

MECHANISMS OF FLASH SINTERING IN CUBIC ZIRCONIA

John Axel McNutt Downs

E-mail: john.downs @ ing.unitn.it

Approved by:

Prof. V.M. Sglavo, Advisor
Department of Industrial Engineering
University of Trento, Italy.

Ph.D. Commission:

Prof. G.D. Sorarù,
Department of Industrial Engineering
University of Trento, Italy.

Prof. P. Colombo,
Department of Mechanical Engineering
University of Padova, Italy.

Prof.ssa M. Ferraris,
Department of Applied Science and
Technology
Polytechnic of Torino, Italy.

University of Trento,
Department of Material Science and Industrial Technology

23 April 2013

**University of Trento - Department of
Material Science and Industrial Technology**

Doctoral Thesis

John Axel Downs - 2013

Published in Trento (Italy) – by University of Trento

ISBN: 978-88-8443-477-7

To my family

Abstract

The recently discovered flash sintering technique has shown that the application of a sufficiently large dc electric field (E-field) to a ceramic during sintering can cause sintering at temperatures several hundred degrees below conventional temperatures with sintering rates that allow for sintering in seconds rather than hours. This technique has already been demonstrated in wide range of ceramic materials including ionic conductors, electronic conductors, semi-conductors and insulators. The application of this techniques to a large range of materials and the dramatic lowering of sintering temperatures and times means this technique has the possibility to revolutionize the ceramics field.

Because the field of flash sintering is still young, the dominant mechanisms are still yet to be identified. So far, the mechanisms active during flash sintering remain only hypothetical. The key to the mechanism is that it must connect two phenomena controlled by different species: conductivity, which is determined by the fast moving species, and sintering, which is controlled by the slowest moving species. At this point the primary hypothesis is that the high E-fields used cause the nucleation and separation of Frenkel defects allowing for both high sintering rates and high conductivities.

This work aims to identify the mechanisms involved in the flash sintering of cubic 8 mol% yttria stabilized zirconia (8YSZ). This materials has been selected because it was one of the first materials show flash sintering properties, and that it has been very well characterized because of its use as a fast oxygen ion conductor.

This work began with the construction and initial testing of flash sintering equipment. Mechanistic investigations were performed on fully dense presintered samples of various grain sizes and single crystalline samples subject to the voltages similar to those used during flash sintering at constant temperatures between 600°C and 1000°C. Because flash sintering

has a sintering component and electrochemical component, dense samples were used to remove the sintering so observations can be made only on the electrochemical behaviors during these electrical treatments. Additionally, the range of E-fields used for flash sintering of green 8YSZ samples was increased by an order of magnitude from the 150 V/cm to 2250 V/cm.

Treatment of fully dense and single crystal samples show that the electrolytic reduction of ZrO_2 to $ZrO_{2-\delta}$ give I-V relations and power dissipations that are similar to those observed in flash sintering of powder samples. Flash sintering using E-field up to 2250 V/cm reveals several relationships between temperature, E-field, current density and power dissipation and their relation to the onset of sintering and densification. Most importantly the onset of sintering can be determined by the power relationship $T_{\text{Onset}} = 2440 E^{-1/5.85}$, where T_{Onset} is the furnace temperature when flash sintering starts in K and E the applied E-field.

Based on these observations, a new mechanism based on electrolytic reduction in the material is proposed to explain the onset and early stages of flash sintering and the observed electrical behaviors. Based on this, the movement of reduced zirconia in the E-field is proposed as a possible sintering mechanism.

Table of Contents

1	INTRODUCTION	1
2	BACKGROUND	7
2.1	SINTERING OF TECHNICAL CERAMICS	7
2.1.1	<i>Free Sintering</i>	<i>7</i>
2.1.2	<i>Pressure Assisted Sintering Techniques</i>	<i>17</i>
2.1.3	<i>Electro-magnetic Field Assisted Sintering Techniques</i>	<i>18</i>
2.2	ZIRCONIA: STABILIZATION, DEFECTS, AND CONDUCTIVITY	20
2.2.1	<i>Structural Stabilization and Defects:.....</i>	<i>20</i>
2.2.2	<i>8 mol% Ytria-Stabilized Zirconia Defect Structure 21</i>	
2.2.3	<i>Conductivity in 8YSZ</i>	<i>28</i>
2.3	ELECTROCHEMICAL CHARACTERIZATION TECHNIQUES	31
2.3.1	<i>Impedance Spectroscopy</i>	<i>31</i>
2.3.2	<i>Direct Current Methods</i>	<i>32</i>
3	STATE OF THE ART	37
3.1	FLASH SINTERING	37
3.1.1	<i>Sintering Behavior:.....</i>	<i>39</i>
3.1.2	<i>Electrical Behavior:.....</i>	<i>40</i>
3.1.3	<i>Flash Sintering in Different Materials:</i>	<i>47</i>
3.1.4	<i>Effect of Particle size</i>	<i>50</i>

3.1.5	<i>Microstructure</i>	51
3.1.6	<i>Proposed Mechanisms:</i>	53
3.2	SIMILAR ASSISTED SINTERING TECHNIQUES	54
3.2.1	<i>Flash-sinterforging</i>	54
3.2.2	<i>Grain Welding:</i>	55
4	MATERIALS, EQUIPMENT, AND	
	CHARACTERIZATION	57
4.1	MATERIALS	57
4.1.1	<i>Zirconia Powder</i>	57
4.1.2	<i>Single Crystals</i>	58
4.1.3	<i>Binders</i>	58
4.1.4	<i>Sample Preparation</i>	59
4.2	4.2 CHARACTERIZATION EQUIPMENT	64
4.2.1	64
4.2.2	<i>Dilatometry</i>	64
4.2.3	4.2.2 SEM	64
4.3	ELECTRICAL CHARACTERIZATION AND FLASH	
	SINTERING	66
5	RESULTS AND DISCUSSION	73
5.1	UNASSISTED SINTERING BEHAVIOR	73
5.1.1	<i>Binder Burnout</i>	73
5.1.2	<i>Constant Heating Sintering</i>	75
5.1.3	<i>Densification and Grain Growth</i>	76
5.1.4	<i>Conductivity</i>	77

5.2	HIGH VOLTAGE FLASH SINTERING	79
5.2.1	<i>Introduction</i>	79
5.2.2	<i>Experimental</i>	80
5.2.3	<i>Results and Discussion</i>	80
5.2.4	<i>Sinter Mapping</i>	92
5.3	FLASH BEHAVIOR IN FULLY DENSE 8YSZ	94
5.3.1	<i>Introduction</i>	94
5.3.2	<i>Experimental</i>	95
5.3.3	<i>Results and Discussion</i>	97
5.4	FLASH BEHAVIOR IN SINGLE CRYSTAL YSZ.....	108
5.4.1	<i>Introduction</i>	108
5.4.2	<i>Experimental</i>	108
5.4.3	<i>Results and Discussion</i>	109
5.4	COMPARISON OF SYSTEMS	113
5.5	MECHANISMS AND FLASH SINTERING	115
6	CONCLUSIONS AND OUTLOOK.....	119
	APPENDIX 1: KRÖGER-VINK NOTATION	131
	APPENDIX 2: GRAIN GROWTH.....	133
	APPENDIX 3: FLASH SINTERING OF EXTRUDED 10GDC CYLINDERS IN DILATOMETRIC SETUP.	135
	CURRICULUM VITAE	137

1 Introduction

Global warming and the associated global climate changes are becoming increasingly observed and understood. These changes include extreme weather events, drastic ecosystem changes, and sea level rise as a result of the Antarctic ice cap melting. Such changes have resulted in, and have the potential to cause, extensive damage and are being credited with causing extreme weather events and drastic ecosystem changes such as drought that can and is resulting in widespread famine [1]. These changes are occurring because the average global temperature has been rising an average of 0.3°C per decade since 1979, a slight, but significant change that has been faster than any normal cyclic temperature change seen in geologic history [2–6].

This increase in temperature is a direct result of anthropogenic emissions of several gasses, the so-called greenhouse gases, which act to trap solar radiation close to the earth's surface causing a net overall heating. Though these gases are naturally present in the atmosphere and are necessary to maintain temperatures so Earth is a habitable planet, in excess, the additional solar forcing that they cause can be dramatic even in small concentrations. The most common of these gases, and the one with the highest total radiative forcing, is carbon dioxide, CO_2 . The bulk of anthropogenic CO_2 emissions are a result of burning carbon-based fuels, coal, petroleum, and natural gas, the back bone of the modern energy production system [2], [7–9]. As a result, atmospheric CO_2 concentrations have increased from ~ 316 parts per million (ppm) in 1960 to 379 ppm in 2005, and continue to rise [2].

In order to slow, and hopefully stop, the climb of the average global temperature, large-scale efforts are being made to curb carbon emissions. The typical goal sought after by climate scientist is to level CO_2 concentrations between 400 – 600 ppm [10]. It is believed that leveling CO_2 concentrations in this range will minimize climate change events that are being observed while still being achieved by economically reasonable methods in a feasible time scales. Many different methods of curbing carbon emissions have been proposed, but the first and primary focus of political and scientific efforts is on the substitution of traditional carbonaceous fuels that have become the foundation of modern electric and heat production with alternative, carbon neutral sources [10]. These fuels—coal, natural gas, and petroleum—are slowly being replaced by alternative

carbon neutral sources—nuclear, wind turbines, solar panels, concentrating solar power plants, etc.

The main focus of alternative energy research is focused on the equipment used for the production of the energy. There is, however, an enormous opportunity to minimize energy at the point of use the energy cycle by implementing various efficiency practices [11], [12]. It has been estimated that increasing efficiency by cost effective means can reduce energy use of the building and industrial sectors by 29% of their energy use today [13]. Typical examples include, but are not limited to, switching to energy efficient and smart lighting and heating systems, better building insulation, and the reduction of vampire loads.

Efficiency measures are as applicable to small home private users as they are to large-scale industrial processes. On the industrial level, and specifically relating to the ceramics industry, there is no exception. First, the ceramics industry is the largest raw materials industry. It encompasses traditional materials such as cements, glasses, refractories, and clays as well as advanced ceramic materials used in electronics, nuclear fuel, biological systems, and other technical applications. [14–16]. Production and processing of these materials inherently consumes a large amount of energy due to the necessity of high processing temperatures required to produce an industrially useful final product [14]. The melting temperatures of these materials are too high for the traditional forming processes used to produce polymeric or metallic items, like casting and forging, and they are typically too hard (typically >8 on the Mohs hardness scale) to be formed by traditional cutting operations like sawing, milling, and drilling. [14]. Instead, solid-state processes must be exploited on preformed, near net shaped components that have been produced from starting powders by heating the material to a sufficiently high temperature for a sufficiently long time. In traditional clay ceramics this treatment is the commonly known as firing.

Advanced ceramics are characterized by their pure chemical composition, giving them specific engineering attributes required [17]. For the advanced ceramics, the solid state forming process is called sintering. A ceramic powder of the desired chemical composition that will give the desired engineering properties is formed into a near net shape. Usually the part is held together with the aid of some sort of binding agent. This piece is said to be in its green state. It has a very low mechanical strength and a very limited density, typically between 30 and 50% of the materials theoretical full density, making it commercially useless. To increase the mechanical strength and density, the green component is sintered by a heat treatment at a temperature that is between 60 and 80% of the materials melting

temperature, and held at that temperature for several hours. At these temperatures, diffusional processes are enabled allowing for the movement of material causing densification. Long hold times are required to allow these processes to reach completion, ideally finishing when full density is achieved and the desired engineering property reaches a maximum.

Two common technical ceramics, alumina (Al_2O_3) and yttria-stabilized zirconia (YSZ), require sintering treatment at $1400^\circ\text{C} - 1650^\circ\text{C}$ for 2 – 6 hours [18]. In order to reach and maintain these sintering temperatures, there is an inherently high energy consumption in the form of electricity or natural gas, and furnaces must be made with expensive, exotic materials in order to withstand these temperatures and times.

The demand for advanced ceramic materials is increasing. In addition to the development and discovery of novel uses for new ceramic materials, especially in biological, catalytic, electronic, communication, and armor applications [14], [19], they are also becoming essential materials in the drive to make current fossil fuel based energy production systems more efficient. Ceramic coatings are becoming increasingly used in combustions systems allowing for higher operating temperatures that are not possible with metallic components, permitting higher thermal efficiencies, thus reduced fuel use for the same fuel use, or increased energy output for the same fuel use. Ceramic materials are also a necessary material for many of the alternative energy systems: photovoltaic solar cells, solar thermal heat exchangers, high efficiency and high capacity batteries, and intermediate and high temperature fuel cells.

Clearly, reducing sintering temperatures and times can save vast amounts of energy. As the ceramics industry continues to grow due to high material demands, energy use in this sector will continue to grow. Additionally, energy will become more expensive forcing ceramic materials to become more expensive slowing overall efforts for efficiency in other sectors eventually slowing efforts for the development of alternative energy sources and efficient combustion engines.

Many different technologies have been developed or are in the process of being developed that are able to lower sintering temperatures and shorten sintering times. Methods include the addition of sintering aids which enhance diffusion rates or allow for faster sintering by creating a liquid phase; pressure assisted sintering such as hot pressing, sinter forging, and hot isostatic pressing (HIP)[15], [18], [20]; and the use of electro-magnetic radiation as is the case in spark plasma sintering (SPS) [21] and microwave assisted sintering [22]. Each exploits various sintering processes and

mechanisms, and often has the benefit of improving the quality of the final product.

In 2010, a new assisted sintering process was discovered. This sintering involves the application of a direct current (dc) electric field (E-field) to a green body while it is being heated to normal sintering temperatures. What was observed was that with a high enough E-field, sintering temperatures began to dramatically drop, even reducing temperatures by hundreds of degrees while sintering times were reduced from hours to seconds [23]. Due to the high sintering rates and the sudden nature the onset of sintering, the name coined for this assisted sintering process is “flash sintering” [23]. What characterizes flash sintering is the sudden onset of sintering at temperatures several hundred degrees lower than the sintering temperatures required for conventional sintering and other assisted sintering techniques. Using this technique, sintering times are reduced to seconds rather than nominal treatment times of hours. Additionally, flash sintering has been shown to occur in several different materials with a wide arrange of electrical characteristics including ceramics that are electronically conducting, ionically conducting, and electronically insulating.

The flash sintering technique has the potential to revolutionize the ceramic industry by lowering energy use, resulting in lower carbon emissions as a direct result of the lowered processing temperatures and times. However, the flash sintering process is still in its nascent stages. Despite the demonstration of the occurrence of flash sintering in a wide range of ceramic materials, the process is difficult to control and the active mechanisms remain unknown leaving the prediction and control of flash sinter behavior difficult. In order to fully utilize and exploit the possible advantages flash sintering has to offer, and in order for it to be adopted at an industrial scale, the underlying mechanisms at work must be understood.

The present work sets out to investigate the mechanisms of flash sintering using cubic zirconia as a model system while further expanding the phenomenological knowledge of the field. Cubic zirconia has been chosen because it was one of the first materials to be shown to have flash sintering behavior, and because it is a very well characterized material from both an electrical and chemical point of view. The main approach to identifying active mechanisms is to measure the flash sintering-like behavior that occurs in samples that have already been sintered, thus removing the effect of the sintering itself. Additionally, in order to observe the effects of grain boundaries, these specimens have been prepared with various grain sizes, and their behavior will also be compared to single crystal samples free of

grain boundaries. Based on the observations made in these systems, the mechanisms active at onset and initial stages of flash sintering are proposed.

2 Background

2.1 *Sintering of Technical Ceramics*

2.1.1 Free Sintering

Technical ceramics, characterized by their chemical purity, are sought for various reasons including their structural and chemical stability over a range of temperatures, especially at very high temperatures, their high hardness, and their high fracture toughness. All these properties arise from the strong atomic bonding that defines ceramic materials. These advantages, however, cause several difficulties when trying to produce a useful component of a given ceramic material. The high stability at temperature and very high melting temperatures make the forming of parts by traditional processes used for metallic and polymeric materials like casting and forging. High hardnesses make tool wear an issue, thus requiring the use of expensive and exotic materials necessary for cutting operations. The tendency of ceramics to be brittle often makes these cutting operations futile because the risk of fracture or the introduction of flaws into the material that make fracture more likely. If cutting is done, feed rates can be very slow making this step expensive.

As a result of these limitations, ceramic items are instead manufactured by means of the sintering process. The sintering process is a near net shape fabrication technique where a ceramic powder is first formed

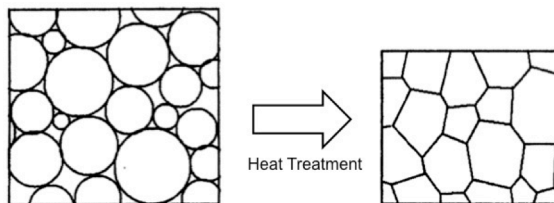


Figure 2.1: The sintering process is the densification of a green powder body to a fully dense body. Modified from [18]

by various methods into a low density, low mechanical strength part. This part has little use because it has no useful engineering properties. The part is then subject to a heat treatment, where diffusional process fill in the pores of the powder bringing the part to high density where the desired properties, whether they be mechanical, electrical, optical etc., are reached. The sintering process is shown in Figure 2.1. Due to the elimination of pores, sintering is accompanied by an overall shrinking.

Starting powders have the desired chemical composition of the final part. The overall chemical composition can be determined by the powder itself, or by a mixture of several different ceramic powders that during sintering interdiffuse to give the desired final composition. Powder sizes range from ~ 10 nm – >100 μ m with the most common sizes being 1 μ m – 10 μ m [20]. The powders are typically mixed with a binding agent that improves the mechanical behavior of the item after it is formed into its low density, near-net-shape so it can be more easily handled. This untreated state is known as the green state.

Green components are then sintered at a sufficiently high temperature to enable solid-state diffusion processes that allow for mass transport eliminating the pores between the powder particles and increasing density. Densities are measured as a percentage of the theoretically perfect density of the material being used. If the treatment temperatures are high enough and the treatment long enough, the part can achieve a density near 100% of the theoretical density (Figure 2.1), where all porosity is eliminated. Typical sintering treatments are done at 50% to 80% of the ceramic's homologous temperature (T_H), the melting temperature on an absolute scale. Heating schedules can be varied and can become very complex in order to deal with the elimination of binders and to activate specific diffusion to ensure as dense a material as possible.

The densification process occurs as the result of matter transport to the contact points between the powder particles. As matter collects at these points, the points grow into surfaces called necks, where a grain boundary

develops as an interface between the differently oriented lattices of the two particles. Necks grow pores are eliminated and only grain boundaries are left between the particles. The evolution of pores and grain shape during sintering is shown in Figure 2.2. Sintering progresses from (a) packed particles to (b) neck formation (c) interconnected pore network and finally to (d) full density [24].

Several diffusional processes can be activated and depending on the material and temperature (Figure 2.3). They differ in the source of the matter and the mode of diffusion. For all process the sink is always the neck free surface. Only the diffusional processes that transport matter from the neck core to the neck surface allowing for the elimination of the porosity and densification. This leaves only two processes, lattice diffusion and grain boundary diffusion from the neck core. A third mechanism that leads to

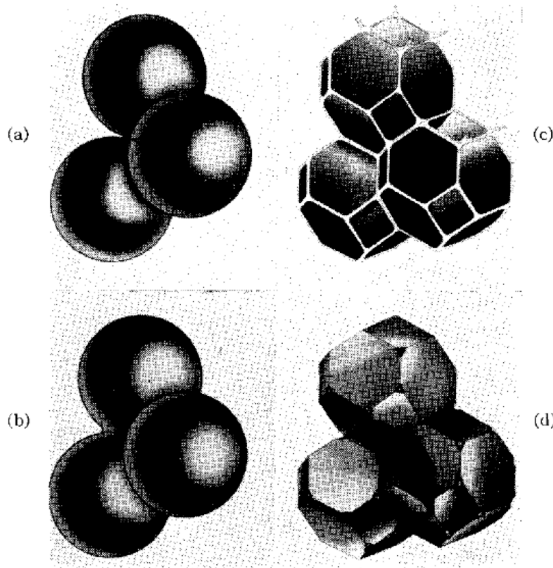


Figure 2.2: Progressive steps of sintering: pressed powder in (a) neck formation (b), porous network at the grain edges (c) fully sintered ceramic (d) [24]

densification is the movement of dislocations by plastic deformation to the pore, but this will be ignored because it requires the use of large externally applied pressures to cause dislocation movement.

Free sintering is sintering without the application of any external forces. The thermodynamic driving force for densification is the elimination of high-energy free surfaces by increasing the area of the lower energy grain boundaries between particles. The overall change in energy is given by:

$$(2.1) \quad \Delta E_{densification} = -(\gamma_{SV}\Delta A_{SV} - \gamma_{GB}\Delta A_{GB})$$

where $\Delta E_{densification}$ is the reduction of energy driving densification, γ_{SV} the free surface energy of the ceramic, ΔA_{SV} the change in free surface area,

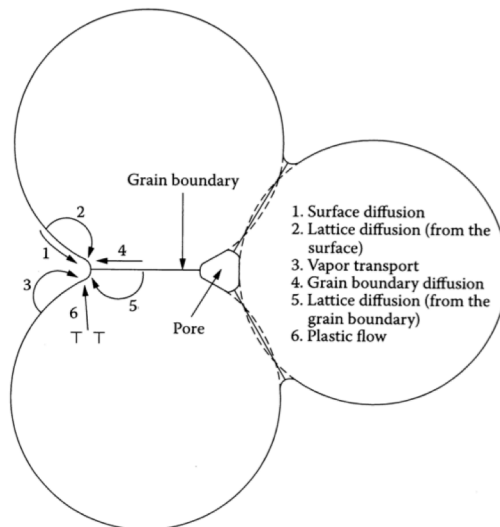


Figure 2.3 Sintering Diffusional processes and their path activated during heat treatment. For sintering, only grain boundary diffusion, 4, and lattice diffusion from the grain boundary, 5, is of interest[18]

γ_{GB} the surface energy of the grain boundary, and A_{GB} the change in grain boundary surface area [18].

The creation of a grain boundary requires the elimination of two free surfaces into one grain boundary so $\Delta A_{GB} \approx \Delta A_{SV}/2$ giving:

$$(2.2) \quad \Delta E_{densification} = -\Delta A_{SV}(\gamma_{SV} - \gamma_{GB}/2)$$

The free surface energy γ_{SV} is usually higher than the grain boundary surface energy γ_{GB} meaning that the elimination of grain boundary surface is energetically favorable ($\Delta E_{densification} < 0$) resulting in densification and sintering.

Even though densification is energetically favorable, a means for the diffusion of matter must be available for the sintering to occur on reasonable time scales. In ceramic materials, lattice diffusion is takes place by movement of atoms through different lattice defects (discussed in section 3.2). Grain boundary diffusion takes place by movement on atoms through the disorder of the grain boundary. There must also be a driving force that is given by the difference in either a concentration or in a difference of chemical potential.

At the initial stages of sintering, where there is little or no neck formation, concentration gradients are controlled by the curvature of the free powder particle surfaces and the curvature of the neck, the concentration of vacancies, C_v , can be determined by the Gibbs-Thompson equation:

$$(2.3) \quad C_v = C_{ov} \left(1 - \frac{\gamma_{SV} K \Omega}{kT} \right)$$

Where C_{ov} is the vacancy concentration at a standard state, K the curvature, Ω the atomic volume of the diffusing species, k the Boltzmann constant, T the temperature in K [18]. This gives C_v that are higher on convex surfaces, the particle free surface, and lower on concave surfaces, the neck free surface [25]. Thus neck formation is favored. In latter stages of sintering, a chemical potential difference arises between the atoms at the grain boundary and the atoms at the free surface of the pore. The potential driving diffusion at a given temperature, μ , is given by [26]:

$$(2.4) \quad \mu = \Omega \left(\frac{2\gamma_{gb}}{G} + \frac{\gamma_{SV}}{r} \right)$$

where r pore radius and G the grain or particle diameter. The driving force is composed of two components, one related to the convex nature of the grain acting as the sources and one related to the convex nature of the pore surface at the neck acting as a sink.

Considering these driving forces, and general diffusion rate equations the densification rate equation is:

$$(2.5) \quad \frac{1}{\rho} \frac{d\rho}{dt} = \frac{AD\gamma_{SV}\Omega}{\rho G^m kT}$$

Where ρ is the density, A a numerical constant, D the diffusion constant for either lattice diffusion or grain boundary diffusion, γ_{SV} the free surface area, G the average grain size. The exponent m is 3 if lattice diffusion is dominant and 4 if grain boundary diffusion is dominant [25].

2.1.1.1 *Improving free sintering behaviors:*

Given equation (2.5), there are several different steps that can be taken in order to modify and improve the sintering behavior for a given material. Desired improvements are shortening sintering times, lowering sintering temperatures, or a combination of the two. Using only the power preparation these improvements can be done by:

1. Decrease powder size, G
2. Increase temperature, T
3. Change diffusion coefficient, D
4. Increase green density, ρ_o

The most effective method to improve sintering behavior, and densification rates is the reduction of the powder size, G . Reduction of G reduces diffusion distances whether diffusion takes place by grain boundary diffusion or lattice diffusion. A small change in the starting particle size has a dramatic effect because of the diffusion exponent, m .

Reduction of powder size has its advantages, but reducing grain size makes the handleability of the powder more difficult [20]. Reaching smaller powder dimensions also requires the input of more energy and time when powders are prepared by mechanical means or a change of preparation method if starting powders are prepared chemically. A balance between savings gained during the sintering cycle must be compared with the losses of the new powder preparation and processing methods.

Because sintering is a diffusional process, increasing the sintering temperature, T , would be the easiest way to increase densification rates by making atomic movement easier. Before doing this, two things must be considered. First, increasing sintering temperature may activate other processes such as grain coarsening and the recrystallization and precipitation of secondary phases. These may result in desired or undesired increases in the performance of the ceramic. Choosing a sintering temperature is often choosing the temperature that balances the advantages of having shorter

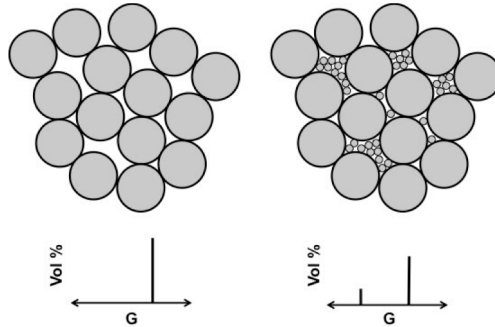


Figure 2.4: Grain packing and the effect of having a bimodal grain size distribution to increase initial density.

processing times while still maintaining some control on these secondary processes.

Increasing sintering temperatures must also be weighed with the limitations of furnaces and their energy use. As temperatures increase, furnaces must be made with more exotic materials that are able to reach and resist the desired sintering temperature. The energy costs required to reach and maintain these temperatures may also become prohibitive.

Several different methods can be used to modify the diffusion coefficient, D , but this is often difficult because it is a property of the material. The first would be the use of different additives that form a secondary phase, often liquid, at the grain boundaries that act as a pipeline for faster rates of diffusion. The addition of amounts less than 0.2 mol% of MgO in Al_2O_3 , can reduce sintering temperatures and result in a finer microstructure.

Increasing the starting density, ρ_0 , effectively moves the starting point of sintering to a more advanced stage before heat treatment takes place. The idea is to maximize contact between powder particles, reducing the starting porosity that must be eliminated and maximizing the points of contact between particles where diffusion takes place. Increasing the pressures used to prepare green specimens ensures that all agglomerates, a

culprit of high initial porosities, are broken and that the porosity of green specimen is determined by the smaller powder particles and not the large agglomerates. However, the high hardness of ceramics and sometimes of the agglomerates formed can result in pressure limitations of the die being exceeded before any benefit of increased density is achieved.

Tailoring the distribution of powder sizes can also ensure a lower starting porosity. Having a bimodal distribution of powder diameters provides a green compact with a matrix with a porosity determined by the larger particle that is then filled in by the smaller particles (Figure 2.4). This increases starting density and, increases contact points between larger powder particles, and provides smaller grains with high diffusion rates a previously discussed. Tailoring the powder distribution can also be very difficult, and increases the complexity of powder processing.

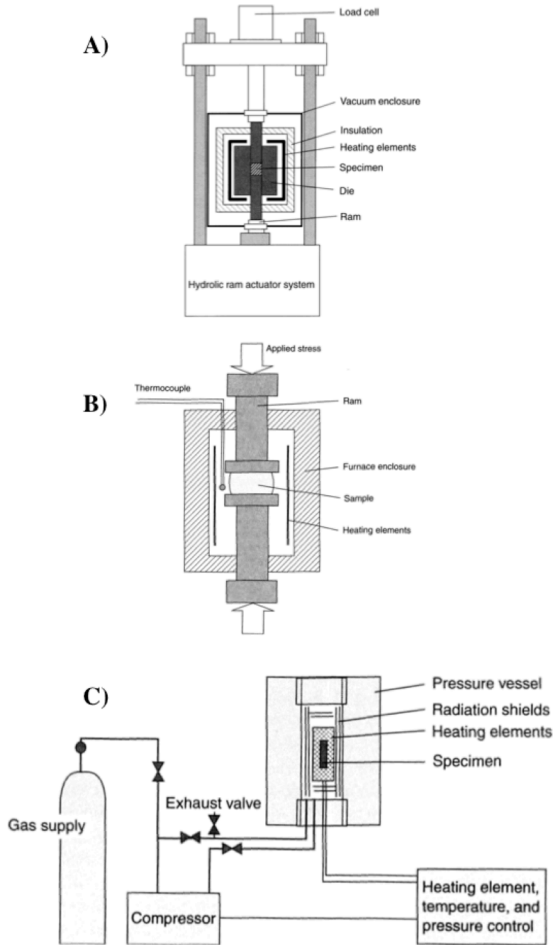


Figure 2.5: Schematics of pressure assisted sintering techniques. A) Hot-Pressing B) Sinter Forging C) Hot Isostatic Pressing (HIP) [26]

2.1.2 Pressure Assisted Sintering Techniques

Free sintering is effective for sintering and can be done without any specialized equipment. It has the disadvantage that very high temperatures and long times at those temperatures are required to get a sufficiently dense material and for very high temperature materials, like zirconium diboride, ZrB_2 , and boron carbide, B_4C , full density is nearly impossible using commercially available furnaces. This requires the use of very specialized furnaces that are still usually incapable of reaching the required temperatures. In order to minimize these requirements, many techniques have been developed to lower sintering temperatures and sintering times.

The family of pressure-assisted techniques, are the most common, involve the use of applying an external pressure to the material. Externally applied stresses change vacancy concentrations by creating zones of tension and compression changing the concentration of vacancies, C_v , and changing the diffusional driving force to sintering, μ . The creation of these vacancies is further assisted by the stress concentration that occurs due to the porosity, much like the stress concentration that occurs in bulk materials that are put into tension or compression.

The three most common pressure-assisted sintered techniques vary on how the external pressure is applied and the way the powder is held. Schematics of these three techniques are shown in Figure 2.5. The first technique, hot pressing, uses the application of a uniaxially applied pressure to a powder that is contained in a die restricting that restricts the radial motion of the powder. Due to this radial restriction, the applied pressure, P_z , gives rise to a hydrostatic pressure P , etc.

The second method, sinter forging, is similar to hot pressing but there is not die restricting radial motion. For the sample to maintain its integrity at the start of sintering, it usually needs to be presintered. By permitting radial motion, shear stresses in the material allow for particle

rearrangement and the refinement of the microstructure as a result of the nucleation of new particles.

The third pressure-assisted technique is Hot Isostatic Pressing (HIP). It uses a high-pressure gas to apply a hydrostatic pressure during the sintering cycle. HIP has an advantage in that it allows for the pressure assisted sintering of very complex geometries. But it requires the use of specialized furnaces that are able to maintain pressures.

2.1.3 Electro-magnetic Field Assisted Sintering Techniques

Another common form of assisted sintering is the use of various electro-magnetic fields during sintering. The most commonly used method is Spark Plasma Sintering (SPS). This method combines hot pressing with application of an E-field. In SPS, a ceramic powder is placed in a graphite die, and uniaxially pressed. A current is applied to the die and sample, and depending on the conductivity of the powder used, the current passes completely through the die, or partially through the sample and partially through the die. This current causes heating of the die and sample by joule heating. Because of the high currents used, heating rates can reach 100s °C/min without the use of a furnace. Current and pressure schedules can become very complex, leading to the many different sub-groups [27]. SPS has very high sintering rates as a result of temperatures that can be reached and the use of an applied pressure. However, rates are higher than expected for either of these phenomena meaning that the presence of E-fields and currents are affecting sintering rates. Unfortunately, due to the complex nature of the SPS process: pressure, high Temperature, and E-fields, it has been very difficult to decouple influence of each of the three effects.

Microwave sintering is another E-field assisted sintering. This technique involves heating samples by both furnace and then by microwaves. When compared to conventional sintering, microwave sintered samples densify much faster, and at lower temperatures [28]. The active mechanism is considered to be the resonance of the dipoles in the ceramic that cause heating. Sintering temperatures can be lowered by several hundreds of degrees, but because microwave sources are usually fixed at 2.45 GHz, the effectiveness of the coupling depends heavily on the properties of the material being sintered.

The field-assisted sintering techniques (FAST) are the last method of electromagnetic field assisted sintering. The work on these is also the preliminary work of what has become the field of flash sintering. Here, low strength E-fields, either alternating current (ac) [29] or direct current (dc) [30] are applied to a part during sintering. The result is accelerated sintering rates and reduction in the amount of grain growth. The application of small E-fields has also been shown to change diffusional properties and deformation stresses during sinter forging and tension tests allowing for high

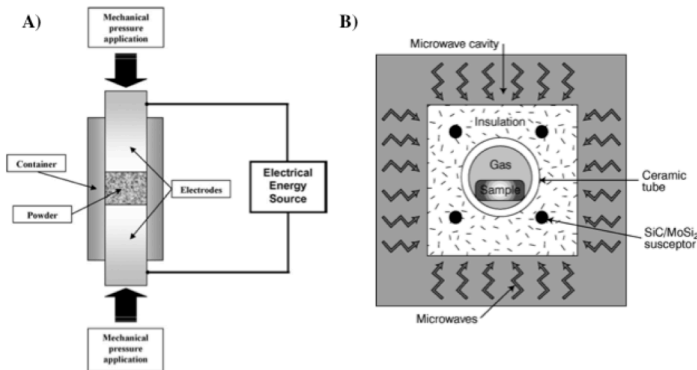


Figure 2.6: Schematics of sintering setups for electromagnetic field assisted sintering. A) Spark Plasma Sintering (SPS) [27] B) Microwave sintering [78] .

amounts of strain and superplasticity in zirconia and alumina ceramics [31–35]. Additionally, small E-fields <4 v/cm have been shown to reduce grain growth during the annealing of 3YSZ [36].

2.2 Zirconia: stabilization, defects, and conductivity

2.2.1 Structural Stabilization and Defects:

Pure zirconia dioxide (ZrO_2), zirconia, has a monoclinic unit cell at room temperature. At $1170^\circ C$ it goes through a change to a tetragonal structure and above $2370^\circ C$ has a cubic structure. Upon cooling there is a martensitic phase change tetragonal \rightarrow monoclinic phases with an associated volume expansion of $\sim 5\%$ and shear strain of $\sim 7\%$ [37], [38]. These two drastic changes result in large stresses that fracture the material. Pure zirconia itself has little engineering use because of this tendency to fracture. It is the higher temperature tetragonal and cubic phases that are of interest, but they must be stabilized at lower temperatures, consequently avoiding the fracture that arises from the monoclinic/tetragonal phase transition.

Stabilization of the tetragonal or cubic phases is achieved by the addition of an aliovalent metal oxide to the pure zirconia. An aliovalent ion would be any metal ion that has a formal charge different from the $+4$ charge of zirconium atom in ZrO_2 . The presence of the aliovalent ions causes the defects to develop in the zirconia lattice because it is forced to maintain charge neutrality. At sufficient concentrations of metal ions, the defects strain the zirconia structure sufficiently to stable the tetragonal or cubic structure. Stabilized zirconia is identified by the equivalent mol% of the dopant metal oxide that has been added to zirconia. Typical stabilizing oxides are the divalent metal oxides: CaO (calcia), MgO (magnesia) and SrO (strontia); trivalent M_2O_3 oxides: Sc_2O_3 (scandia) and Y_2O_3 (yttria); and

pentavalent metal oxides V_2O_5 (vanadia), Hf_2O_5 (hafnia), and Ta_2O_5 (tantala) [39].

2.2.2 8 mol% Yttria-Stabilized Zirconia Defect Structure

For the purpose of this work, only cubic stabilized, 8 mol% yttria-stabilized zirconia (8YSZ) has investigated experimentally. This material stabilization was chosen as the model system and because its electrical, thermal, and structural behaviors have been well characterized due to interest as its use as a fast oxygen ion conductor.

2.2.2.1 Intrinsic Defects

Stoichiometric ZrO_2 has a fluorite unit cell. This cell is face center cubic with the oxygen anions at tetrahedral sites coordinated by 4 zirconium cations and a cubically coordinated zirconium cations surrounded by 8 oxygen ions, see Figure 2.7 [40].

The ideal unit cell would be repeated infinitely in a bulk material. However, entropic effects cause disorder of the perfect lattice by moving atoms from their ideal lattice site one of various different positions. The

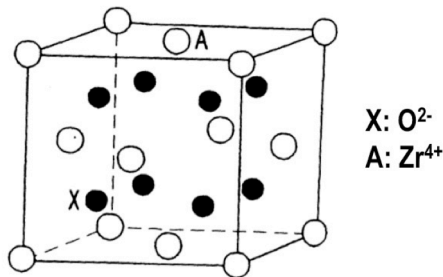


Figure 2.7: The fluorite unit cell of stoichiometric Zirconia [79]

atoms moved from their ideal lattice position and the empty lattice sites left behind are called lattice defect. The amount of disorder depends on the temperature of the system and the enthalpy of formation for various defects. Because the formation of these defects occurs spontaneously in the stoichiometric structure, they are called *intrinsic defects*.

Three different intrinsic defects can form giving rise to disorder and are of important concern for the sintering behavior of flash sintering, they are: cationic Frenkel disorder, anionic Frenkel disorder, and Schottky disorder. These defects are described using Kröger-Vink notation which gives information on the species of the defect, the location of the defect, and the resulting effective charge by moving the atom in question depending on its position with regards to an ideal lattice site in the perfect structure. This notation is discussed in Appendix 1.

Frenkel disorder is a defect that is caused by the movement of a single atom from its ideal location to an interstitial site (Figure 2.8). Cationic Frenkel disorder occurs when the atom in question is a cation, and anionic Frenkel disorder when the atom in question is an anion. The formation of Frenkel defects causes the formation of a defect pair that consists atom that has moved to an interstitial site and the vacancy left at the original site of the now interstitial atom.

In order to determine the equilibrium state of the Frenkel disorder, the formation of the defect can be as the chemical reaction for compound ZrO_2 :



for cation disorder caused by the formation of zirconium ion interstitials, and:

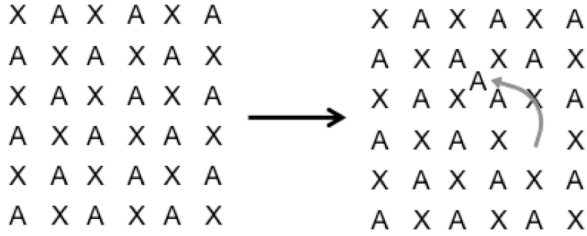


Figure 2.8: Example of cationic Frenkel Defect in compound AX. The atom A has moved to an interstitial position resulting in the addition defect left at the site formerly occupied by A.



for anionic disorder caused by the formation of oxygen ion interstitials. *Nil*, corresponds to the ideal lattice the state with out any defects of Zr_{Zr}^x and O_o^x .

If the concentrations of these defects are low, the ideal system can be considered a dilute solution allowing for the determination of equilibrium concentrations using the lass of mass action. For cationic Frenkel (CF) defects this gives:

$$(2.8) \quad \frac{[Zr_i^{\cdot\cdot}][V_o^{\cdot\cdot}]}{[Zr_{Zr}^x][O_o^x]} = K_{CF} = \exp\left(\frac{\Delta S_{CF}}{k}\right) \exp\left(\frac{\Delta H_{CF}}{kT}\right)$$

and similarly for anionic Frenkel (AF) defects:

$$(2.9) \quad \frac{[O_i''] [V_o^{\cdot\cdot}]}{[Zr_{Zr}^x][O_o^x]} = K_{AF} = \exp\left(\frac{\Delta S_{AF}}{k}\right) \exp\left(\frac{\Delta H_{AF}}{kT}\right)$$

where K_i is the equilibrium constant at a given temperature T in degrees K, ΔS_i is the energy change due to enthalpy, ΔH_i is the enthalpy of formation of the defect pair, and k is the Boltzmann constant. The equilibrium constant

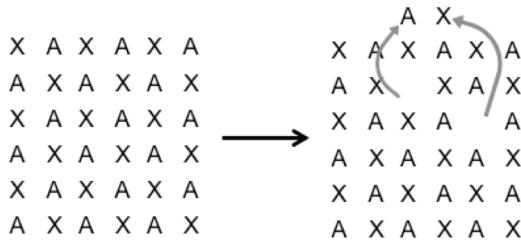
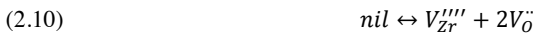


Figure 2.9: Schottky disorder in compound AX. The stoichiometric pair AX is removed from the lattice and placed on a free surface creating a pair of vacancy defects.

K is an indication of the change in free energy of the system, ΔG , due to the formation of the defect.

Schottky defects are third mode of intrinsic disorder. In this case, a stoichiometric set of atoms are removed from their lattice sites and placed on a free surface of the system leaving behind an equally charged set of vacancies, see Figure 2.9.

In ZrO_2 , the reaction for Schottky defect formation is given by:



Because the atoms are moved to a free surface, they do not create defects themselves. Only the vacancies left behind after their removal constitute the defects formed. The equilibrium reaction is given by:

$$(2.11) \quad \frac{[V_{Zr}''''][V_O^{\bullet\bullet}]^2}{[Zr_{Zr}^x][O_O^x]} = K_S = \exp\left(\frac{\Delta S_S}{k}\right) \exp\left(\frac{\Delta H_S}{kT}\right)$$

2.2.2.2 *Extrinsic Defects*

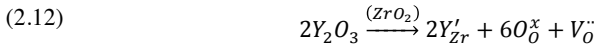
Extrinsic defect result from the addition of aliovalent dopants to pure zirconia. The law of charge neutrality dictates that the dissolution of any aliovalent dopants must be counteracted by something that balances the missing or additional charge. Four crystalline defects can act to compensate for an unbalanced charge and depend on how the additional atoms are substituted into the zirconia structure. Due to steric hindrances as a result of atomic radius and/or the formation of highly charged defects there are usually limitations of how the aliovalent atom can be placed into the lattice.

As discussed in section 2.2.1, the stable phase of stoichiometric ZrO_2 is monoclinic. The addition of aliovalent metal oxides is used to stabilize the higher temperature tetragonal and cubic phases, which are structurally stable. Normally in ionic compounds, four different types of defects can form. Each depends on where the dopant metal oxide cation atoms are supported when diffusing into the existing ZrO_2 lattice, and whether the aliovalent atoms is a donor impurity or an acceptor impurity. Donor impurities will have a formal charge that is positive when substituted into the lattice at a cationic site while an acceptor will have a negative formal charge. The possible defect that can form in order to balance the missing or excess charge due to the dissolution of a certain metal oxide in to the zirconia lattice are:

1. Substitution of donor atom at lattice site creating cationic vacancies
2. Substitution of donor atom at interstitial site creating cationic interstitials
3. Substitution of acceptor atom at lattice site creating anionic vacancies
4. Substitution of acceptor atom at interstitial site creating cationic interstitials

In the case of ZrO_2 doped with Y_2O_3 , yttrium is a donor impurity. That is, when Y^{3+} ions are substitute Zr^{4+} , atoms in the ideal ZrO_2 lattice, the

resulting net charge will be -1. To balance the resulting net negative charge, two possible defects can be created:



To understand which of these substitution are preferred, one must consider both the size of and charge of the interstitial species. In the case of the first substitution, there is only the creation of one oxygen vacancy. This has a charge of two and does not cause considerable stress the crystal lattice with its absences. In the case with an interstitial Yttrium atom, a relatively large cation with a high charge is placed into an interstitial site. Both of these are energetically unfavorable. For this reason, the accepted way of substitution of Y_2O_3 in ZrO_2 is the formation of oxygen vacancies, eqn (2.12).

2.2.2.3 *Extrinsic Electronic Defects*

So far, only stoichiometric compositions of ZrO_2 or Y_2O_3 - ZrO_2 have been considered. In normal environments, 8YSZ normally maintains its stoichiometry. However, in atmospheres with very low or very high partial pressure of oxygen (P_{O_2}), it is possible that oxygen is absorbed or expelled from the system as it attempts to equalize with its surrounding. In the Y_2O_3 - ZrO_2 system, these deviations from stoichiometry result in electronic defects.

In conditions with low P_{O_2} , oxygen leaves the crystal system creating oxygen vacancies. Conditions with high P_{O_2} cause the absorption of oxygen that is most easily accommodated at an interstitial site. The formation of these defects cannot be balanced by the defects described before because the system with regards to intrinsic and extrinsic defects is

already in equilibrium. To maintain charge neutrality of the crystal system electrons are left behind as atomic oxygen is created and eliminated from the system. In the case of the Y_2O_3 - ZrO_2 system and considering that yttrium is substituted at zirconium sites creating oxygen vacancies, the addition of oxygen results in:



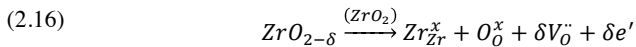
Here, $V_O^{\bullet\bullet}$ is replaced by two electron holes, h' , maintaining the +2 charge. Elimination of oxygen from the solid system results in:



The creation of neutral oxygen at its lattice as oxygen gas is balanced by positively charged $V_O^{\bullet\bullet}$ and negatively charged electrons, e' , maintaining a zero net charge.

2.2.2.4 *Intrinsic Electronic Defects*

Intrinsic electronic defects arise from the change in oxidation state of the constituent components. In the case of metal oxides, this would mean the change in oxidation state of the metallic species. For ZrO_2 the preferred state is Zr^{4+} . However, it can be reduced to states of +3, +2, +1, and 0. Considering the substitution of ZrO into ZrO_2



The variation of stoichiometry by δ created vacancies that are compensated by the creation of electrons.

2.2.3 Conductivity in 8YSZ

8YSZ is utilized because of its ability to conduct oxygen ions with a minimal conduction of electrons over a large range of oxygen partial pressures. This is one reason why 8YSZ is commonly used as an electrolyte in solid oxide fuel cells (SOFCs).

The transport of charge in oxygen ion conductors can be viewed as the movement of V_{O}^{\bullet} or the movement of $\text{O}_{\text{O}}^{\times}$ in the opposite direction as the result of an applied E-field. These movements are equal and opposite. Vacancies have a positive net charge so their movement is in the opposite direction of electronic current.

This conductivity arises from the extrinsic yttria doping and the resulting creation of oxygen vacancies. In general, regardless of the dopant used, increasing the amount of dopant increases the conductivity of the zirconia due to an increase of V_{O}^{\bullet} concentrations. However, at high concentration, there can be an excess of V_{O}^{\bullet} . This excess results in

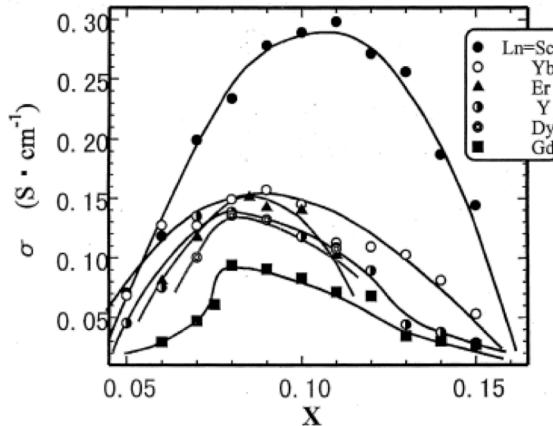
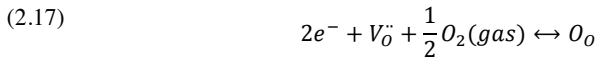


Figure 2.10: Ionic conductivities in zirconia for varying amounts of different dopants [80].

electrostatic hinderances there is the formation of electrostatically bound defect complexes that impede conduction, see Figure 2.10. In yttria-stabilized zirconia, the maximum conductivity is achieved with a doping of 8 mol% yttria. This amount stabilizes zirconia's cubic phase.

If an ionic conductor is placed in an electrical circuit, there are two different charge carrying species. In the metal wires, electrons act as the charge carrying species and oxygen vacancies as the charge carrying species in the ionic conductor. As a result, there must be a chemical reaction at the electrodes that allows for the change of charge carriers. The electrode reactions are given by:



At the cathode, the forward reaction occurs. The elimination of oxygen vacancies in the 8YSZ with oxygen taken from the surrounding environment, and requires two electrons from the electrode. At the anode, the reverse reaction takes place. Oxygen vacancies are created at the cost of oxygen at the lattice. The lattice oxygen leaves the system as gaseous oxygen and two electrons are liberated for every vacancy created.

Because of this reaction, there is a resistance at the electrodes. This resistance is determined by the rate of the reaction, which can be limited by the reaction or by the current applied.

Generally, for ionic conductors, the conductivity follows the Arrhenius trend because it is an activated diffusion process. Materials of this type are governed by the Arrhenius equation:

$$(2.18) \quad \sigma = \sigma_0 e^{\frac{-A}{kT}}$$

where σ is the conductivity ($\Omega^{-1} \text{ cm}^{-1}$) at temperature T in degrees K , σ_0 is the the conductivity at a standard value, and A is the activation energy of conductivity for the given material. This has to do with the ease of moving oxygen ions through the material. As temperature increases, the conductivity increases. Published values for A are shown in

Table 2-1.

Typically, zirconia has two regimes, defined by two different activation energies. At temperatures below 600°C , oxygen vacancies form defect complexes. This results in a) less vacancies available for conduction and b) and electrostatic resistance making vacancy movement more difficult. The result is a slightly higher activation energy A . Above this temperature, the thermal energy is high enough that defect complexes dissociate and all vacancies that arise from the yttria doping are available as charge carriers. This results in lower activation energies at high temperature.

Table 2-1: Activation energy for the conductivity in YSZ prepared by different methods. (Grain boundary impedance denoted GB)

Author	Method	Preparation	E_a (eV)
Rajeswari, K et al. [41]	Impedance	SPS 8YSZ	Bulk: 1.02 – 1.53 GB: 0.79 – 1.86 Total: 0.96–1.80
Abelard and Baumard [42]	Impedance	Conventionally sintered 13.5YSZ	Bulk: 1.03 GB: 1.16
Abelard and Baumard [43]	2-pt DC	12YSZ Single Crystal	Bulk Imp.: 1.29 Bulk DC: 1.17 – 1.13
Badwal [44]	Impedance	7YSZ	Bulk: 103 GB: 108
		10YSZ	Bulk: 114 GB: 111

2.3 *Electrochemical Characterization Techniques*

Several different techniques exist to characterize electrochemical circuits like those that include ionic conductors like 8YSZ. These techniques, to various degrees, are used to measure the electrical properties of the circuit. Some techniques allow for clear measurements of the different chemical processes involved in the circuit like the previously mentioned charge transfer reaction.

2.3.1 Impedance Spectroscopy

Impedance spectroscopy is a characterization method that uses small amplitude alternating current (ac) E-fields of different frequencies to excite different electro-chemical processes. This technique has the advantage that it is able to distinguish different electrochemical process and characterize those processes by their resistance and capacitive response. Based on the circuit response, an equivalent circuit of resistors and capacitors or constant phase elements can be assembled to model the response of the system in question. The electrochemical behavior of a system can be estimated if there is some reasonable hypothesis of the processes in question. Because there are an infinite number of electrical circuits that can be developed to fit a measurement, a reasonable knowledge of the possible processes involved in the electrochemical behavior is necessary to consider which equivalent circuits are reasonable. In solid ionic conductors like zirconia, measurements usually aim at determining the different responses of the bulk of the material and the grain boundaries of the material.

In order to have useful measurements, impedance spectroscopy measurements must be made in the linear response regime of the process in question and the response must be stable on during the period of the measurement. Typical excitement voltages are on the order of 100 mV and frequencies $10^{-2} - 10^5$ Hz [45], [46]. A bias voltage can be used to shift the

zero point of the measurement, but the full range of excitement voltages must remain in the linear response regime [45].

Because impedance spectroscopy is able to separate response of different electrochemical processes, it has the advantage that the effect of the electrodes and the charge transfer reaction can usually be characterized or eliminated from the response of the material in question. In many direct current (dc) characterization techniques the electrode effect is difficult to separate and can bias results considerably because the effect of the charge transfer reaction can be considerable [47].

In zirconia materials, impedance spectroscopy has been used to provide many of the baseline electrochemical behaviors that are used in this work. However, impedance spectroscopy cannot be used to characterize the behaviors of zirconia at the voltages in flash sintering because a) the electrical response of the material is not linear and b) the response is not stable either in time or temperature.

2.3.2 Direct Current Methods

Characterization techniques using direct current (dc) E-fields have the advantage because they involve a much simpler experimental setup than impedance spectroscopy. These techniques also have the advantage in that they are much more dynamic. Measurements do not need to be done in the linear regime of the sample and the material in question does not to have a stable response.

Dc techniques have the disadvantage in that only the total response of the circuit can be analyzed. One must also pay close attention to the experimental setup, specifically to the effect of the electrodes used.

2.3.2.1 Two-probe method

The simplest dc characterization technique is to measure the current response of a system with the application of a voltage by means of two opposing electrodes. The current response to a known power supply

voltage or the voltage response to a constant current is easily measured. An example setup is shown in Figure 2.11a.

This technique has its advantages in its simplicity, but several spurious effects can be measured in the response affecting the overall sensitivity and biasing result. First, due to the simplicity, it is more difficult to measure transient effects like capacitance. Usually only resistances are measured. The risk with 2-point measurements in electrochemical circuits is measuring extra resistances that do not pertain directly to the activities in the material of interest. The most common example is the additional measurement of the resistance of the connecting wires. At high temperatures where the electrochemical responses of ceramic materials are concerned, the resistance of these wires can become considerable and cannot be ignored. Furthermore, electrode reactions can dominate the circuit response. This is true in ionically conductive materials, especially in the high current regimes encountered during flash sintering where this reaction can dominate and mask the response of the material under investigation.

2.3.2.2 *Four-probe methods*

The simplest way to avoid the issues arising from the use of two electrodes is to use a separate pair of electrodes to measure voltages of the system at a point where wire and/or electrode effects can be eliminated. The use of two separate electrodes, here referred to as the voltage-probes, is known as a 4-point, 4-probe, or the Kelvin technique.

I-V characterization is performed by measuring the voltage response at the voltage probe to a certain current that is measured in series with the material. Currents leaked to the voltage probe usually are only nA, so they are considered negligible in most measurements, but if the circuit current is also on the order of nA or μA , this leakage must be considered. This effect must be considered at low temperatures where total currents are very low.

If there is no charge transfer reaction at the electrodes or if it has been previously determined that this reaction is negligible in the regime being characterized, the voltage-probe can be attached directly to the electrodes (Figure 2.11b). This configuration removes the resistance of the wires used to connect the circuit and is known as a pseudo 4-probe measurement. If there is a considerable charge transfer reaction, the voltage-probe must be separated from the electrodes (Figure 2.11c). Doing so, removes both the wire resistance, but also the resistance that arises from the charge transfer reaction.

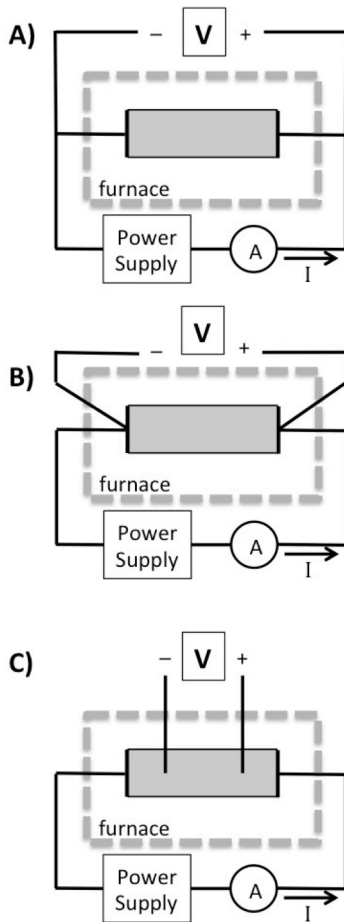


Figure 2.11: dc probe configurations. A) 2-Point measurement B) Simple 4-point measurement C) 4-point measurement

3 State of the Art

3.1 Flash Sintering

Flash sintering is a novel assisted sintering technique first discussed by Colonna *et al.* [23] for the 3 mol% yttria-stabilized zirconia system (3YSZ). These simple experiments utilized a direct current (dc) electric field, ranging from 15 to 120 V/cm, applied to a uniaxially pressed green sample, as it was free sintered. What was observed was that above a certain E-field strength, sintering began to occur at temperatures lower than expected and at rates so high that sintering to full density occurred in seconds rather than the typical isothermal treatment times of hours. This combination of lowered sintering temperatures and high sintering rates was nominated as flash sintering because of the high rates that were achieved [23].

Flash sintering distinguishes itself from other electromagnetic

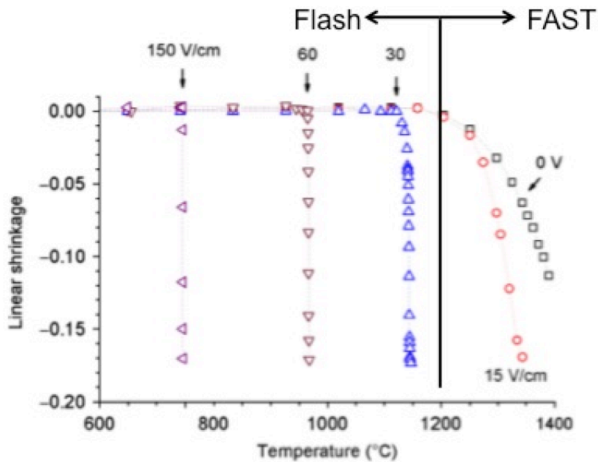


Figure 3.1: Dilatometric curves for the behaviour of 8YSZ under various dc electric fields. The division between FAST and flash sintering regimes is shown. Adapted from [51].

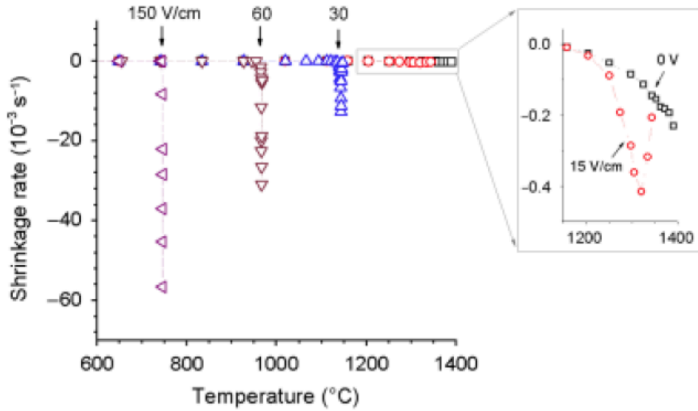


Figure 3.2 Sintering rates for flash sintering of 8YSZ. The rates corresponds to the sintering curves shown in Figure 3.1 [51].

field assisted sintering techniques first in that it is a free sintering technique. The distinction from microwave sintering makes is easy to make, because of the obvious differences between the use microwaves and a dc E-fields and currents. There are no applied external pressures like it SPS [48], though the effect of E-fields during sinterforging is being investigated [49]. Second, the sample is primarily heated by a furnace, rather than by the electric currents themselves. Third, the voltages and currents used, therefore the total energy used in flash sintering are much lower than the energies is SPS techniques [50]. Fourth, the E-fields used so far in flash sintering are static and they remain constant throughout the sintering treatment as long as power supply current limits are not met. Reaching these limits results in reduction of the E-field to maintain the maximum current. Typical SPS schedules involve the pulsing of the applied current, another reason why it is known as Pulsed Electric Current Sintering (PECS) [27].

3.1.1 Sintering Behavior:

Flash sintering was first discussed by Cologna *et al.* [23]. The flash sintering behavior is described for 3YSZ. In this work, flash sintering is carried out by applying a dc E-field to a uniaxially pressed, dog bone-shaped green body. The dog bone is suspended in a vertical furnace, where an externally mounted digital camera measures length change. The suspended sample is heated at a rate of 10 °C/min until a flash sintering event occurs or the furnace temperature reaches normal sintering temperatures. What was observed was that the sintering behavior fell into two different regimes depending on the strength of the E-field. They are called the FAST regime, (Field Assisted Sintering Technique), and the flash sintering regime. Between the two regimes, there is a critical transition E-field, E_{crit} , that has been estimated to be 30 V/cm for 8YSZ [51]. The sintering behavior characteristic of the two different regimes can be seen in the dilatometric measurements shown in Figure 3.1. In the FAST regime, where the applied E-field is less than E_{crit} , sintering behaviors resembles conventional sintering (0 V/cm). Sintering starts at the same temperature, but sintering rates are higher resulting in higher sintering strains for the same temperature. This behavior is attributed to the slowing of grain growth under the influence of an E-field [36] [[30]. This behavior is similar to that of SPS and other FAST techniques, which is why it has been classified as a FAST sintering technique[29], [30].

When the applied E-field exceeds E_{crit} , sintering behavior changes dramatically. Above E_{crit} the flash sintering regime begins. In this regime, sintering starts to occur at furnace temperatures lower than the temperature observed with no E-field and in the FAST regime. It is important to note that these temperatures are furnace temperatures. There can be a significant heating of the sample due to the high current passing through the sample resulting in joule heating (see section 3.1.2).

In the flash sintering regime, sintering rates also become phenomenally high. In 8YSZ maximum sintering rates in the absence of and E-field, while being heated at 10 °C /min were $\sim 0.2\% \text{ s}^{-1}$. By applying an E-field in the FAST regime, but below the critical E-field, rates are on the order of $0.5\% \text{ s}^{-1}$. In the flash regime, shrinkage rates reach more than $1\% \text{ s}^{-1}$, and as high as $6\% \text{ s}^{-1}$ for 150 V/cm [51]. For a green compact that starts with a relative green density of 50%, to reach 100% density, linear shrinkage should be 23.1% if uniform in all three directions. With sintering rates as high as $6\% \text{ s}^{-1}$ sintering occurs in <4 seconds, at what is effectively the same furnace temperature. This is indicated by the near vertical sintering curves seen in Figure 3.1. In the FAST regime, during constant heating sintering, sintering occurs over the range of $\sim 200^\circ\text{C}$ or in 20 minutes. With no field applied sintering occurs over 250°C or 25 minutes and achieves only half the density achieved by FAST and flash sintering.

3.1.2 Electrical Behavior:

3.1.2.1 Voltage, current, and power

Up to this point, all reported flash sintering experiments use constant E-fields applied while a dog bone sample is being heated at a constant rate of $10^\circ\text{C}/\text{min}$. The relation between the applied E-field, the current, and even more so, the power dissipation in the sample have become the focus of the search for mechanisms.

The E-field, E , is calculated as the voltage applied divided by the distance between two electrodes used to apply that voltage. Current is measured, but more importantly, the current density, J , is the normalization of the current per unit area of the sample cross-section perpendicular to the current flow. In the case of dog bone shaped samples, the length to determine E-field is the distance between the holes where the electrodes are from which the sample is suspended, and the area to normalize current density is the cross-sectional area of the dog bone's gauge section. These values are considered constant throughout the entire experiment despite the

occurrence of sintering that will change both the length and cross-sectional area of the dog bone.

With these two values, E and J , the power dissipation of the sample can simply be determined by $p = EJ$. Here, p is the volumetric power dissipation in mW mm^{-3} , E in V mm^{-1} , and J the current density in mA mm^{-2} . The power dissipation can also be determined by finding the total power dissipation, $P = IV$, and dividing it by the effective dog bone gauge section volume.

What characterizes flash sintering is the sudden increase in current at the onset temperature. For reasons that are still unidentified, there is a loss of resistance in the material resulting in a runaway increase in current. Because these experiments are run at constant voltage, the onset of current runaway causes power dissipation to also run away. Interestingly, the onset of this runaway is the sample point at flash sintering occurs (Figure 3.3)

A real power supply cannot supply an infinite amount of current. Normally, the power supply is run at constant voltage (constant E-field) and the total circuit resistance determines the amount of current. If that current reaches a limiting level, a setting on the power supply, the power supply will cut voltage to maintain that current limit. These two conditions result in two different modes of power dissipation [52]. If the power supply is in the constant voltage regime, power is determined by:

$$(3.1) \quad P = \frac{V^2}{R_{Total}}$$

Where P is the power in watts, V the voltage drop across the sample in volts, and R_{Total} the total resistance of the sample ($R_{Total} = R_{Grain\ Boundary} + R_{Bulk}$) in ohms.

When the power supply switched to current control, the equation for power becomes:

(3.2)

$$P = I^2 R_{Total}$$

where I , is the current in amps.

When the power supply is in voltage control, and flash sintering begins, the sample resistance decreases causing current and power to increase according to equation (3.1). When the power reaches the current limit, and the power supply switches to current control, the low resistance begins to cause power to decrease. This switch from voltage to current control creates a power spike in the sample as seen in Figure 3.3.

Power dissipation appears to be the determining factor for the initiation of flash sintering. The power dissipation behaviors in both 3YSZ and 8YSZ are shown in Figure 3.4 [51]. There is a critical power dissipation value of 10 mW/mm^3 that must be exceeded to initiate flash sintering. For low field strengths, 20 and 40 V/cm for 3YSZ and 15 V/cm for 8YSZ, the

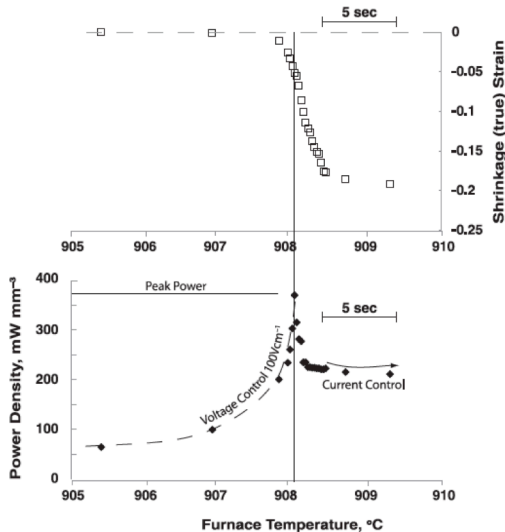


Figure 3.3: Power dissipation and sintering relationships. [52]

power dissipation was not reached consequently, only FAST sintering was observed. When the E-field is sufficiently high and the critical power dissipation is reached before reaching conventional sintering temperatures, flash sintering is initiated. Much like the vertical dilatometric curves, flash sintering is indicated by the near vertical power dissipations.

8YSZ is more conductive than 3YSZ at a given temperature. As a result, for the same E-field, the 8YSZ will reach the critical power dissipation at a lower temperature than the 3YSZ resulting in lower flash sintering temperatures.

3.1.2.2 Joule Heating

If the power dissipation cannot be dissipated by heat transfer processes, there will be a net heating of the sample. Because the heating of the sample results from the resistive heating due to current, it is known as joule heating. In non-linear regimes, the power dissipation can become appreciable, resulting in a significant heating of the sample above furnace

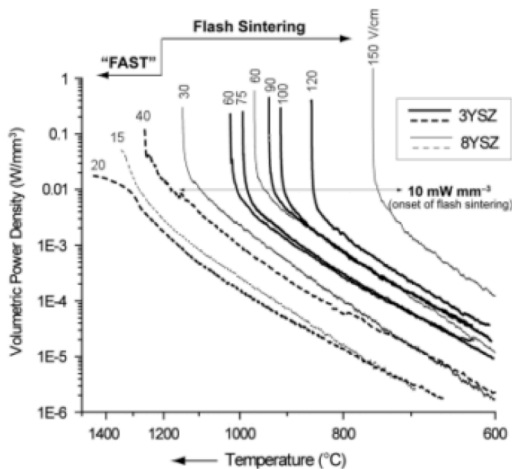


Figure 3.4: Volumetric power dissipation in 3YSZ and 8YSZ during flash sintering experiments[51]

temperatures. This heating can intern affect the diffusional processes

The actual behavior, shown in Figure 3.5, shows that sample heats several hundreds of degrees above the furnace temperature. This temperature rise occurs during the current runaway, and continues to rise even after the power supply switches to current control eventually reaching a stable temperature.

If a sample being flash sinter is assumed to behave as a black body with the power dissipation occurring uniformly in the body, the change in temperature is given by:

$$(3.3) \quad \frac{\Delta T}{T_f} = \frac{P}{4A\sigma T_f^4}$$

where ΔT is the temperature change above the furnace temperature T_f , due to the power P , in a sample with a surface area A , and σ is the Stefan-Boltzmann constant [23], [30].

Comparison of pyrometric results has shown that the estimated temperature change by black body radiation is much lower than what is actually measured. In 3YSZ, the powers measured gave estimates of ΔT of only a few degrees, not the hundreds of degrees that are observed [23].

A more rigorous estimation of heating was done considering that grain boundaries in YSZ have a blocking property, as a result of their higher resistance [36], [53]. This would mean that power dissipation would preferentially occur at grain boundaries.

To estimate the temperatures reached by grain boundaries, the densification rates were compared using equation (2.10). Considering two densification rates, taken at the same density, one arrives at the equation:

$$(3.4) \quad \ln\left(\frac{\dot{\rho}_E}{\dot{\rho}_0}\right) = \frac{Q_B}{R} \left(\frac{1}{T_E} - \frac{1}{T_0}\right)$$

here $\dot{\rho}_E$ is the densification rate for E-field assisted sintering at density ρ , $\dot{\rho}_0$ is the densification rate in the absence of and E-field at density ρ , Q_B is the activation energy of self diffusion, R the gas constant, T_0 the furnace temperature measured when the sample, in the absence of and E-field, is at a constant density ρ , and T_E the estimated temperature [23].

This estimation of temperature change gives a much better estimate of gives a much better estimate of the temperature measured by pyrometric, but tends to over estimate the temperatures. This would be the result of the change of temperature being calculated for the grain boundary

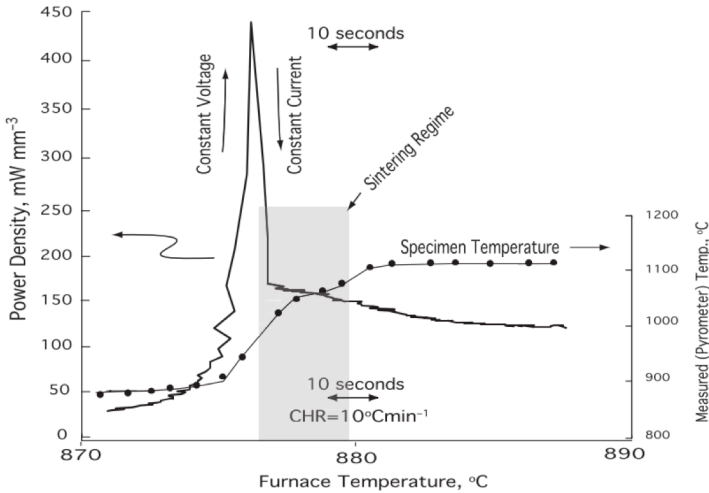


Figure 3.5: Heating behaviour of during flash sinter-forging [52]

that would then heat the sample by conductive heat transfer.

3.1.2.3 Sintering Rates

Using equation (3.4), the sample temperatures required to achieve the same short sintering times observed during flash sintering can be estimated. In Ref. [52], T_o , was assumed to be 1450°C, a typical unassisted sintering temperature. The ratio of rates was assumed to be ~ 1000 , the ratio between unassisted sintering times of 1 hour (1 hour = 3600 seconds), and the observed flash sintering time of 3.6 seconds. Assuming that the activation energy of self diffusion in 3YSZ is 500 kJ/mol [54], a temperature of 1900°C would be required to achieve the same sintering rates measured in flash sintering of 3YSZ. This calculation is shown graphically in Figure 3.6.

This temperature is hundreds of degrees higher than those observed by pyrometric measurements of flash sintering. This calculation shows that the observed sintering rates are not solely a result of joule heating

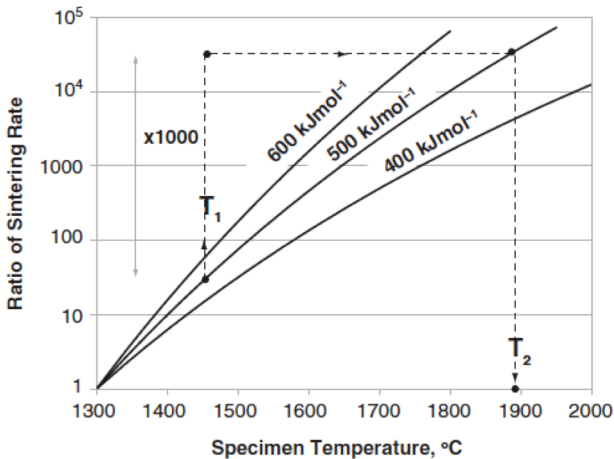


Figure 3.6: Temperatures required to achieve observed sintering rates in 3YSZ [52].

in the sample. There is joule heating, but the effect of the E-field and current play a very important, but still unexplained, role in the flash sintering behavior of a material.

3.1.3 Flash Sintering in Different Materials:

In the short time since the first report of flash sintering, the behavior has been demonstrated in several different classes of materials based on their mode of carrying current. These results demonstrate the huge potential that this technique has for the entire ceramics field.

3.1.3.1 Ionic Conductors

The first class of materials that was demonstrated to have flash sintering behaviors was the ionic conductors. So far, all materials have been oxygen ion conductors. The first material ever flash sinter was 3 mol% yttria-stabilized zirconia (3YSZ) [23] this was followed shortly by 8 mol% yttria-stabilized zirconia (8YSZ) [51]. Recently, flash sintering has been demonstrated in 20 mol% gadolina-doped ceria (20GDC) [55] and 10 mol% gadolina-doped ceria (20GDC) [Azzolini, A., Downs, J.A., Sglavo, V.M. *unpublished work*]. These materials all are of interest because of their use as fuel cell electrolytes. Additionally, flash sintering has been demonstrated in hydroxyapatite, a common bioceramic used as a bone filler [Naik, K., Downs, J.A., Sglavo, V.M. *unpublished work*].

In YSZ materials, the estimated E_{crit} is 30 V/cm, above that E-field, flash sintering have been attempted with fields up to 120 V/cm in the case of 3YSZ and 150 V/cm in the case of 8YSZ. With these E-fields these materials have been sintered at furnace temperatures as low as 850°C and 750°C respectively.

3.1.3.2 Insulators

Flash sintering has also been attempted on pure alumina (Al_2O_3) [56]. For pure samples, E-field reached 1000 V/cm only minimal FAST

sintering behavior was observed. However, with the addition of 0.25 wt% MgO, a common alumina sintering aid, flash sintering behavior was observed for fields of 500 and 1000 V/cm. Flash sintering did not occur with a field of 250 V/cm implying and E_{crit} between 250 V/cm and 500 V/cm.

Interestingly, the flash sintering started at a point where the dog bone was already partially sintered. Both fields showed an initial phase of FAST sintering then, the onset of flash sintering behavior. Additionally, the critical power dissipation for the onset of flash sintering was similar to the much more conductive zirconia.

3.1.3.3 *Electronic Conductors*

Early publications on flash sintering focused on materials commonly used as fuel cell electrolytes, resulting in other work investigating the flash sintering behavior of other fuel cell components. Flash sintering has been reported in electronically conducting cobalt manganese oxide (Co_2MnO_4). This material is used as a coating on fuel cell interconnects to prevent migration of chromium for stainless steel interconnects to the electrolyte where the chromium acts to poison the electrolyte reaction.

Because Co_2MnO_4 is electronically conductive, the conductivity is much higher than in either ionic or insulative materials. The effect of the high conductivity results in the requirement of low voltages (<12.5 V/cm) and high currents (13 A) to achieve high densities by flash sintering rather than the 100 V/cm-1000 V/cm required in YSZ or alumina.

The sintering behavior is shown in Figure [57]. There is an apparent transition between FAST behavior and flash behavior that occurs with an E-field of 5 V/cm. Flash sintering begins, but does not proceed to high densities, instead, there is a transition to more FAST like sintering behavior. It is also interesting to note that the critical power density for the onset of flash sintering remains the same as that observed in 3YSZ, 8YSZ, and alumina

3.1.3.4 *Semi-Conductors*

Flash sintering has been reported in the perovskite strontium titanate (SrTiO_3) [58]. Typically, conductivity arises in SrTiO_3 as a result from deviations from stoichiometry by the addition of dopants, much like in yttria-stabilized zirconia [59]. In the pure material, where deviation from stoichiometry is minimized, the conductivities observed indicate that there is a deviation from stoichiometry.

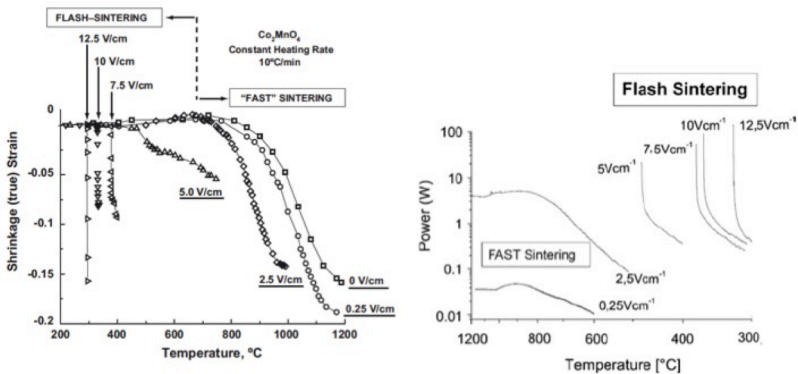


Figure 3.7 Dilatometric and power dissipation behaviour of flash sintered Co_2MnO_4 [57].

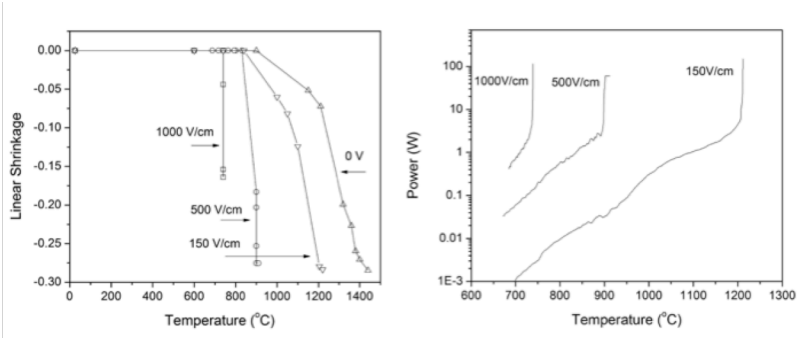


Figure 3.8: Dilatometric and power dissipation behaviour of flash sintered SrTiO₃ [58]

3.1.4 Effect of Particle size

In unassisted free sintering, the particle changes sintering behavior dramatically as a result of shorter diffusion distances, and a smaller pore volume that needs to be filled (less mass movement). In flash sintering, this densification behavior is also manifested. Interestingly, for the same E-field, reducing the particle size also decreases the flash sintering temperature [60].

The effect of particle on flash sintering of 3YSZ is shown in Figure 3.9. First, in the absence of an E-field, sintering rates and the degree of densification increase with decreasing particle size. This has to do directly with the change in particle size. With the application of an E-field of 100 V/cm, two observations can be made from the dilatometric data. First, for a smaller particle size, the temperature of flash sintering is lower than that for large particle sizes. There is a difference of furnace temperature of 120°C between the 1 μm sample (D50 = 0.33 μm) and the 10 μm sample (D50 = 3.08 μm). Second, for smaller particle sizes, the final densification is higher, only the smallest particle size was reported to reach a density of 96%. Similarly, the strain rate of sintering for the 1 μm sample is more than 4.8% s⁻¹, while the 10 μm sample is only 1.7% s⁻¹. This is attributed to the shorter

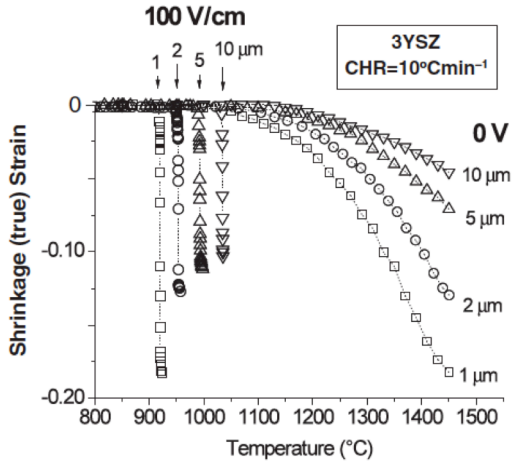


Figure 3.9: Effect of particle size on the flash sintering behaviour of 3YSZ. [60]

diffusion distances for smaller particles, much as the case in unassisted sintering.

3.1.5 Microstructure

Microstructural results for flash sintered ceramics are extremely

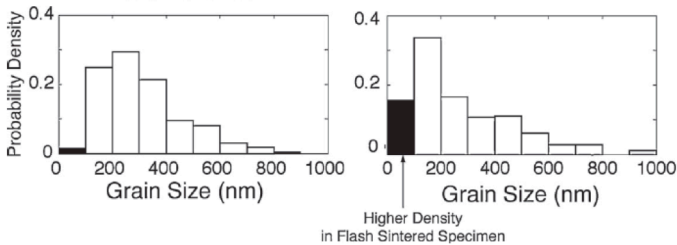


Figure 3.10 Grain size distribution of conventionally sintered 3YSZ (left) and 3YSZ flash sintered with 100 V/cm (right) [60]

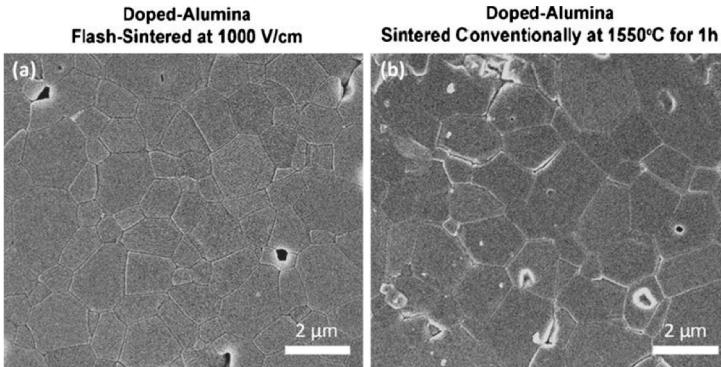


Figure 3.11: Microstructure of MgO-doped alumina flash sintered with 1000 V/cm (left) and conventionally sintered (right) [56].

variable. This likely has to do with the uncontrolled nature of the flash sintering. There is wide variation with respect to different E-fields and when flash sintered samples are compared to conventionally sintered materials.

In 3YSZ, flash sintering with 100 V/cm results in a slightly refined microstructure. The grain size distribution in the flash sintered material shows a much larger proportion of grains less than 100 nm, and reflect closely the initial particle size distribution of the starting powder (Figure 3.) [60]. This would indicate that in flash sintering, there is a reduction of grain growth as has been observed in dense samples annealed with E-fields [36]. The joule heating at the grain boundaries is believed to thermodynamically pin the boundary, minimizing coarsening in a similar mode observed in the annealing of fully dense 3YSZ [36].

In alumina, there is again an observable influence of the E-field on grain growth and the final microstructure (Figure 3.11) [56]. When flash sintered with an E-field of 1000 V/cm, the sample reach full density with an average grain size, $G = 0.8 \mu\text{m}$, while the conventionally sintered specimen had an average grain size $G = 1.9 \mu\text{m}$. Much like in alumina, there was microstructural refinement, but in alumina, there was still a considerable

amount of grain growth when compared to the starting powder's particle size of 100-300 nm.

In the highly conductive Co_2MnO_4 , very similar microstructures and grain sizes are achieved for conventionally sintered, FAST sintered, and flash sintered specimens despite the sintering temperatures being 1180°C, 1177°C, and 336°C respectively. In flash sintered samples, there was a higher elimination of the interconnected porosity [57].

3.1.6 Proposed Mechanisms:

In order to further exploit flash sintering behaviors, it is critical to know the mechanisms that are causing this behavior. To be rigorous, the mechanism must account for a change in conductivity, which is controlled by the fastest moving charge carrying species, and sintering, which is controlled by the slowest moving species. The hypothesis that has been proposed several times for the cause of flash sintering is the nucleation of Frenkel defects [23], [49], [52], [56], [60], [61]. Because the sample is conducting, the movement of oxygen is not an issue. This means that these defects must be primarily zirconium ions that are forced into interstitial sites resulting in $\text{Zr}_i^{\bullet\bullet\bullet}$.

Normally these defects, in this case $\text{Zr}_i^{\bullet\bullet\bullet}$ and $V_{\text{Zr}}^{\bullet\bullet\bullet}$, are electrostatically bound to each other and cannot move on length scales needed for sintering. In the presence of the E-fields used for flash sintering, defects can decouple. Once defects are decoupled, they would be able to move in the E-field. Their movement results in the sintering effect, and because they are charged, their movement would result in an increase in current thus satisfying the two requirements.

3.2 *Similar Assisted Sintering Techniques*

3.2.1 **Flash-sinterforging**

Flash sintering is a free sintering technique; there are no externally applied pressures. The idea of applying an E-field has also been applied to the already existing sinterforging technique. Sinter forging is a pressure assisted sintering technique that, utilizes the application of an external pressure the long axis of a cylindrical sample that is not restricted to in the radial direction. The applied pressure changes diffusion rates because it nucleates extra defects that increase diffusion gradients and increase the effective internal sintering pressure. In flash sinter forging, and E-field is applied through the long axis of the sample, during the sinter forging. Results have been reported for 3YSZ [49].

For flash-sinterforging, in condition where the applied pressure is held constant at 5 MPa and the applied E-field is varied, the sintering behavior is nearly equal to free flash sintering. Increasing the E-field, lowers the onset temperature, and results in sintering rates that, again, allow for sintering in seconds. Compared conventional sinterforging, the application of the E-field appears to cause a softening of the material. In the absence of the field, volumetric strains reach <20%. With the E-field, volumetric strains easily reach 60%, where the experiment was stopped.

When the E-field is fixed at 100 V/cm and the applied pressure is changed, increasing pressure decreases the onset temperature. In free flash sintering the onset temperature was slightly higher than 900°C. With an applied pressure, of 1.5 MPa results in approximately the same results: 916°C. Increasing pressure, decreases onset temperature, with 12 MPa, the onset temperature was lowered to 850°C. Increasing the applied pressure also increases the maximum sintering rates from 4% s⁻¹ for 1.5 MPa and up to 9% s⁻¹ for pressures above 7.5 MPa.

3.2.2 Grain Welding:

Grain welding is a corollary technique to flash sintering, that utilizes alternating current (ac) E-fields with a tuned frequencies rather than the dc E-fields used in flash sintering. This techniques takes advantage of the fact that grain boundaries and the material bulk conduct differently depending on the frequency of the ac E-field applied. The frequency used for sinter welding is chosen so that the majority of the conductivity takes place at the grain boundary causing grain joule heating and a similar flash sintering effect.

A typical experiment is done by heating an isostatically pressed cylinder to a constant temperature 800°C – 1000°C. The compact is subject to bursts of the ac field, with a frequency of 1000 Hz in the case of zirconia, with a certain voltage[62], [63]. The voltage is maintained, for a certain amount of time, typically less than 30 seconds, or until a current limit is reached.

This technique has the advantage that it is highly controllable. Depending on the voltage or current limit, the extent of sintering can be highly controlled an sintering can be done in several steps by bursts or current [64]. If the duration of the application is long enough and the current high enough, temperatures can even be high enough to melt the material [63].

There is also the advantage that very fine microstructures can be maintained. Unlike in flash sintering, which shows a range of microstructural results after flash sintering, grain welding can consistently give results with very fine microstructure. A typical result for the grain welding of 8YSZ with an E-field of 120 V/cm at 1000 Hz for 5 seconds at 800°C is compared to a conventionally sintered sample at 1300°C is shown in Figure 3.12.

Much like in flash sintering, there is joule heating in the sample, but the overall heating does not explain the overall results. Similar mechanisms to those active in flash sintering should be activated by this method of electric field assisted sintering [63].

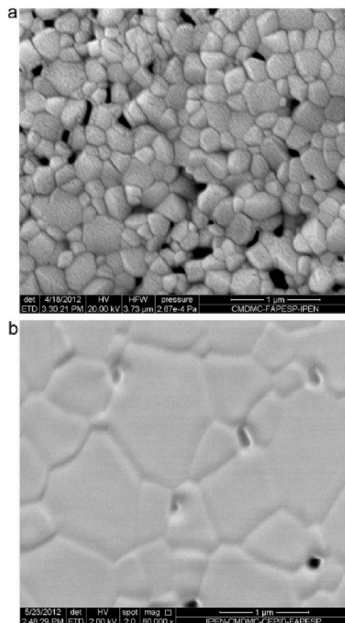


Figure 3.12: Microstructure of a) grain welded (120 V/cm, 1000 Hz, 800°C, 5 seconds) and b) conventionally sintered 8YSZ (1300°C) [63]

4 Materials, Equipment, and Characterization

4.1 Materials

4.1.1 Zirconia Powder

All polycrystalline experiments, for those done on flash sintering from a green state and for those done with presintered specimens, utilized a commercially available 8 mol% yttria-stabilized zirconia (8YSZ) (TZ-8Y Lot: Z805550P Tosoh, Corp., Shunan, Japan) powder. Analyses supplied with the powder show nominal crystallite size of 250 Å and specific surface area of 13.1 m²/g with the minor chemical components shown in Table 4-1. This powder is very low in SiO₂ a common contaminant that can dramatically change electrical properties because of its segregation to grain boundaries restricting the paths for oxygen vacancy conduction, thus changing the electrical properties of sintered samples [65]. An SEM image of the powder as provided is shown in Figure 4.1. The granulated powder shows a spherical morphology with granules ranging from ~10 μm to ~100 μm. The surface of a single granule shows that the surface is not perfectly smooth, and that the individual crystallites are ~200 Å.

Table 4-1: Chemical analysis of Tosoh 8YSZ powder used. Crystallite size 250 Å and surface area 13.1 m²/g Lot: Z805550P.

Component	Y ₂ O ₃	Al ₂ O ₃	SiO ₂	Fe ₂ O ₃	Na ₂ O
Weight	13.23	<0.005	<0.002	0.003	0.071
Percent					

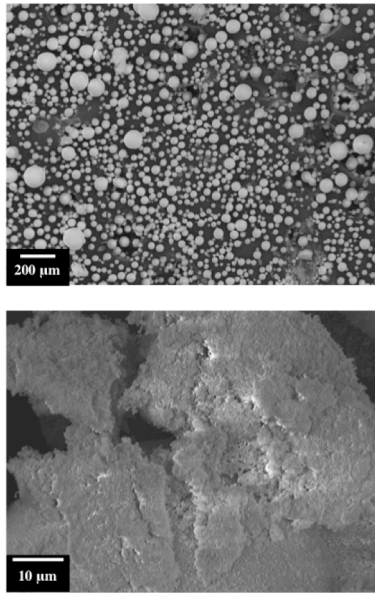


Figure 4.1: 8YSZ Powder Used. A) Granulated powder as provided, B) Surface of an individual granule showing individual crystallites.

4.1.2 Single Crystals

Single crystal samples were cut from a bulk piece of yttria-stabilized zirconia (Ceres Corp, Niagara Falls, NY, USA). Several rectangular samples were cut from the same piece in the same direction. The crystallographic direction of these pieces was not known, but all specimens have the same crystallographic direction.

4.1.3 Binders

Two different organic binders were used to increase the green strength of specimens. The amounts used were determined to minimally affect the final sintering behavior and leave minimal residues after

treatments at sintering temperatures whilst still giving them the desired handleability.

4.1.3.1 B1000

For specimens prepared by uniaxial pressing, Darvan B1000 (Rohm and Haas France SAS, BP, France) was used as a binding agent. B1000 is a commercially available acrylic binder emulsion commonly used for tape and slip casting application. It has a T_g of -26°C and relative pH of $\sim 9-10$ [66].

The binder was added to the zirconia powder on a weight percentage basis considering only the solid acrylic components of the binder emulsion. The powder was mixed with 5 wt% binder, mixed with enough double-distilled water to form a paste. The paste was mixed well for at least 5 minutes, then allowed to dry overnight at 60°C . After drying, the cake was crushed until a fine powder was achieved.

4.1.3.2 Hydroxypropyl methylcellulose

For extrusion, pastes were prepared with Hydroxypropyl methylcellulose (HPMC)(Sigma-Aldrich, Average Mn $\sim 90,000$) as the binder. This polymer is a commonly used thickener and binder for ceramic extrusion [67].

Pastes were prepared with 0.2 wt% HPMC. This amount of was used because it gave pastes high flowability, allowing for minimization of extrusion pressures, while giving the wet extrudate enough resistance so that it did not deform during drying and allowed dried samples to be handled easily without breaking.

4.1.4 Sample Preparation

4.1.4.1 Uniaxially pressed Samples

The powder prepared with the B1000 binder was uniaxially pressed with 150 MPa into either dog bone shaped samples with the shape shown in Figure 4.2 or into disks with a diameter of 25 mm. The dog bone shape is slightly modified from the shape reported in Ref [56] for other flash

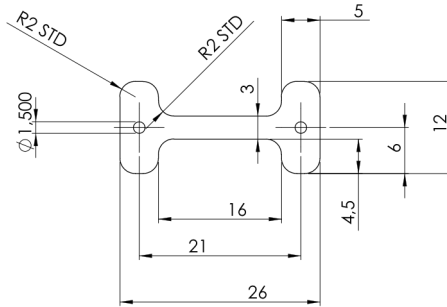


Figure 4.2: Die used to uniaxially press dog bone shaped samples. All dimensions are in mm. The effective gauge section considered for electrochemical measurements is shaded in gray.

sintering experiments. The shape of the dog bone allows for its suspension between two wire electrodes by the holes in the dog bone handles. It has no sharp corners in the transition from the handles to the gauge section, allowing for smooth transitions in current density and for current lines to be well developed and parallel as they pass through the gauge section. The concentration of current in the gauge section forces any sintering behaviors to preferably take place in the gauge section. Sharp angles are avoided to minimize any constriction points that result in anomalous effects such as spurious local heating and/or sintering.

To determine the preliminary grain growth behavior of this powder disks with a diameter of 25 mm were uniaxially pressed with 150 MPa. The disks were then treated at various temperatures to determine the densification behavior and grain growth behavior at those temperatures.

4.1.4.2 Extrusion

Cylindrical shaped samples were prepared by extrusion. Before extrusion, the ideal paste recipe was determined. An ideal paste has a solid loading, the powder: powder + liquid volume ratio, that has the correct amount of liquid phase to just fill in the spaces between powder particles. If there is too little liquid, the liquid phase forms a thin film covering the powder surfaces while the mixture remains in a powder state. If the amount of liquid phase is too high, there a liquid phase forms between particles, resulting in a suspension. For this powder, the liquid phase that consists of 0.2 wt% HPMC acting as a binder and thickener, the ideal solid loading was determined to be 39% by slowly adding the liquid phase drop by drop to the 8YSZ powder during mixing until a workable paste formed.

Using a solid loading of 39%, extrusion pastes were prepared according to the recipe in Table 4-2. First, the HPMC and zirconia powders were dry-mixed. Then double-distilled water was slowly added to the powder mixture while being agitated in a vertical mixer. After all the liquid phase was added, the mixture was allowed to mix until a uniform paste formed.

Cylindrical shaped samples were extruded in-house built ram extruder (Figure 4.4). Before the final extrusions, the paste was subject to two treatments of high shear mixing by extruding the paste through a holed disk installed in the extruder (Figure 4.3). These steps served to further homogenize the paste and break any agglomerates that remained in the paste

Table 4-2: Recipe used for extruded samples. The solid portion corresponds to a 39% solid loading.

Paste Component	Volume %	Weight %
8YSZ Powder	39	79.2
HPMC	--	0.2
Distilled H ₂ O	61	20.6

after the initial mixing. After high shear mixing, samples were extruded through a die 5 mm in diameter and 9 mm long with a ram speed of 10 mm/min, giving an extrudate speed of 212 mm/s. Extrusion took place until the extrusion force reached 2.5 kN, corresponding to the operating limit of the extruder, or until the ram travelled its full distance. The extruded cylinders were collected and dried overnight in a desiccator with silica salts, then in an oven at 110° C for at least 6 hours. Samples were cut from the dried rods. The dried samples had a relative green bulk density of 48.5% determined geometrically, and a binder content of 0.25 wt.% confirmed by TG.



Figure 4.3: Die setup used for high shear mixing of 8YSZ paste before extrusion [81]

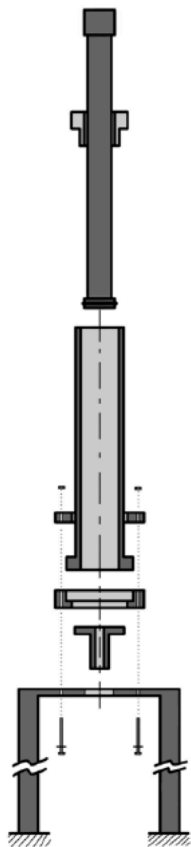


Figure 4.4: Ram extruder used for extrusion of 8YSZ cylinders [81]

4.2 4.2 Characterization Equipment

4.2.1

4.2.2 Dilatometry

The sintering behavior of the sample in the absence of and electric field for both pressed and extruded samples was obtained using a Linseis L75 dilatometer (Linseis GmbH, Bolzano, Italy). Samples were heated at 10°C/min to 1550°C. A correction curve to account for the expansion of the sample support and dilatometer push rod was determined using an alumina standard heated at the same rate and to the same temperature.

4.2.3 4.2.2 SEM

Sample microstructures were examined using a JEOL JSM-5500 Scanning electron microscopy (SEM). Samples were first metalized with a layer of gold-palladium by sputter coating for 45 seconds to ensure electrically conductive surface. Images were taken using an accelerating voltage of 10 kV.

4.2.3.1 Grain Size Measurements

To measure the average grain size in sintered samples, they were cut using a low speed saw then ground using a series of SiC paper, from 80 grit to 1200 grit. Samples were then polished using diamond paste to down to 1 μm . Polished samples were thermally etched in the same furnace that was used for sintering at temperature 50° C lower than the sintering temperature for 25 min. Samples were then metalized as described above.

Grain size measurements were done using the line intercept method counting at least 500 grains and 6 different images taken from several different positions on the polished and etched surface. Grain size was corrected by a factor of 1.57 assuming a log-normal grain size distribution and tetrakaidecahedron shaped grains [18], [68].

4.2.3.2 *Density*

Sample densities were measured before and after sintering. The green density before sintering was measured on the pressed or extruded samples geometrically. For uniaxially pressed samples, only the thickness was measured with the diameter of the pressed disks or the area of the dog bones already known. For extruded samples, the extruded diameter was measured by taking two diameter measurements orthogonal to each other. The length was measured after the ends were squared and cleaned with 800 grit SiC paper.

Sintered density was measured by the Archimedes method using the equation [69]:

$$\rho_{sint} = \frac{W_{dry}}{W_{dry} - W_{susp}}$$

The suspended weight, W_{susp} , was measured with a balance (Gibertini Analytic Balance) setup to make measurements of samples suspended in distilled water. Before measurement, samples were infiltrated with water by placing the samples under vacuum for 20 minutes dry. Then, while still under vacuum, were submerged in water. The sample were then left for 30 minutes submerged in water under vacuum to remove any remaining air that may have been left in the open porosity of the sintered material. After the submerged measurement, samples were dried overnight at 110°C, then the dry weight, W_{dry} , was measured.

4.2.3.3 *Pyrometry*

Joule heating can be significant in flash sintering, causing sample temperatures to be significantly different from furnace temperatures that were measured by thermal couple [52]. To determine the difference, certain experiments were performed using a pyrometer to measure the actual sample temperature.

Pyrometric measurements were made using an IRCON Ultimax UX-20 infrared thermometer (Square D Co., Niles, IL, USA) was used. It uses a silicon sensor and has a range from 600°C to 3000°C. Sample temperatures were recorded using the 0-1 V output of the device.

A calibration of the voltage-temperature relationship was done from 600°C to 1200°C using a sintered target prepared from the same powder used to prepare the specimens. The target temperature was measured by an S-type thermocouple that was touching the target surface. The target and thermocouple were mounted inside an alumina housing that served to reduce the effect of radiation reflected from the furnace walls and to minimize the effect of convection across the sample to get a more accurate measurement of the thermocouple.

4.2.3.4 Thermogravimetry

Thermogravimetric/ Differential Thermal Analysis (TG/DTA), was performed on the powder prepared with B1000 and the paste prepared with HPMC to determine the burnout behavior of the two binders. Analyses were performed using a Netzsch, ST 409 TG/DTA (Netzsch GmbH, Germany). Samples were heated in an alumina crucible at 10°C/min to 1500°C in static air. Pure alumina powder in an alumina crucible was used as the DTA reference.

4.3 Electrical Characterization and Flash Sintering

4.3.1.1 Power Supplies

Two different power supplies were used to perform electrical characterization, flash sintering, and to characterize flash like behavior in fully dense specimens. The first power supply (Sorensen DLM300-2, Calpower Srl, Como, Italy), nominated 'PS:DLM300', was used for measurement with E-fields that required voltages less than 300 V. This

power supply was able to provide a maximum current of up to 2 A, while in current control mode.

The second power supply (Glassman EW Series, Tektronix Srl, Milano, Italy) used was used for experiments with E-fields that required applied voltages between 300 V and 5000 V. This power supply is nominated 'PS:GM5000'. Because of the power limitations of this power supply, the maximum current limit was 120 mA when the power supply was operating in current control mode. The

Both power supplies' voltage and current limits could be controlled manually or by computer by means of voltages inputs controlled by a Data Acquisition System (DAQ), (NI USB-6009, I.R.S – National Instruments, Padova, Italy) connected to the controlling computer. Both control methods were used depending on the experiment being performed.

4.3.1.2 Voltage and Current Measurement

Voltage and current values were collected by two means. Both power supplies had a voltage and current monitor outputs. Outputs were connected to the measurement computer by means of the same DAQ that was used to control the power supply used. These values were used only to confirm that data that was collected.

High accuracy data for current and voltage was take using either a Keithley Model 2000 (Keithley Instruments Inc., Cleveland, OH) or Keithley Model 2100 digital multimeter (Keithley Instruments Inc., Cleveland, OH). Both DMMs had a 6-½ decimal place precision and were used interchangeably for current and voltage measurement, the different between the two being the mode of interfacing with the computer. The Keithley 2000 communicated via GPIB and the Keithley 2100 via USB. For voltages in excess of 1000 V, only the Voltage Monitor output from the power supply could be used as a measurement due to DMM limitations.

4.3.1.3 Electrical Characterization Configuration

4.3.1.4 Vertical Configuration

Most experiments were performed using the vertical configuration (see Figure 4.5) this is the standard configuration of flash sintering experiments in literatures. This configuration, the furnace is mounted vertically, and the sample suspended from its electrodes. The sample was monitored from below by either a video camera or by pyrometer. Measurement by both was not permitted due to space restrictions.

The current that passed through the sample was monitored by DMM connected in series on the negative side of the circuit. Voltage was monitored in three different ways depending on the experiment:

- 1 By 4-Point measurement across the current carrying electrodes, with voltage probes outside the furnace
- 2 By 4-Point measurement across two separate electrodes, with voltage probes at the electrodes
- 3 By the power supply Voltage Monitor

For flash sintering experiments, using PS:DLM300, sample voltage was taken on the current carrying electrodes, just outside of the furnace. This setup is less accurate for measuring the true voltages dealt with during measurements due to additional resistances that arise from the electrodes, which can be considerable at high temperature and high current, and the contact resistance at the electrode zirconia interface where a charge transfer reaction must take place, which can also be considerable at high currents.

Experiments used to characterize the behaviors in fully dense and single crystalline specimens used the 4-point methods. Fully dense sample permitted the handling that allowed for the application of two separate electrodes wrapped around the sample separate from the electrodes applying the voltage. The use of two separate electrodes a known distance apart allowed for a much more accurate measurement of E-fields present during flash sintering like behavior because all electrode and contact resistances can be separated from the voltage measurement taken [47]. In this configuration,

2-point values were taken as the voltages given by the power supply Voltage Monitor output.

For measurement using PS:GM5000, only the Voltage Monitor output was used for voltage measurement. The voltages provided with this power supply exceed the limitations of the DMMs so only the power supply Voltage Monitor was used. All experiments using the PS:GM5000 were done at a fixed voltage, so accurate current measurement was considered more important.

For all configurations, the furnace temperature was measured using an S-type thermocouple connected to the measurement computer by a NI TC-01 (I.R.S – National Instruments, Padova, Italy). The TC-01 had a built in cold junction correction. The thermocouple was mounted within 2 mm of the center of the samples in order to measure furnace temperature near the sample.

4.3.1.5 Dilatometric Configuration

A second method for flash sintering and I-V characterization specifically for extruded sample used a modified dilatometer (402E, NETZSCH-Gerätebau GmbH, Germany), to hold and measure sample length changes, see Figure 4.5. The use of the dilatometer permits much more accurate measurement of length changes than measurement by camera. The measurements by camera are limited by the quality of the image, the frequency the images are taken at, and the tendency of the sample to shift and rotate during sintering changing the calibration of the measurement scale. With the dilatometer, samples are held in place with the push rod, giving a physical measurement, and measurement with sampling frequencies up to 5 Hz, rather than the ~ 1 Hz permitted by the camera.

The pressure applied by the push rod was <10 Pa. This value is much lower than the pressures used in pressure assisted sintering methods,

which are on the order of MPa. The push rod was considered to have negligible effect on the sintering behavior of the specimens.

Electrical characterization in the dilatometric setup was done only by the 2-point method. Two platinum disk shaped electrodes were placed at either end of the sample that was then mounted in the dilatometer. Sample voltages were measured just outside the furnace between the current carrying electrodes. Only the PS:DLM300 was used with this configuration. The use of the extruded samples allowed for a much wider range of E-fields and currents by modification only of the sample length.

Like in the vertical configuration, an S-type thermocouple mounted within 2 mm of the sample was used to measure the furnace temperature at the sample.

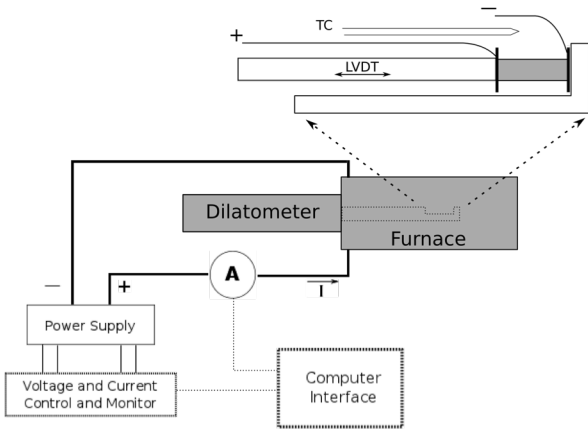
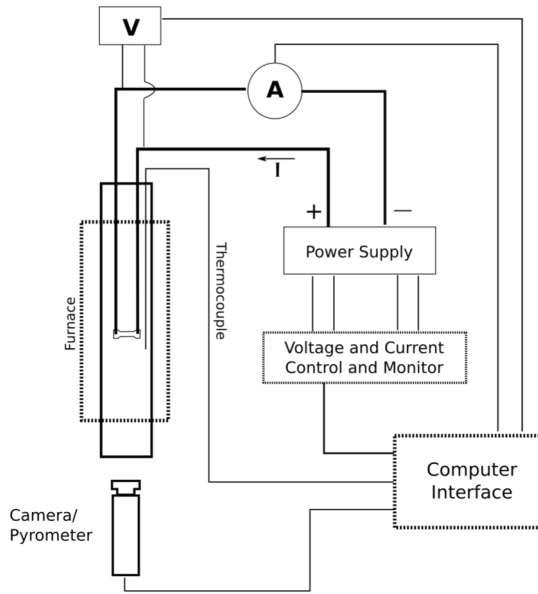


Figure 4.5: Experimental Setup for vertical configuration (above) and dilatometric configuration (below)

5 Results and Discussion

5.1 *Unassisted Sintering Behavior*

Several base line measurements and characterizations were made to understand the conventional sintering behavior of this 8YSZ prepared by the methods that will be utilized to measure the flash sintering behavior. From these, the differences that arise during flash sintering and flash sintering electric treatments will be clear.

5.1.1 **Binder Burnout**

The first step of a sintering process is the elimination of any binders present in the sample. Two different binders were used for sample preparation: Darvan B1000, an acrylic binder, and HPMC, a cellulosic binder. The complete elimination of these binders is important because residues left after burnout can affect the overall electrical behavior of the

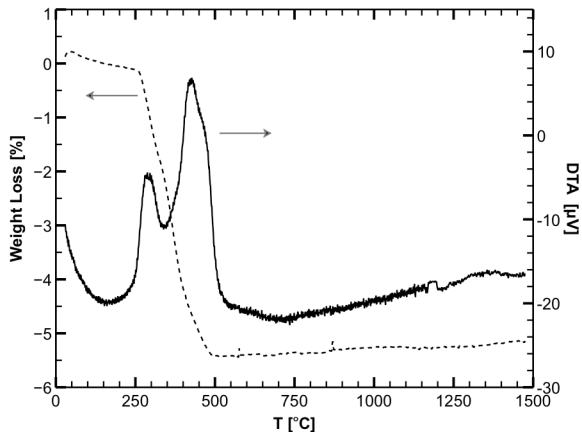


Figure 5.1: TG/DTA 8YSZ powder used for uniaxial pressing prepared with 5 wt% B1000 as a binder

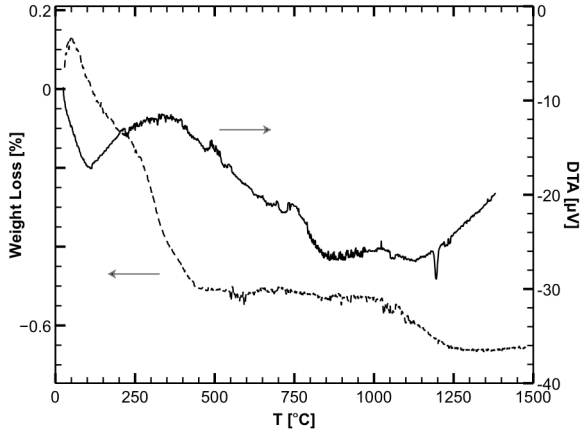


Figure 5.2: TG/DTA of extruded sample with 2 wt% HPMC as a binder

samples at higher temperatures. The binder burnout can also coincide with flash sintering where the heating that accompanies current runaway can cause sudden burnout and failure of the sample due to the expansion of the burnout gases. TG/DTA allows for the observation of the burnout behavior as well as the behavior of the zirconia powder at higher temperatures to see if there are any other weight losses of reactions during heating. The powder with B1000 added, was measured in its powdered state and the powder with HPMC was measured as a dried piece of the extruded paste.

Results from TG/DTA analysis show that binder burnout for both binders occur in the same range, 250 – 500 °C. The actual fraction of binder added was 5.5 wt% for the powder prepared with the B1000 (Figure 5.1) and 0.5 wt% for the paste used for extrusion prepared with HPMC (Figure 5.2).

For B1000, the flatness of the TG and DTA at high temperature indicates that there are no carbon residues left from the binder burnout that could effect conductivity values less than 900°C.

For HPMC, the TG results, show that there is a very slight weight loss at high temperature, between 1000°C and 1250°C. This is the

temperature range where any carbon left from burning of the HPMC would decompose. The amount of weight change due to this decomposition is <0.2 wt%. Because the high temperature weight change is so small, it has not been considered significant to results. Only the low temperature burn off of the HPMC is considered for flash sintering experiments.

The stability of the DTA curves after burnout for both of the binders indicate that there are no phase transformation or other reaction up to 1550°C.

5.1.2 Constant Heating Sintering

Flash sintering experiments were run at constant heating rates of 10°C/min. The conventional sintering behavior at this heating rate was determined by dilatometry and was assumed to represent the sintering behavior of the samples suspended in the hot zone of the furnaces used for flash sintering.

Nominal sintering behavior for samples prepared by uniaxial pressing with and without 5 wt% B1000 binder and extruded with 0.2 wt% HPMC are shown in Figure 5.3. The presence of either binder shifts the start of sintering to higher temperatures by the same amount. This shift has likely occurred because of the space that was previously occupied by the binder before burnout, the extra space results in longer times to form necks between particles at the initial stage of sintering. The burnout of B1000 is also accompanied by a reconsolidation of the powder, seen as the step down from 200°C – 300°C. However, this reconsolidation still does not provide a high enough contact between particles to account for the voids left by the binder after burnout.

Considering the reconsolidation in the sample prepared with B1000, all samples show similar sintering profile with a final strain of 22% at 1550°C.

5.1.3 Densification and Grain Growth

Grain growth experiments were performed in three different furnaces. Different furnaces have different sintering behaviors because of variations in temperature distributions resulting in differences in what the measured furnace temperature and the real temperature at the sample being sintered or annealed. Grain growth is a diffusional process so slight variations of temperature can significantly change the resulting microstructure. Before grain growth experiments, samples were sintered at different temperatures to determine the minimum temperature for each furnace to ensure a sintered density of >98%. Above these temperatures, different sintering temperatures and times were investigated to observe the effect on the final grain size of the dense samples. Treatments and results are shown partially in Figure 5.4, and all treatments are shown in Appendix 2.

Based on these results, 4 different treatments were used to determine the behaviors in fully dense samples of different grain sizes. The treatments

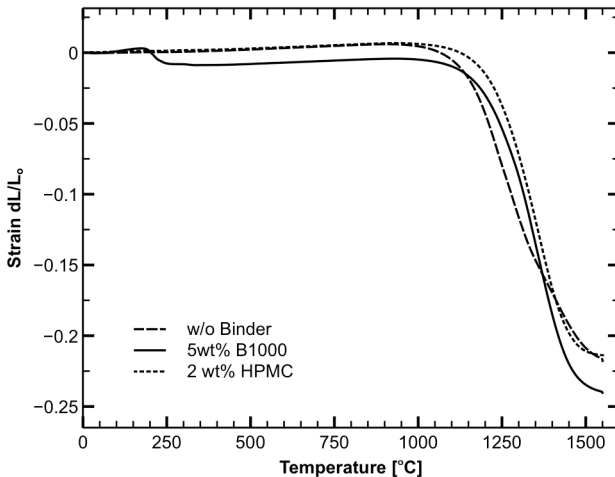


Figure 5.3: Dilatometric behaviour of 8YSZ prepared with 5 wt% B1000, 0.2 wt% HPMC binders and without binder. Heating at 10°C/min to 1550°C

were sintering at 1400°C for two hours, 1600°C for two hours, 1550 for 12 hours, or 1600 for 17 hours giving average grain sizes, G , of 0.60 μm , 3.76 μm , 5.30 μm , and 11.47 μm respectively.

5.1.4 Conductivity

Conductivity measurements were taken on two sintered samples. The first was sintered at a low temperature of 1300°C for 2 hours and the second at a high temperature of 1575°C for 2 hours representing the lower and upper average grain sizes.

Bar shaped samples cut from presintered 25 mm uniaxially pressed disks. Silver paste was baked onto the ends of the long side of the bar at 900°C for 1 hour. The bars were then heated at 2°C/min from 450°C to 850°C with 1 volt applied while measuring the resulting current. Normal measurements would take fewer points with longer times spent at

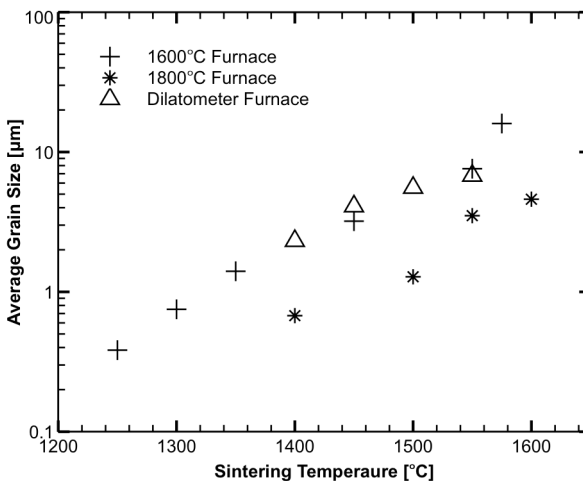


Figure 5.4: Grain growth behaviour as a function of sintering temperature and furnace. Samples were sintered at sintering temperature for 2 hours and free cooled

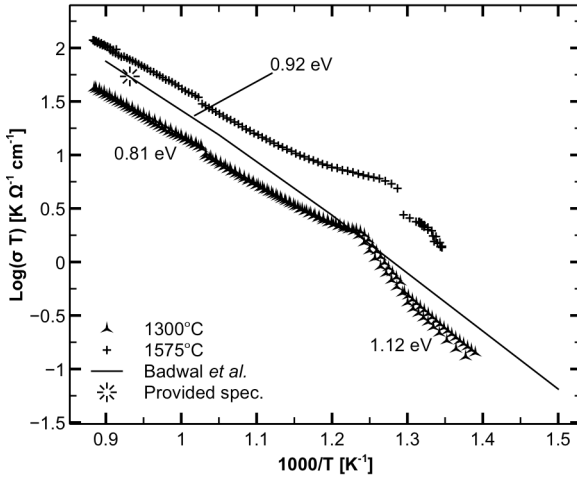


Figure 5.5: Conductivity measurements of samples sintered at 1300C and 1575C compared to literature values found by dc measurements [70].

temperature each temperature in order to ensure that the sample is in equilibrium. The lack of this is the reason for the deviation at $1000/T = 1.25$ (800°C). There would be a polarization process at this temperature that is being excited by the heating-current combination. At the other temperatures this excitement is not present. At low temperature, the activation energy is 1.12 eV and at the upper end of the temperature range is 0.81. The results from Badwal *et al.* [70] divide the two results, and has a slightly higher activation energy at high temperatures, but a similar energy at low temperatures.

The two samples have similar behaviors with respect to activation energy, but the sample sintered at 1300°C has slower conductivity values as a result of the larger fraction of grain boundary. Grain boundaries in zirconia are blocking and more resistive than the bulk of the crystal.

5.2 *High Voltage Flash Sintering*

5.2.1 Introduction

Despite flash sintering being demonstrated in several different materials, results reported up to this point have focused solely on proving that flash sintering occurs in the material, not pushing the limits of the phenomenon. Finding flash sintering behavior is also done by trial and error. Arbitrary fields are applied to a material and their effect sintering behavior is observed. Little work has been done on determining the relation between the applied E-field and the resulting sintering behavior. The determination of E_{crit} , the FAST-flash transition, is only inferred by the observation of the different sintering behaviors.

So far, no work has been shown on what happens when the E-field is increased too much higher values. Reported flash sintering results for 8YSZ have been limited to field strengths of 150 V/cm [51]. The reason for this limitation was the sample geometry and power supply combination. For a field of 150 V/cm, sintering was found to occur at $\sim 750^\circ\text{C}$ and in only a few seconds. Based on the observed flash sintering behavior in this work, E_{crit} was estimated to be ~ 30 V/cm. The relation between E-field and sintering temperature, T_{Onset} , reported suggests an inverse linear relationship i.e. increasing fields lower the onset temperature of flash sintering.

Here, E-fields were increased beyond the previously reported value of 150 V/cm to 2250 V/cm. For the first time, a relation between E and T_{Onset} is shown. In addition, the effects the power dissipation and the current density on densification are also discussed. Based on the conventional sintering behavior and the relationship between E and T_{Onset} , E_{crit} has been determined rather inferred.

5.2.2 Experimental

Dog bones with various thicknesses were prepared by uniaxially pressing with 148 MPa. Various thicknesses were prepared to investigate the effect of varying current density on the sintering behavior of the samples, but the primary samples had a thickness of 2.25 ± 0.05 mm and a relative green density of 49.8%. These samples were suspended in a vertical furnace (Nabertherm RT 50), the desired field was applied, and the samples were heated at 10 K/min until a sintering event occurred.

Two different power supplies were used to apply the range of E-fields used. For fields less than 150 V/cm, the power supply PS:DLM300 used was the same as that used in the results reported in Cologna *et al.* [51]. The current limit setting of the power supply was set at 655 mA. The results with this power supply were used to compare this experimental setup-up and powder preparation to those already reported, and to have point lower in the E-field spectrum, but above the previously estimated E_{crit} of 30 V/cm. The power supply PS:GM5000 was used E-fields of up to 2250 V/cm using these dog bone samples. The current limit for this supply was 120 mA, which was the maximum for the supply.

As a result of the observed flash sintering behavior, samples sintered with E-fields higher than 1500 V/cm were subject to a heat treatment in the absence of the E-field at 500°C in order to burnout any binder in the powder. The sample was then allowed to cool to ambient temperature, the E-field was applied and the sample was subject to the treatment described above.

5.2.3 Results and Discussion

5.2.3.1 Sintering behavior

The sintering behavior fell into two different categories. First, for the dog bone sample sintered with the low E-field ($E < 150$ V/cm, PS:DLM300), high current set-up, sintering proceeded to high densities and

Table 5-1: Sintering Results for flash sintering with E-field up to 2250 V/cm.

Applied Field, E	Current Limit	Onset Temperature, T_{Onset}	Linear Shrinkage	Relative Density	Maximum Power Dissipation
[V/cm]		[°C]	[%]	[%]	[mW/mm ³]
60	655	960	-28.1	86.6	257.7
140	655	768	-24.7	60.4	113.6
350	120	629	-11.8	48.8	827.1
950	120	508	-10.0	51.4	105.9
1425	120	467	-9.7	49.5	374.8
2250	120	378	-8.5	49.0	5285

large shrinkages. Second, for samples sintered in the high E-field ($E > 150$ V/cm, PS:GM5000), low current set-up, final densities were only slightly higher than the starting green density. The sintering results for different E-field are shown in Table 5-1.

The two samples sintered with PS:DLM300 were repeated to test the results of this set-up and 8YSZ with the results reported in Ref. [51]. For both 60 V/cm and 140 V/cm, T_{Onset} was in agreement with the reported data, meaning the set-up and powder were comparable. These two samples also showed the highest final densities and linear shrinkage, with the highest occurring at the lowest E-field.

Moving to high E-fields and changing the power supply to the PS:GM5000, the final densities hardly changed from the green value. Relative density, ~50%, were the same for all samples sintered with this power supply. Observations showed sintering did occur because of the linear shrinkage, and increased handleability and mechanical strength after sintering. The low level of density with the increased mechanical strength means that sintering remained in the starting stages of neck formation.

Finally, T_{Onset} continues to decrease with increasing E-field. With 2250 V/cm, sintering occurred at 378°C.

5.2.3.2 *Power Dissipation*

Because of the low levels of sintering strain and shrinkage, sintering was difficult to measure using the image analysis method described in Ref: [23]. For this reason, the power dissipation results were used to determine the onset of flash sintering. In previously reported works, ([23], [51], [55], [57], [58], [60]), flash sintering occurred at the point of current and power runaway. Because these experiments are run at constant E-field, and all normalization is done with the initial dimensions, the point of current runaway also corresponds to the point of volumetric power dissipation runaway by $p = E \cdot J$, where p is the volumetric power dissipation, E the applied E-field, and J the current density. The results of the power dissipation are seen in an Arrhenius plot for the dog bone shaped samples in Figure 5.6.

In Figure 5.6, a peak in the power dissipation of the sample sintered with 950 V/cm applied can be seen. This peak is attributed to the binder burnout. During burnout, carbon residues are formed, increasing conductivity and therefore power dissipation while they are present. After the burnout process has completed at $\sim 450^\circ\text{C}$, the conductivity and power dissipation return to the nominal values observed in the binder free green dog bones. Because this burnout occurs in a temperature region that interferes with the flash sintering behavior at E-fields higher than 1500 V/cm, any samples with these fields were heat treated so that burnout and flash sintering behavior did not interfere with each other. This burnout peak is also present in the samples sintered with 350 V/cm, but the peak is out of the scale of the plot. It was not seen in the 60 V/cm and 140 V/cm samples because the current with those E-fields and the conductivity of zirconia at burnout temperatures remained too low for a current change to be measured.

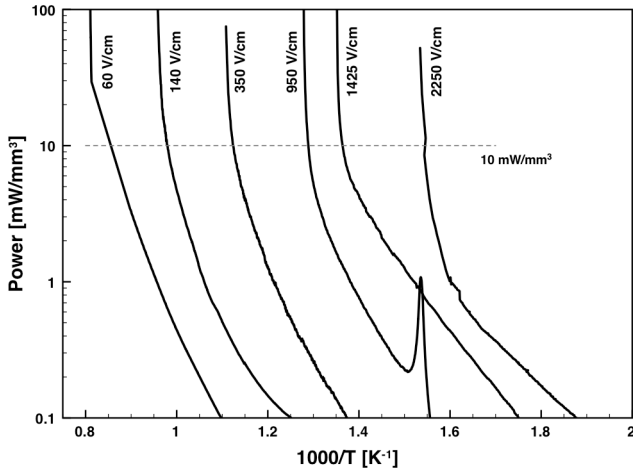


Figure 5.6: Power dissipation of dog bone shaped samples.

5.2.3.3 *Onset Temperature*

The flash sintering temperatures shown in Table 5-1 were taken as the temperature where the power dissipation curve becomes vertical. The plot of the flash sintering temperature with respect to applied E-field is shown in Figure 5.7. The results previously reported for the flash sintering of 8YSZ are shown [51]. The results for 60 V/cm and 140 V/cm are in agreement with these results.

In Figure 5.7a it can be seen that increasing the E-field continues to decrease the temperature at the onset of sintering and current runaway. Previously, the relationship between the applied E-field and the onset temperature appeared to be linear. However, increasing the E-field above 150 V/cm reveals that the decreasing trend continues, but that it is non-linear. To sinter at lower temperatures, it requires a higher E-field.

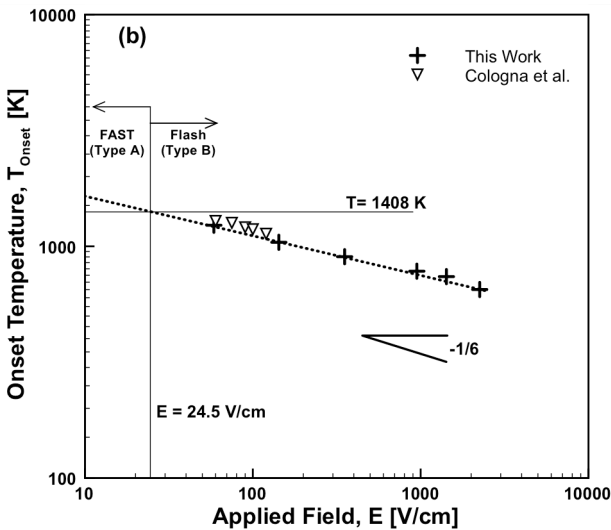
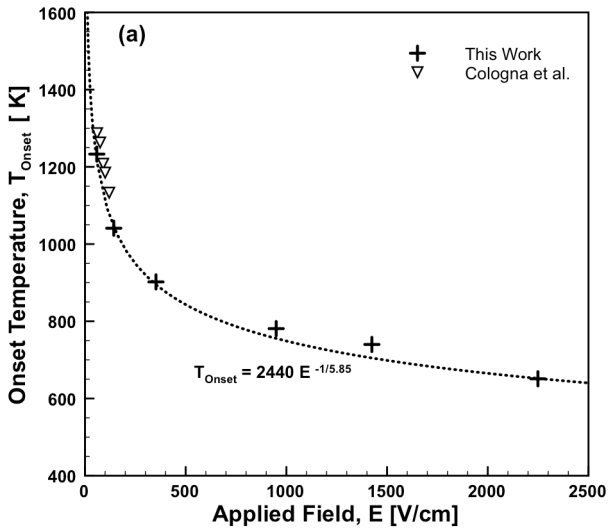


Figure 5.7: Flash sintering onset temperature with respect to the applied E-field

Plotting the results on a log-log scale (Figure 5.7b) shows that there is a power relationship between the applied E-field, E, and the resulting temperature at the onset of sintering, T_{Onset} . The line of best fit is given by the power equation:

$$(5.1) \quad T_{Onset} = 2440E^{-1/5.85}$$

where T_{Onset} is given in K and E in V/cm.

Typically, sintering phenomena are shown on Arrhenius plots because diffusion is an activated process. Taking the same points and plotting them is shown in Figure 5.8. Typically, activated processes have a negative slope to the data, signifying that increasing temperature increases the effect that is under investigation. Here, the opposite is true. This would mean that the temperature is retarding the effect. The slope of the line gives an activation energy of -1.17 eV. This is nearly the same magnitude of the activation energy of conductivity found for the fully dense sample at low temperatures, and for the values of activation energy of conduction found in literature

The reasons for the fit equation given in equation (3.1) and the negative activation seen in the Arrhenius plot are still unknown and are still being investigated. The fit to the power equation may have many explanations and may include ionization of one of the species in the 8YSZ or electrolysis. The activation energy is likely related to the conductivity change at different temperatures.

5.2.3.4 *Thickness and current density*

The lack of sintering at high E-fields is believed to occur as a result of a lack of sufficiently high current density that results in very little matter movement and the resulting sintering. The samples that sintered to higher densities using the PS:DLM300 power supply reached current

densities at the set power supply current limit of 87 mA/mm², nearly 4 times that reached with the samples sintered with the PS:GL5000 power supply. Because increasing the power supply current limit was not an option, it was already at its maximum of 120 mA, the sample geometry was modified to try and increase current densities.

Sample modifications were done in two ways. First, dog bone sample were prepared with different thicknesses, with the smallest having a thickness of 1.7 mm, and tested with an E-field 950 V/cm. Samples thinner than this were prone to break. Reducing the thickness allowed for only a modest increase in the maximum current density from 17.8 mA/mm² to 23.5 mA/mm². The flash sintering behavior of the thin dog bones mimicked closely the behavior of the thicker samples. The sintering onset temperature agreed with the temperature found for the thicker samples sintered with the same E-field, but there were no noticeable differences in the densification

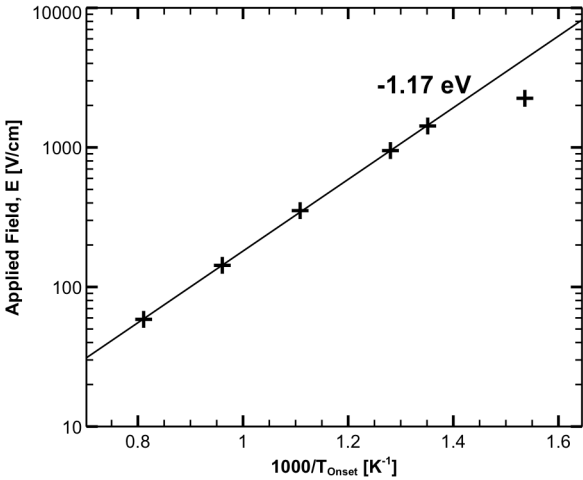


Figure 5.8: Arrhenius plot of the effect of furnace temperature, T_{Onset} , on the E-field, E, required to start flash sintering

behavior.

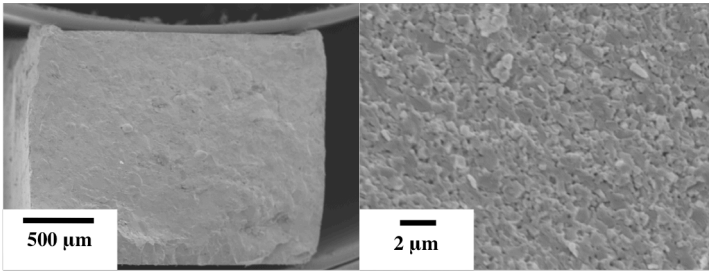
A second method that is currently being investigated is the use of extruded rods that are much easier to prepare with thicknesses that can be used to reach sufficiently high E-fields with the power supply PS:DLM300 that can provide considerably higher current densities. Preliminary results using the dilatometric setup demonstrate that with a different sample configuration gives results for the onset of flash sintering predicted by equation (3.4). However, there are observations of similar short-circuiting type behavior. At this point, this behavior may be attributed to a lack of sufficient electrode contact forcing short-circuiting, or if this is comparable to the behavior observed in the dog bones. With the higher current densities and the occurrence of short-circuiting, there are issues pertaining to the melting of the platinum electrodes.

Results for preliminary flash sintering of 10GDC using the dilatometric setup are shown in Appendix 3. These results for the first time show flash sintering in extruded samples, 10GDC, and using such an experimental setup.

5.2.3.5 *Microstructure*

Much like the densification behavior, the microstructural behavior behaved differently depending on which power supply was used. Typical microstructures for both regimes are shown in Figure 5.9. Here the fracture surface of the dog bone transverse to the gauge section of the sample sintered with PS:DLM300 with 60 V/cm is shown. The dog bone shows uniformity in the sintering behavior across the entire cross-section. The fracture surface shows that there is remaining porosity and that particles are well connected with an approximate size of 1 μm .

60 V/cm



950 V/cm

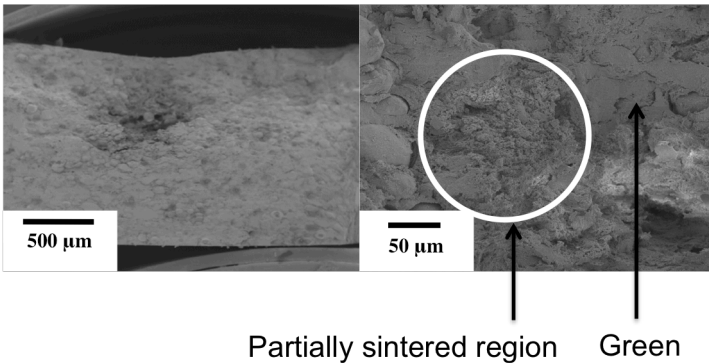


Figure 5.9 SEM micrographs of samples flash sintered with 60 V/cm and 950 V/cm.

The samples sintered with PS:GM5000, showed the typical sintering pattern seen in the sample sintered with 950 V/cm. An area of local sintering was seen near the center axis of the gauge section. Often, cracking originating from the center of the area of local sintering formed towards the corners, indicating that this area indeed underwent local sintering while the outer region of the dog bone did not sinter, or at least experience only small amounts of sintering. Examining the central region, a small area of local sintering is observed. This is the area where the current

short-circuited through the sample, causing the slight amount of sintering. Outside of this region, the microstructure appeared to remain green or remain in the early stages of sintering.

5.2.3.6 Flash sintering predictions and limitations

5.2.3.6.1 Sintering at room temperature

Given the fit equation (3.1), one may consider what E-field is required in order to sinter at room temperature. Taking 300 K as room temperatures, an E-field of 211.4 kV/cm would be required to sinter at a temperature of 300 K if the given trend holds to E-field of this magnitude and to such low temperatures. For these dog bones, that have a gauge length of 2.1 cm, a voltage of 444 kV would be required to sinter. With a current of 87 mA/mm² which is sufficient for densification, this would be a 2.6 kW power supply. Both power supplies used for flash sintering have a maximum power rating of 300 W.

5.2.3.6.2 Sparking

In reality, sintering at room temperature would be very difficult because the actual circuit used in these experiments is not as simple as assumed. In reality, the circuit also has a capacitive element composed of the atmosphere surrounding the sample between the electrodes. At low E-fields, it is acceptable to ignore this component. At higher E-fields, there is the risk of sparking. In fact, this was reported for flash sintering of alumina, which required E-fields in excess of 2 kV/cm [56]. At these E-fields, the atmosphere, air in this case sparks due to Townsend breakdown

Townsend breakdown in gases occurs much like it does in a dielectric material. Electrons accelerated between two electrodes can achieve a high enough energy that their collisions with other atoms in the air between the electrodes can cause the emission of more electrons resulting in an avalanche of electrons that eventually for a current carrying spark.

The Paschen limit is an empirical limit for determining the voltage breakdown limit of a gas between two flat plate electrodes. The breakdown

voltage is a function of the electrode spacing and the pressure of the gas between them. Both are essentially measures of the distance an electron has to accumulate energy in a give E-field. The electrode spacing, d , gives the potential, and the pressure, P , is a measure of the spacing between gas atoms that and electron has between collisions. If an electron has enough distance in a strong enough field, then sparking will occur. The Paschen equation is given by:

$$(5.2) \quad V_{Br} = \frac{Bpd}{C + \ln(pd)}$$

$$(5.3) \quad C = \ln \left(\frac{A}{\ln \left(1 + \frac{1}{\gamma} \right)} \right)$$

where, V_{Br} , is the breakdown voltage in kV, p the pressure in torr, d the distance in centimeters, The parameters A and B , are empirical parameters given by 15 1/cm-torr, 365 V/cm-torr, and γ is the third ionization coefficient given by 10^{-2} [71] .

The equation, modified for the temperature (a pressure effect) is given as:

$$(5.4) \quad V_{Br} = 24.2 \left(\frac{293pd}{760T} \right) + \frac{6.08}{d} \sqrt{\frac{293pd}{760T}}$$

where, V_{Br} , is the breakdown voltage in kV, p the pressure in torr, d the distance in cm.

Given the setup used in this work, we assume that wire electrodes behave as plate electrodes and are separated by a gap, d , in dry air at 1 atmosphere (760 torr) at the furnace temperature. The E-field where breakdown occurs, E_{Br} , is given by:

$$(5.5) \quad E_{Br} = \frac{V_{Br}}{d} = 24.2 \left(\frac{293pd}{760T} \right) + \frac{6.08}{d} \sqrt{\frac{293pd}{760T}}$$

Given this equation, upper E-field limit for the onset of sintering can be determined for different sample sizes. In Figure 5.10, the curve fitted to the results as well as the Paschen limit for different thicknesses of 10 cm, 10 μ m,

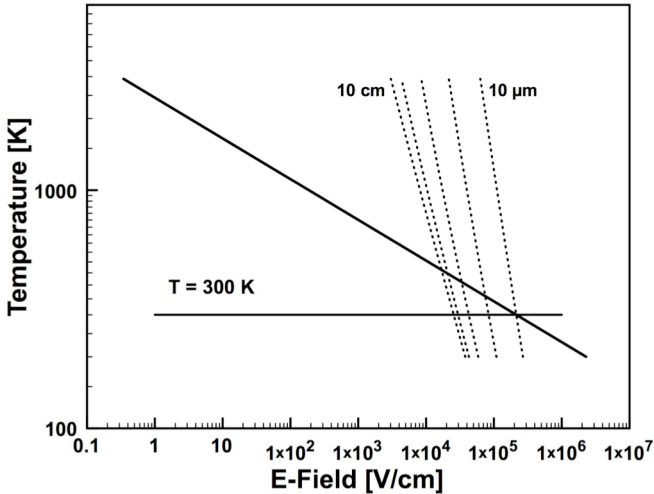


Figure 5.10: Flash sintering onset behaviour extrapolated to room temperature with Paschen limits for the prediction of sparking at different electrode spacing between 10 cm and 10 μ m.

2.1 cm (This work), 1 mm, 100 μm , and 10 μm (Typical fuel cell electrolyte thickness), are calculated.

At high enough temperatures, and high enough fields, the Onset temperature curve intersect the Paschen limits, meaning that sparking is more likely than conduction through 8YSZ at this temperature.

For the dog bones used here, with an electrode separation of 2.1 cm, sparking would occur at an E-field of 18 kV/cm and a temperature of 167°C. To sinter at room temperature, samples would have to reach $\sim 10 \mu\text{m}$.

These predictions remain completely hypothetical. In practice, sintering starts at lower E-fields and higher temperature for the gap of 2.1 cm. however, this sparking is inconsistent and many different factors may play a role. First, Paschen limit is derived for the sparking behavior between two flat plate electrodes. The use of 2 cylindrical electrodes can change the potential fields that are actually in practice. Second, sparking has also been observed between the sample and the electrode. Here, gaps can be very small an immeasurable because of the way samples are suspended from the wires that are used. The most likely system that these predictions can estimate would be a plate like sample sandwiched between two plate electrodes. This would closely represent the Paschen system. However, work flash sintering of Co_2MnO coatings show that this sort of configuration shows the tendency to create area of local flash sintering when a similar short-circuiting behavior to that seen in these high E-field samples [Anshu, Montanaro, D., Sglavo, V.M., unpublished work].

5.2.4 Sinter Mapping

We propose a mapping of the different sintering behaviors of the material depending on applied E-fields and the furnace temperatures. The mapping of 8YSZ is shown in figure Figure 5.11. The mapping shows the dominant sintering mechanisms of a green sample that are dominant depending on the combination of temperature and E-field.

The different regions are the same as those shown in Figure 5.10 with the addition of the conventional sintering temperature (1408 K), the critical E-field 24.5 V/cm, and the melting temperature (3000K).

With E-fields less than E_{crit} , and lower than the conventional sintering temperature or for E-fields higher than E_{crit} at temperature that lie below T_{Onset} as predicted by equation (3.1), the sample behavior purely as an ionic conductor with a conductivity σ . For E-fields less than E_{crit} , if the furnace temperature exceeds the conventional sintering temperature, the sample enters the FLASH sintering regime. If E is higher than E_{crit} and the temperature is on or above the predicted T_{Onset} -line, the sample will flash sinter. The upper limit for the applied E is when sparking starts. This limit will be dependent on sample geometry. There is an additional limit at high temperatures where kinetics would dominate as discussed by Raj [52]. At temperatures > 2050 K diffusion would allow for sintering rates that are comparable with flash sintering rates. This regime is completely theoretical

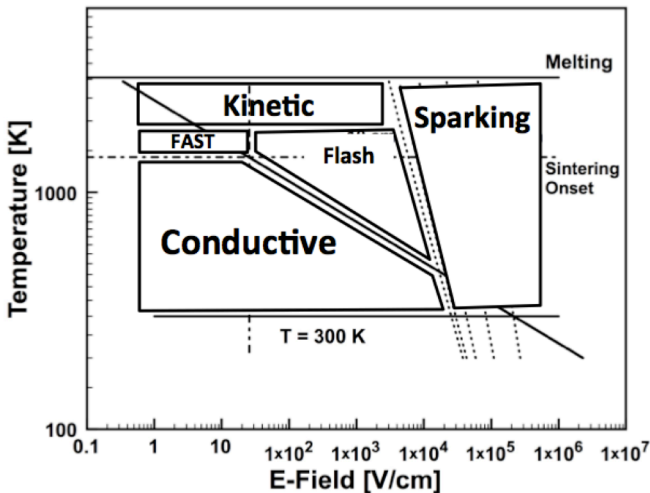


Figure 5.11: Mapping of sintering behaviour of 8YSZ under the influence of a dc E-field

because a sample would have already sintered if were heated to these temperatures with or without an applied E-field.

5.3 *Flash Behavior in Fully Dense 8YSZ*

5.3.1 Introduction

The effect of grain boundaries is of interest in flash sintering. Sintering is a boundary phenomenon, so mechanisms active in the grain boundaries in flash sintering conditions are of interest. Previous works have shown that grain boundaries in E-field assisted sintering are pertinent to the heating behaviors during flash sintering of zirconia [23], [51], and they play a role in coarsening mechanisms in E-fields [36]. The starting particle size also plays a role in the sintering [60].

To examine the effect of the grain boundaries, presintered samples have been prepared. Examining flash like behaviors on these samples and examining the results with respect to grain size allows for inferences on the effect of grain boundaries and there influence on the flash like behavior in sintered samples.

5.3.2 Experimental

Dog bone and disk samples were presintered and to have average grain sizes of $0.60\ \mu\text{m}$, $3.76\ \mu\text{m}$, and $5.30\ \mu\text{m}$ and $11.47\ \mu\text{m}$, samples 1400, 1600s, 1600L, and Large respectively. The microstructures are shown in Figure 5.12 and Figure 5.13.

Two different test configurations were used to observe the flash sintering-like behavior in fully dense samples. The first was much like flash sintering experiments with dog bones suspended from the holes in the dog

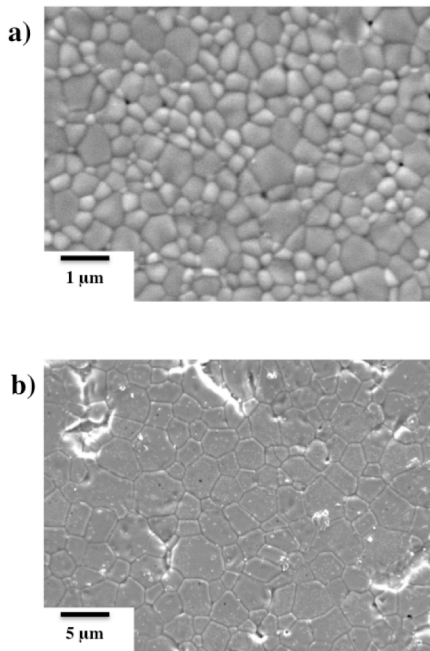


Figure 5.12: Microstructure on polished and thermally etched surface for samples sintered at (a) 1400, $G=0.60\ \mu\text{m}$ and (b) 1600s $G=3.76\ \mu\text{m}$.

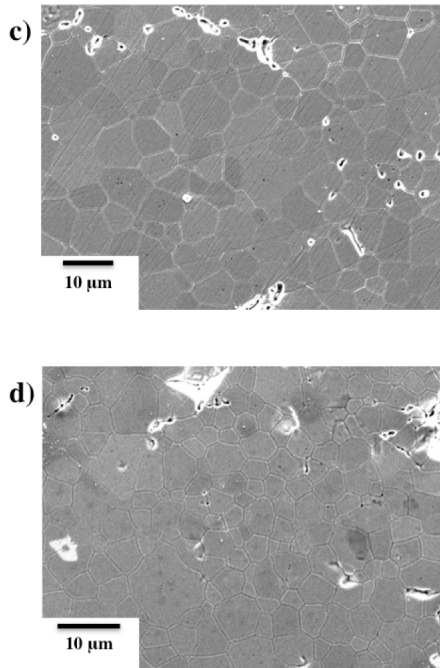


Figure 5.13: Microstructure on polished and thermally etched surface for samples sintered at (e) 1600L, $G=5.30 \mu\text{m}$ and (d) Large $G=11.47 \mu\text{m}$.

bone handles between two platinum wires that acted as the current carrying electrodes. Platinum wires were used as the 4-point voltage probe, wrapped around the section of the dog bone. Because these samples used all platinum electrodes, they were heated to 600°C, 800°C, and 1000°C. The samples were allowed to equalize at temperature, and then the power supply voltage was ramped at 5 V/min while monitoring sample current and temperature. The voltage was ramped until a current runaway event occurred while measuring the 4-point voltage, current, furnace temperature, and sample temperature.

Bars were cut from the disk and silver electrodes were baked on to the bar ends at 900°C for 1 hour. Again, voltage probes were Pt wire wrapped around the samples. The bars were suspended in the vertical configuration with the pyrometer focused on the center of the bar between the voltage probe electrodes. The use of silver electrode limited these samples to temperatures of 600°C and 800°C. Because of this, they were used primarily to examine the heating characteristics because the pyrometer target fell completely on the sample, where on dog bones the gauge section was slightly too small for to completely cover the area where the pyrometer sensor area was aimed.

Bar samples also served to observe the effect of the a different geometry. The difference between the two was unnoticeable both for I-V behavior and heating. Results were taken as the best, cleanest data, usually being the dogbone sample. The way the voltage probes were made, by wrapping wire around the sample, made measurements in the larger bar samples more noisy because of the difficulty of making the wire perfectly parallel to the electrodes.

Voltage results were normalized by the disances between the electrodes giving the E-field, and by the sample cross-sectional area transverse to current giving the current desnisty, J . The lengths for the dog samples are shown in Figure 5.14. The cross-sectional area was taken as the area of the dog bone gauge section. For bar samples, the configuration was similar, and on similar length scales.

5.3.3 Results and Discussion

5.3.3.1 *Flash behavior in fully dense 8YSZ*

From the beginning of this work, the behavior of dense 8YSZ at high voltages was uncertain. Typically, 8YSZ is used at very low voltages in fuel cells and oxygen sensors, where voltages do not exceed more than a few volts.

The typical E-J behaviors of fully dense 8YSZ at different temperatures are shown in Figure 5.15. The samples prepared with $G = 0.60 \mu\text{m}$ is shown here, but it is indicative of the response for all sample preparations. Solid lines indicate the 4-point voltage response and dashed lines the 2-point voltage response. As is observed in flash sintering experiments, there is a point at which there is the onset of an unstable current runaway, indicated by the current response J becoming vertical.

There is a difference, ΔE , between the 2-point and 4-point measurements at a constant system current value J . This difference is the result of other voltage drops in the system. The primary drop will occur at high currents due to the charge transfer reaction at the electrodes. Other resistive voltage drops include the resistance of the electrode wires especially at furnace temperatures. These, however, are considered insignificant with regards to the charge transfer reaction resistance.

Increasing temperature decreases the E-field where current runaway takes place. This is expected in 8YSZ because of the activated nature of conductivity. Increasing temperature increases conductivity so reaching the

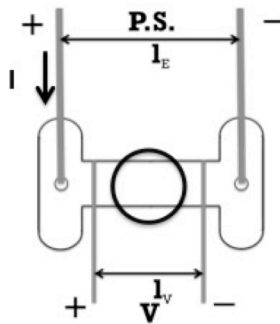


Figure 5.14: Wiring setup for measuring the flash-like behaviour in fully dense sample. 2-point voltages are normalized by length l_E and 4-point voltage probe measurements by l_V . Pyrometric measurements were taken over the area indicated by the circle in the sinter of the dog bone gauge section.

critical values for the start current runaway are reached with smaller E.

This critical value for the onset of current runaway remains an issue of power dissipation as is the case in the flash sintering of green YSZ samples [23], [51]. In Figure 5.16, the same results from Figure 5.15 are shown with slightly changed axes and lines indicating constant power dissipations. The critical power dissipation remains continues to around 10 mW/mm^3 . Here, the transition occurs between 10 mW/mm^3 and 20 mW/mm^3 whether the response is considered from 2-point or 4-point measurements.

The effect of the power supply transition from voltage control to current control can also be seen. These transitions are indicated by the discontinuous and sudden decrease of E at high current densities.

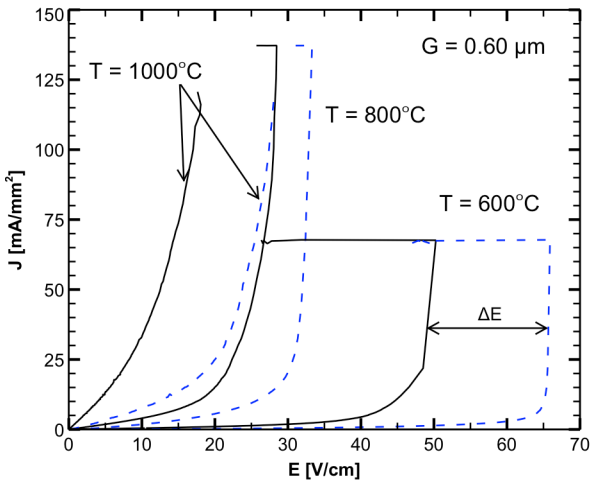


Figure 5.15: Typical current response of dense samples at different temperatures, here given by the sample 1400 with $G=0.60 \mu\text{m}$.

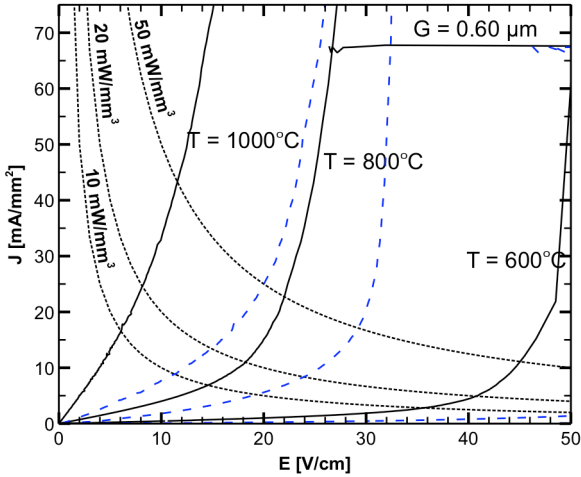


Figure 5.16: E-J response with constant power dissipation lines, $G=0.60 \mu\text{m}$.

5.3.3.2 Charge carrier transition, ΔE

The difference of the two E-field measurements, $\Delta E = E_{2pt} - E_{4pt}$, were taken at constant J. The E-J response with the difference is shown in Figure 5.17, with typical response represented by $G=0.60 \mu\text{m}$ at 600°C and 800°C . A clear maximum is observed that occurs a J that divides the samples' behaviors in a low E ohmic region, and the region of current runaway. This response was observed for all samples measured at furnace temperatures of 600°C and 800°C . At 1000°C , ΔE showed variable results for some samples, it reached a maximum like already shown and in others it reached a maximum value, but it did not decrease, instead it leveled off at a relatively constant value.

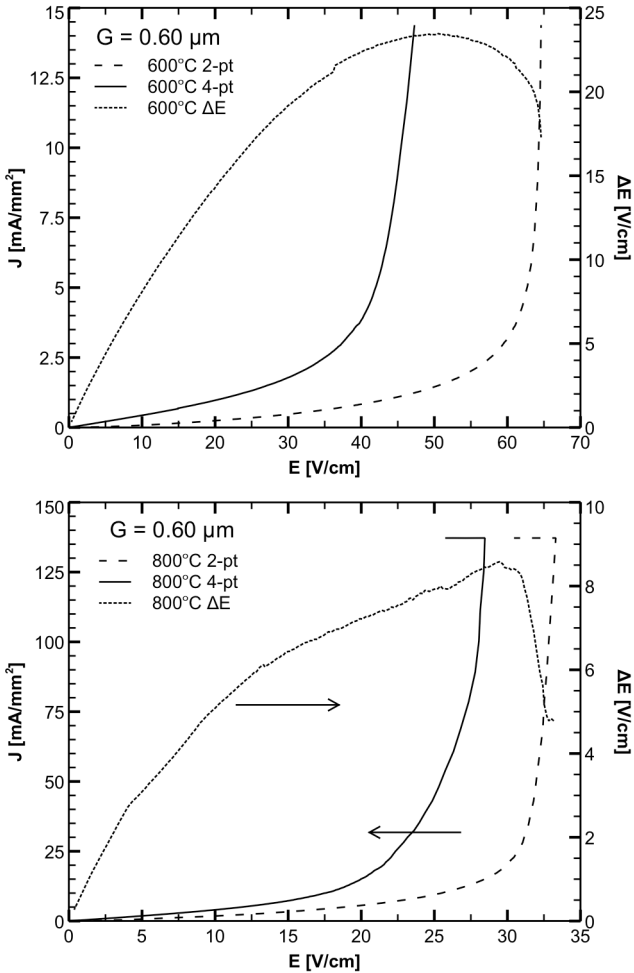
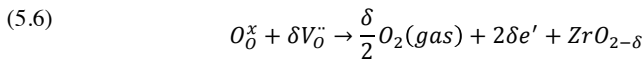


Figure 5.17: Difference, ΔE , of 2-point and 4-point measurements showing a maximum in the difference. Upper plot: 600°C, $G=0.60 \mu\text{m}$, Lower plot: 800°C, $G=0.60 \mu\text{m}$.

At the lower temperatures, the ΔE peak occurs at a current density that signals the onset of other observed transition including the increase in conductivity and the current runaway as well as and start of heating in the sample. In Figure 5.18, the transition voltage, the peak of ΔE_{max} , is indicated in the plots of σ vs. E, T vs E. At ΔE_{max} there is a clear transition in the conductivity, where it begins to leave its 'low E' behavior and increase non-linearly. Following shortly, the sample temperature begins to increase.

This transition is believed to occur due to the nucleation of electronic charge carriers at the cathode. Below the ΔE_{max} the reaction $\frac{1}{2}O_2(gas) + V_O^{\cdot\cdot} + 2e' \rightarrow O_O^x$ is sustained, and the current can be sustained by the consumption of gaseous O_2 at the expense of $V_O^{\cdot\cdot}$. At ΔE_{max} , the current and this reaction can no longer be sustained by the reaction providing resulting in an accumulation at the electrode of $V_O^{\cdot\cdot}$. In order to maintain currents, the crystal itself is used as an oxygen source resulting in the reduction of zirconia:



The vacancies that are not filled by cathodic reaction with gaseous oxygen react with lattice oxygen, partially reducing the zirconium while creating additional electrons. At the cathode, electrons are usually consumed in the cathodic reaction. Now that they are being created, there is an additional charge carrier in the system and the zirconia becomes a mixed conductor. The mixed conduction means that the resistance at the electrodes is no longer completely determined by the charge transfer reaction. Because electrons can now cross from the electrode to the sample directly, a much less resistive step that is observed as a drop in the voltage between the 2-point and 4-point voltage measurements.

The blackening that is observed in the samples after being subject to flash-like treatments supports this. Figure 5.19 shows samples treated at 800°C for each different grain size. This blackening has been reported as the result of reduction of the Zr atom [72], [73]. The amount of blackening increases from small grain size to largest, a similar effect observed in electrolytically reduced samples with oxygen blocking electrodes [73]. When comparing single crystalline to polycrystalline results with the blocking electrodes, the polycrystalline sample showed a slow propagation of the reduction from when compared to single crystals treated with the same voltage. This retardation was attributed to the blocking properties of grain boundaries that act to impede the reduction from. In this case, the electrodes are both open to the atmosphere, so oxygen exchange can occur at both ends of the current, but the results with grain size agree that for smaller grain sizes, more grain boundaries. Increasing grain size reduces the amount of grain boundary, thus, electrolysis has larger areas to take place in the individual grains.

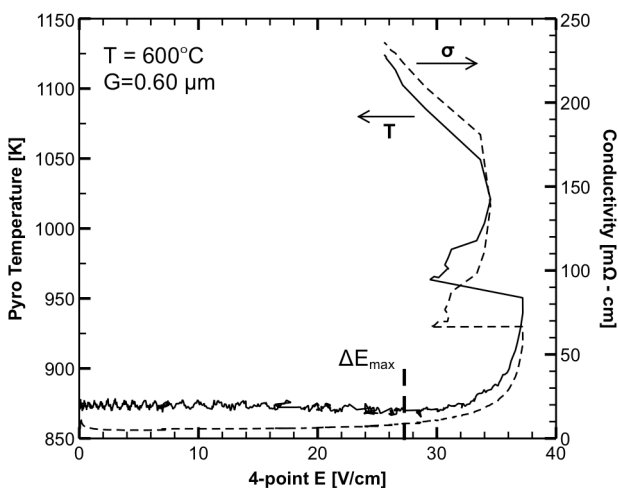


Figure 5.18: Transitions in conductivity and sample temperature that occur at ΔE_{\max} .



Figure 5.19 Blackening observed after flash treatment at 800C. Sample grain size increases from left ($G=0.60 \mu\text{m}$) to right ($G=11.47 \mu\text{m}$). The cathodic reaction occurred at the under hole.

Values of ΔE at their maximum vary range widely. Values are as low as a few V/cm to as much as 30 V/cm, and there is no regularity in the maximums. More importantly, the values of 2-point measurements can be as much a 60% of the values measured by 4-point measurement. First, this difference would indicate that the quality of the contact between the sample and the electrodes varied from one test to another, and that this contact plays a significant roll Secondly, and more importantly, up to this point, all flash sintering results reported use only 2-point measurements. The difference in the values has been noted in impedance spectroscopy measurements, and resulted in several reported result being nullified. For flash sintering, especially in the very nonlinear conditions, it is necessary to get an accurate measurement of the actual E-field acting with in the sample.

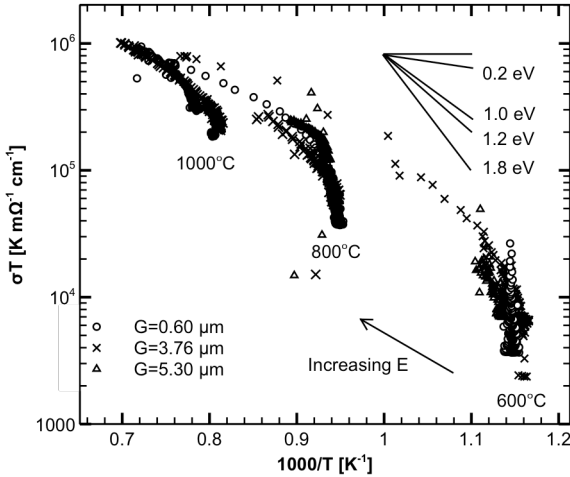


Figure 5.20 Change in conductivity during while V is ramped at 5 V/min. Samples started at furnace temperatures of 600°C, 800°C, and 1000°C. Samples finish at 1440 K (1167°C)

5.3.3.3 Conductivity Behavior

Flash sintering is characterized by the sudden increase of current due to an apparent loss of resistivity/ increase in conductivity. Reported results do not examine this effect because only furnace temperatures were measured. Because of the heating in the sample, it is necessary to consider the sample temperature for the conductivity. This loss of resistance is also unstable, meaning that measurements of the conductivity cannot be considered quantitatively. It is however interesting to observe the behaviors in this transient state.

Table 5-2 Total Activation energies of conductivity for fully dense samples prepared with different grain sizes.

Sample	Average grain size, G	Ea
1400	0.60 μm	1.03 eV
1600s	3.76 μm	0.90 eV
1600L	5.30 μm	0.85-1.19 eV
Large	11.47 μm	Data insufficient

Conductivity results are shown in Figure 5.20. The results for low E conductivities, give activation energies shown in Table 5-2. Activation energies vary, but they are within the range of values reported in literature. These values are very rough estimates because they are taken from only 2 or 3 points, and during transient measurements. A more refined set of measurements would give more accurate values of activation energy.

In fully dense samples, there is the interesting result of an increase in conductivity at constant temperature, indicated by the vertical lines. Then at the value that conductivity that corresponds to the transition at ΔE_{\max} , begins to heat and naturally, conductivity increases. At high current and temperatures, samples tend to the same point. Here, the power supplies have reached their current limits, and power dissipation levels after the peak have stabilized to a constant value. Regardless of the starting temperature, for the current limit used, and if the samples are left to stabilize, they all tend towards the same final temperature of 1440 K (1167°C).

5.3.3.4 *Grain size and runaway*

The main interest at the start of this work was to observe the effect of grain size on the flash sintering like behavior of dense samples. The effect of grain size on the 4-point E-field at the transition that occurs at ΔE_{\max} is shown Figure 5.21. The results are shown for samples measured at furnace temperatures of 600°C and 800°C. At 1000°C, the ΔE_{\max} was only observed for 1 sample. The results behave in two different ways depending on grain size and are divided by a local minimum at $\sim 3 \mu\text{m}$. For larger grain sizes, $> 3 \mu\text{m}$, increasing grain size increase the transition voltage by $\sim 1.12 \text{ V/cm}$ per μm of grain size. This means that there is an increase in the grain boundary resistance that adds $1.12 \text{ mV/grain boundary}$ for every $1 \mu\text{m}$ the average grain size increases, assuming a brick layer model with cubic grains of equal size. The increase in voltage is found from $v_{Br} = E_{Br}G$, a typical value to gauge the breakdown characteristic in ZnO varistors. V_{br} is the voltage drop

per grain boundary at breakdown with the E-field E_{Br} . Below $3 \mu\text{m}$, higher E-fields are required to initiate flash behavior.

We propose that these behaviors are a result of two different competing mechanisms that determine the total resistance of the material, and as a result, how difficult it is for the sample to reach critical power densities to initiate flash behavior by $p = V^2/R$. The first, is the increase of total resistance due to the increase of the number grain boundaries as grain size decreases. Grain boundaries have a blocking effect as a result of oxygen vacancy depletion arising from preferential yttria segregation to the grain boundary. This makes it more difficult for a vacancy to move through the grain boundary [74]. By increasing grain size, the effects of grain boundaries are minimized and conduction is dominated by bulk conductivity. At very low grain sizes, there is the possibility that the amount of grain boundary can result in increased total conductivities due to grain boundary pipelining. This however occurs in sample $< 0.5 \mu\text{m}$ and is not applicable here [41], [74].

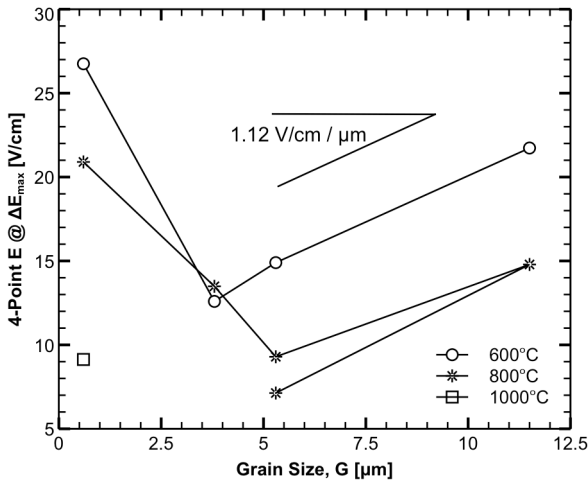


Figure 5.21: The effect of average grain size on the E-field required to initiate flash behaviour.

Because of the high voltages and currents here, electrolysis of the sample must also be considered in addition to the more traditional factors of bulk and grain boundary resistance. Here, increasing grain size reduces the effective E-field drop per grain and the potential developed across the grain meaning for large grains; thus, a higher potential is required to initiate electrolysis with the single crystal behavior being the limiting case (discussed in section 5.4).

At a critical grain size the effects of these two mechanisms are minimized and result in a minimum of the E-field required to initiate current runaway. This minimum occurs where the two mechanisms change dominance. The minimum appears to be temperature dependent with an estimated minimum grain size of 3.0 μm at 600°C and 5.5 μm at 800°C

5.4 *Flash Behavior in Single Crystal YSZ*

5.4.1 Introduction

Because grain boundaries are of such interest, it is beneficial to compare the behavior of a single grain in the absence of grain boundaries. This is rather difficult to do in a polycrystalline samples, instead, a single crystal of zirconia can be used as model for individual grain.

5.4.2 Experimental

A bar of single crystalline zirconia was cut from a larger piece of zirconia. The bars were polished on all sides with 1200 grit SiC paper to minimize the effects surface defect could have on the electrical behavior. Silver paste was used as the electrodes and baked onto the crystal at 900°C for 1 hour. Platinum wire was wrapped around the bars to be used as the voltage probes for 4-probe measurements.

The samples were suspended in the vertical flash sintering configuration with the largest side oriented towards the bottom of the furnace. The single crystal was heated to 600°C or 800°C and allowed to equalize. It was then subject to a voltage ramp of 5 V/min until current runaway took place. Voltage was measured at the voltage probes and the power supply while the current in the circuit and sample temperature was monitored by pyrometer.

5.4.3 Results and Discussion

Single crystal results showed a similar E-J behavior to those found in polycrystalline samples. The E-J behavior at 600°C is shown in Figure 5.22. Again, there is a similar current runaway and a large difference in ΔE at constant current density. However, unlike in polycrystalline samples, ΔE does not show reach a peak value as was seen in the polycrystalline samples.

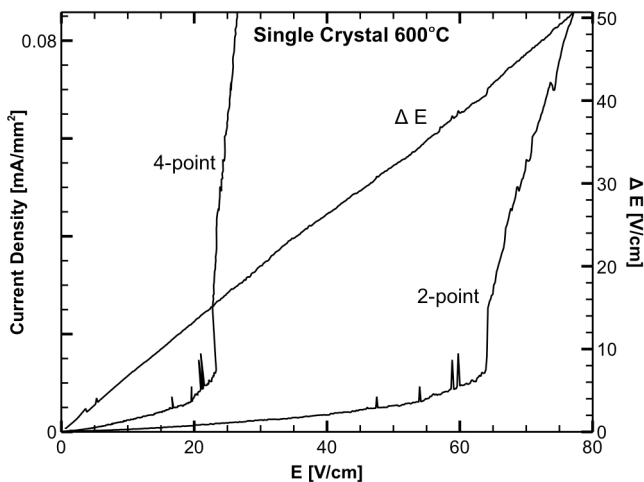


Figure 5.22: Current response J to applied E -field, E , for single crystalline YSZ. 2-point response is the results for the Voltage applied at the electrodes, and 4-point for the response measured at the voltage probes. ΔE is the difference of the two taken at the same current density, plotted with respect to the 2-point E .

Instead, it continues to increase, at a constant value with respect to current density.

The change of the samples temperature, measured by pyrometer, with respect to the volumetric power dissipation is shown in Figure 5.23. Measurements done with a furnace temperature of 600°C appear as a close cluster because the very low currents resulting in low power densities. For both furnace temperatures, the single crystal shows no change in temperature despite both displaying current runaway events. This signifies that grain boundaries must be present if there is going to be any heating in the sample.

After samples were removed from the furnace, they showed a blackening originating from the negative electrode. This blackening is characteristic of the reduction of zirconium atoms. Similar results were obtained in single crystal samples that were encased in airtight glass so that a pure blocking electrode was obtained at the cathode [73]. The electrolysis pattern and the proposed reactions from Ref. [73] are shown in Figure 5.25. In this work, electrodes were open to the atmosphere so they were not automatically blocking, but the same electrolytic pattern was observed. In inert atmospheres, the mass transfer has been shown to be the rate limiting step [75]. This limitation is considered to be the reason for electrolysis in these single crystals. The current is believed to reach such levels that the mass transfer limits of the charge transfer reaction creating a virtual blocking electrode. There are not enough charge carriers to provide the current, so the missing carriers are created by the reduction of the Zr atoms creating electronic defects to maintain the charge movement. In controlled atmosphere experiments, this sort of blackening occurs when oxygen activities are $\sim 65 \cdot 10^{-55}$ at 600°C and 10^{-44} at 800°C [76]. At oxygen activities lower than this, and if the sample is allowed to equalize, the dominant charge carrier becomes electrons. In these samples, this result is only localized because it occurs only at the electrode, not throughout the sample.

The transition at 600 is shown closer in Figure 5.22. At high E and J , where blackening occurs, there is a quadratic relationship that develops, $J \propto E^2$. In TiO_2 , this has been attributed to interface phenomena between at the electrode [9].

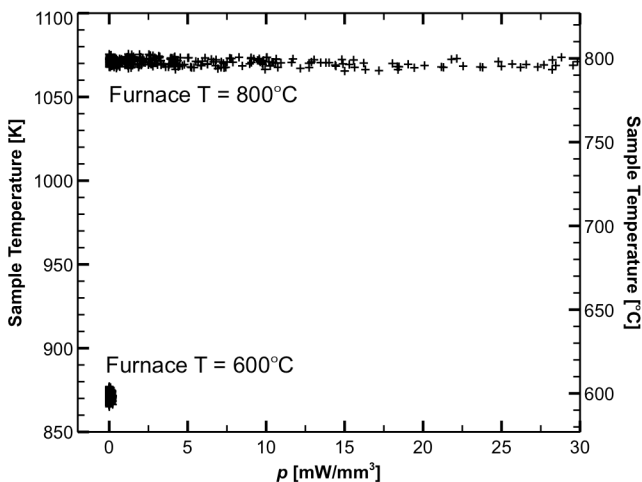


Figure 5.23: Temperature change of single crystal samples, measured by pyrometer as a function of the volumetric power dissipation in the samples

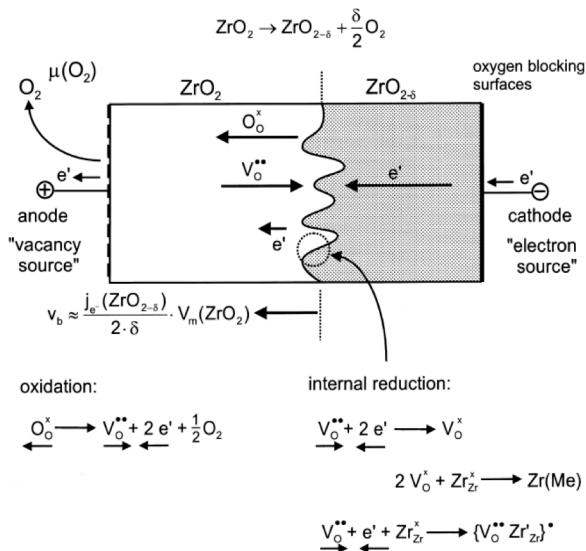


Figure 5.25 The blackening pattern observed in single crystals and the proposed reactions involved in single crystal reduction [73]

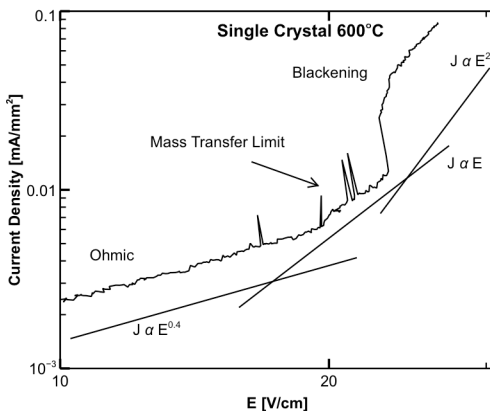


Figure 5.24 The transition of at a single crystal at 600°C from ohmic behaviour to mass transfer limitations to the electrolytic blackening of the crystal

5.4 Comparison of systems

The behaviors shown during flash sintering are very similar to those displayed in the ZnO system. This material is used as a circuit protector because of its ability to pass a minimal amount of current, up to a certain voltage. At this voltage, ZnO shows very high non-linearity and the ceramic allows for high currents to pass, essentially shorting the circuit and protecting the circuit that it is protecting from over voltages.

A typical ZnO behavior is shown in Figure 5.27. Plotting the I-V response for these measurements, the results for the samples treated sintered at 1400°C ($G=0.60 \mu\text{m}$) is shown in Figure 5.28. The effect of preparation of grain size at 600°C is shown in Figure 5.27. The behavior is very similar to the behavior of the ZnO varistor.

For samples with the same grain size, the effect of temperature is evident in the ohmic region. This has to do with higher conductivities at higher temperatures. In the breakdown region, there are differences where higher temperatures lead to lower breakdown field strengths. This would be

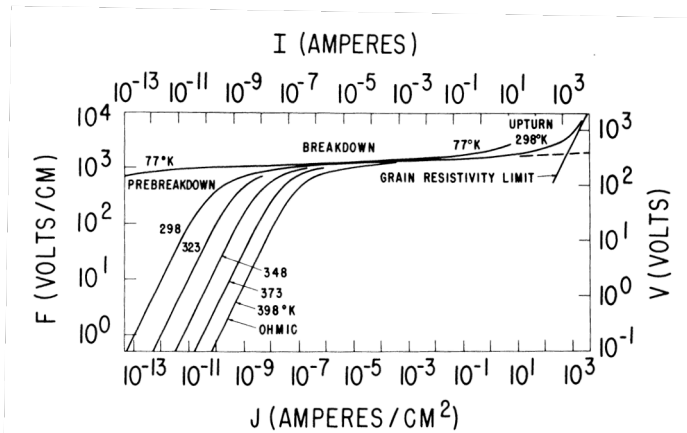


Figure 5.26: Classical I-V behaviour of ZnO varistor [82]

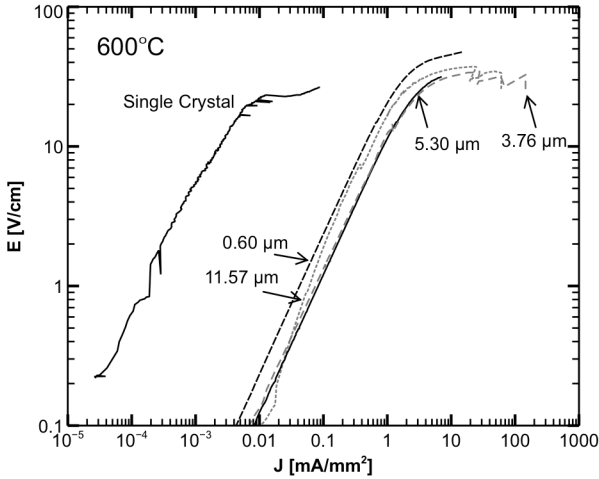


Figure 5.27 ZnO-type breakdown in dense 8YS with different average grain sizes at a furnace temperature of 600C

the effect of the critical power dissipation of 10 mW/mm^3 that has been observed time and time again.

For the same temperature, it is difficult to distinguish the different behaviors for samples with different grain sizes. There is a trend that finer grain sizes have lower current densities for the same E, but this trend is inconsistent, and the variations are within the experimental error so non conclusions can be made.

Most importantly, the electrolytic behavior in single crystals is very similar to the behavior of polycrystalline samples see Figure 5.27. The breakdown E-field is the same as all the samples prepared with grain sizes $>1 \mu\text{m}$. The single crystal has a lower conductivity than the polycrystalline samples, so it is shifted to lower J for the same E.

These similarities can be used to identify the different region so the polycrystalline samples.

5.5 Mechanisms and Flash Sintering

Several different results have been presented, regarding what are the initial stages of flash sintering when a given sample is still a loose structure of powder, and at the end stages of sintering, where the sample has reached near full densities.

Based on the observations made here, the proposed mechanism for the initiation of flash sintering is the electrolytic reduction of zirconia. In single crystal and polycrystalline samples, the electrical behaviors resemble those of flash sintering very closely. It is clear that in single crystals, the electrolytic reduction is the causes of the sudden current runaway. The reduction occurs because of the kinetics of the cathodic electrode, the recombination of oxygen vacancies with molecular oxygen from the air becomes limiting. As current continues to increase either due to heating in constant voltage experiments, or by increased voltage, there is a ‘build up’ of vacancies at the cathode that remain unreacted. This build up causes the

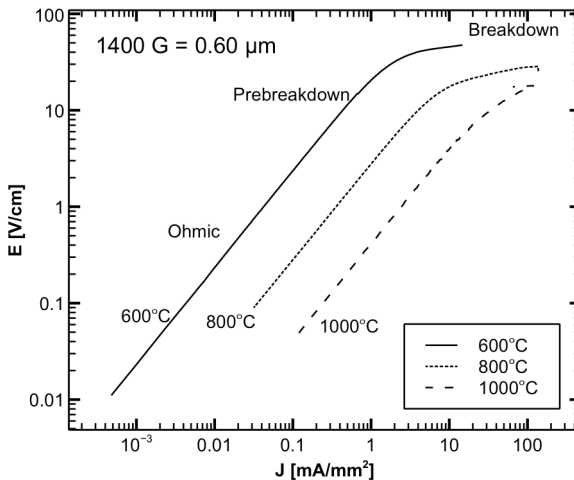
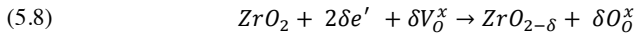


Figure 5.28 ZnO-type breakdown in 8YSZ with an average grain size of 0.60 μm at different furnace temperatures.

accumulation of positively charged species. The crystal must maintain charge neutrality, so electrons are taken from the electrode and are captured by the vacancy by:



creating a neutral vacancy. This vacancy is now immobile because its lack of charge. The accumulation of these neutral vacancies changes the stoichiometry of the crystal resulting in a change in the local conditions of the zirconium atoms. Previously each was surrounded by 4 negatively charge oxygen atoms; the presence of a neutral vacancy must be compensated by reducing the oxidation state of zirconium. The overall reaction including the neutralization of the oxygen vacancy is given by:



This reduction first occurs at the electrode creating a layer of reduced zirconia. The interface between the reduced and unreduced zirconia acts as a virtual electrode where the reduction reaction continues resulting reaction front that moves through the crystal [77]. This reduced zirconia is electronically conductive because of low oxygen activities that allow for electronic conductivities to be much higher. Ionic conductivities in the reduced crystal remain the same.

The reduction of the zirconia results in the characteristic blackening that has been observed. Higher conductivities are observed because the reduced crystal has become a mixed conductor. The ability conduct electrons dramatically changes overall conductivity and the shift from the ionic conductivities to enabled electronic conductivities appears as a loss of resistance and results in the observed current runaway.

In fully dense polycrystalline samples, each individual grain acts much as the single crystal. At the electrode, once the mass transfer limit has been reached, reduction occurs much as in the single crystal. In the bulk of the material, grain boundaries act themselves as the electrodes. In zirconia, the tendency of positively charged yttria to segregate to the grain boundaries results in a depletion of oxygen vacancies around the grain boundary making them act as blocking electrodes. Once the voltage drop across an individual grain results in sufficient currents to cause reduction, reduction fronts develop in each individual grain starting from the grain boundary on the cathode side of the grain.

In polycrystalline zirconia, the development of the reduction front at the grain boundaries will eventually cause an interconnected network of reduced areas that can directly carry electrons from one electrode to another. The conduction of electrons in this grain boundary network cause the joule heating that is observed.

These mechanisms can also be applied to the flash sintering behavior. To sinter zirconia, there needs to be the movement of the rate limiting species of Zr. In this case, the movement of oxygen does not need to be considered because of its movement at a charge carrying species.

In the green specimen, the contact points between the grains act as electrodes for each particle much like in each grain in dense samples. This result in similar creation of a reduction front localized at the contact point. In the reduction zone, oxygen vacancies can be neutralized as previously discussed, but they can also form the defect complex of zirconia proposed in Ref. [77] by:



A partially reduced zirconia Zr'_{Zr} ion binds with an oxygen vacancy resulting in a positively charged defect complex. In the field, either the complex can move as unit, or the Zr'_{Zr} can move by walking from vacancy

to vacancy. When the zirconia reaches a neck surface, it can reform stoichiometric ZrO_2 . The creation of the charged zirconium ions in the presence of the E-field would result in enhanced diffusion rates. Because zirconium diffusion is the rate determining mechanism during sintering, this enhancement would result in a net increase in sintering rates.

This mechanism is fundamentally different from the proposed mechanism of Frenkel defect nucleation. Instead of creating the highly charged Zr_i^{++++} as a defect to induce zirconia movement, Zr is reduced Zr'_{Zr} by electrolysis and in doing so can form for defect complexes that would allow the zirconia to 'walk' by forming a series of complexes from oxygen vacancy to oxygen vacancy.

6 Conclusions and Outlook

First, this work resulted in the construction and testing two different flash sintering setups. The first following standard setup used to measure the flash sintering behavior in dog bone shaped samples. The second, new setup is able to measure the sintering behavior in the extruded cylindrical samples.

In fully dense samples, dc electric measurements have shown that their behavior shows similar characteristics that are similar to the behaviors observed in flash sintering of green samples. Specifically, the onset of current runaway and the resulting rise in sample temperature. In green samples, this runaway accompanies sintering. In order to separate the electrical behavior from the sintering behavior, presintered, fully dense samples were used as a model system to understand the electrochemical mechanisms active during active during flash sintering in 8YSZ.

Using dc electrical measurements at constant furnace temperature, the differences between 4-point and 2-point at constant current density in dc electrical measurements, revealed that at the high voltages and currents that are experienced during flash sintering, there is a critical transition in the charge transfer reaction between the electrodes and the 8YSZ. A sudden drop characterizes this transition in the voltage difference at the electrodes signaling a change in the charge transfer mechanism and/ or charge carrier in the zirconia. Most importantly, the point of this transition signals the onset of the current runaway and the start of internal heating of the sample, both are characteristic of flash sintering in green samples. Samples that were subject to measurements that entered this runaway state, displayed a blackening of varying amounts depending on the grain size. Samples with large grain size showed a greater degree of blackening than those with a finer grain size. This blackening is characteristic of the electrolytic reduction of zirconia and a stoichiometric change of the system $\text{ZrO}_2 \rightarrow \text{ZrO}_{2-\delta}$.

Observations with respect to grain size showed that with increasing grain size, the onset of the critical point increased with increasing grain size. This is a result of the combination of a larger volumetric fraction of the more resistive grain boundary and larger effective E-field per grain in finer samples. The increase in grain boundary volume makes the sample more resistive, resulting in higher power dissipations for a given current density samples thus reaching the critical power dissipation, that is also characteristic of flash sintering. However, for the finest grain size the E-field the transition voltage was much higher than expected. This has been attributed to the blocking effect of the grain boundaries.

Single crystals showed similar I-V behavior to the polycrystalline samples. Again, the onset of reduction accompanied the onset of current runaway that occurred at similar E-fields as those observed in polycrystalline samples. This reduction was clearly observed as a stable, progressing front of blackened crystal. The onset of reduction and the resulting change in stoichiometry is a result of the limitations of the mass transfer reaction at the cathode. To maintain charge neutrality in the crystalline lattice, the reduction of the crystal is accompanied by electronic defects.

The introduction of electronic as a result of the change in stoichiometry changes the work function between the zirconia and the electrode thus explaining the drop in voltage that was observed in fully dense samples. This difference and the heating that accompanies runaway were not observed in single crystal samples. This indicated that grain boundaries are unquestionably the reason for heating observed during flash sintering. The lack of an observed change in 2-point and 4-point measurements suggest that the grain boundaries allow for the conduction of the electronic defects while in single crystals, these defects remain trapped in the reduced region.

Flash sintering experiments done on green samples with E-fields up to 2250 V/cm revealed that there is a regular fit $T = 2440 E^{-1/5.85}$ between

E-field applied, E , and the temperature at the onset of sintering, T_{onset} . This has been used to predict the behavior of cylindrical shaped samples that have a very different form factor than the dog bone samples that were used to demonstrate the relationship. The reasons for this fit are still unclear, but they seem to be related to the conductivity change in 8YSZ due to changes in temperature. Using this fit, and the unassisted sintering behavior of this zirconia, the critical e-field was determined to be 24.5 V/cm,

These results show that the critical power dissipation for the onset of sintering remains constant regardless of the E-field applied. The lack of sintering to high densities of the after the onset of the current runaway upon reaching the critical power dissipation of 1-10 mW/mm³, reveal the importance on sufficient current densities to ensure densification. Total power dissipation is not an indication of sintering. Instead, power densities are determined by the current densities. Thus, at lower E-fields, the required current density for densification results in lower powers than those that would be required at very high E-fields.

Based on the observations made in fully dense samples, electrolysis has been determined to be the determining factor for the onset of flash sintering. Reduction of the crystal results in an electronically conductive region that explains the apparent current runaway that occurs. This reduction also can produce charge zirconium species depending on the extent of the reduction. This charge species, in the presence, of the E-field can move much faster. Because the diffusion of zirconium ions is the rate determining step, the creation of these charged, fast moving species can result in faster sintering rates.

More detailed work can to reveal the extent electrolytic reduction has on flash sintering can be performed by flash sintering 8YSZ in various atmospheres with differing oxygen activities. At lower oxygen activities, reduction in the material will be more easily induced, due to mass transfer limits likely resulting in lower flash sintering temperatures for the same E-field. The extent of sintering may also be limited as a result of preferred

electronic conduction by the more reduced particles than by conduction of the reduced species.

Work remains on explaining the T_{onset} applied e-field most likely by seeing how a fit found for other materials with similar ionic conduction properties can be explained by differences in certain electrical properties. Additionally, work is under way investigating the effect of current density at high E-fields in disk shaped sample that the high E-fields to be achieved by smaller voltages permitting the use of a high current power supply that can provide the current densities believed to be necessary for sintering to full density at $E > 300$ V/cm.

Works Cited

- [1] C. Field, V. Barros, T. Stocker, Q. Dahe, D. Dokken, K. Ebi, M. Mastrandrea, K. Mach, G. Plattner, S. Allen, M. Tignor, and P. Midgley, Eds., *Managing the risks of extreme events and disasters to advance climate change adaptation*. Cambridge, United Kingdom and New York, NY, USA: Cambridge University Press, 2012.
- [2] S. Solomon, D. Qin, M. Manning, Z. Chen, M. Marquis, K. Averyt, M. Tignor, and H. Miller, Eds., *Contribution of Working Group I to the Fourth Assessment Report of the Intergovernmental Panel on Climate Change*. Cambridge, United Kingdom and New York, NY, USA: Cambridge University Press, 2007.
- [3] J. Hansen, R. Ruedy, M. Sato, and K. Lo, "Global Surface Temperature Change," *Reviews of Geophysics*, vol. 48, no. 4, p. n/a–n/a, 2010.
- [4] J. Hansen, R. Ruedy, M. Sato, M. Imhoff, W. Lawrence, D. Easterling, T. Peterson, and T. Karl, "A closer look at United States and global surface temperature change," *Journal of Geophysical Research*, vol. 106, no. D20, pp. 23–947, 2001.
- [5] T. M. Smith, T. C. Peterson, J. H. Lawrimore, and R. W. Reynolds, "New surface temperature analyses for climate monitoring," *Geophysical research letters*, vol. 32, no. 14, p. L14712, 2005.
- [6] P. Brohan, J. J. Kennedy, I. Harris, S. F. B. Tett, and P. D. Jones, "Uncertainty estimates in regional and global observed temperature changes: A new data set from 1850," *Journal of Geophysical Research*, vol. 111, no. D12, p. D12106, 2006.
- [7] R. J. Francey, P. P. Tans, C. E. Allison, I. G. Enting, J. W. C. White, and M. Trolier, "Changes in oceanic and terrestrial carbon uptake since 1982," *Nature*, vol. 373, pp. 326–330, 1995.
- [8] R. J. Andres, J. S. Gregg, L. Losey, G. Maryland, and T. A. Boden, "Monthly, global emissions of carbon dioxide from fossil fuel consumption," *Tellus B*, vol. 63, no. 3, pp. 309–327, 2011.
- [9] C. D. Keeling and T. P. Whorf, "Atmospheric CO₂ records from sites in the SIO air sampling network," *Trends: A compendium of data on global change*, vol. 2009, 2005.
- [10] O. Edenhofer, R. P. Madruga, Y. Sokona, K. Seyboth, P. Matschoss, S. Kadner, T. Zwickel, P. Eickemeier, G. Hansen, S. Schlömer, and C. von Sechow, Eds., *Renewable Energy Sources and Climate Change Mitigation Special Report of the Intergovernmental Panel on Climate Change*. Cambridge, United Kingdom and New York, NY, USA: Cambridge University Press, 2012.

- [11] S. Pacala and R. Socolow, “Stabilization wedges: solving the climate problem for the next 50 years with current technologies,” *Science*, vol. 305, no. 5686, pp. 968–72, Aug. 2004.
- [12] International Energy Agency, “World Energy Outlook 2012: Executive Summary,” Paris, France, 2012.
- [13] B. Metz, O. R. Davidson, P. R. Bosch, R. Dave, and L. A. Meyer, Eds., *Contribution of Working Group III to the Fourth Assessment Report of the Intergovernmental Panel on Climate Change (IPCC)*. Cambridge, United Kingdom and New York, NY, USA: Cambridge University Press, 2007.
- [14] W. Callister, *Materials Science and Engineering: An Introduction*, Fifth. John Wiley & Sons, 2000.
- [15] W. D. Kingery, H. K. Bowen, and D. R. Uhlmann, *Introduction to ceramics*, vol. 1032. New York: John Wiley & Sons, 1976.
- [16] C. B. Carter and G. Norton, *Ceramic Materials: Science and Engineering*. Springer Science+Business Media, LLC, 2007.
- [17] “ASTM Standard C1145-06 Standard Terminology of Advanced Ceramics.” ASTM International, West Conshohocken, PA, 2006.
- [18] M. Rahaman, *Sintering of ceramics*. Boca Raton: CRC Press, 2008.
- [19] J. Rödel, A. B. N. Kouna, M. Weissenberger-Eibl, D. Koch, A. Bierwisch, W. Rossner, M. J. Hoffmann, R. Danzer, and G. Schneider, “Development of a roadmap for advanced ceramics: 2010–2025,” *Journal of the European Ceramic Society*, vol. 29, no. 9, pp. 1549–1560, Jun. 2009.
- [20] J. S. Reed, *Introduction to the Principles of Ceramics Processing*. New York: John Wiley & Sons, 1988.
- [21] R. Orru, R. Licheri, A. M. Locci, A. Cincotti, and G. Cao, “Consolidation/synthesis of materials by electric current activated/assisted sintering,” *Materials Science and Engineering R*, vol. 63, no. 4–6, pp. 127–287, 2009.
- [22] M. A. Janney, C. L. Calhoun, and H. D. Kimrey, “Microwave Sintering of Solid Oxide Fuel Cell Materials: I, Zirconia 8 mol% Ytria,” *Journal of the American Ceramic Society*, vol. 75, no. 2, pp. 341–346, 1992.
- [23] M. Cologna, B. Rashkova, and R. Raj, “Flash Sintering of Nanograin Zirconia in less than 5 s at 850 degrees C,” *Journal of the American Ceramic Society*, vol. 93, no. 11, pp. 3556–3559, Jan. 2010.
- [24] R. Coble, “Sintering crystalline solids. I. Intermediate and final state diffusion models,” *Journal of Applied Physics*, vol. 32, no. 5, pp. 787–792, 2009.
- [25] L. C. De Jonghe and M. N. Rahaman, “Sintering stress of homogeneous and heterogeneous powder compacts,” *Acta Metallurgica*, vol. 36, no. 1, pp. 223–229, 1988.

- [26] L. C. De Jonghe and M. N. Rahaman, *Handbook of Advanced Ceramics: Vol. 1: Materials Science*. London, UK: Academic Press, 2003.
- [27] R. Orru, R. Licheri, A. Locci, A. Cincotti, and G. Cao, "Consolidation/synthesis of materials by electric current activated/assisted sintering," *Materials Science and Engineering: R: Reports*, vol. 63, no. 4–6, pp. 127–287, 2009.
- [28] M. A. Jamney and H. D. Kimrey, "Diffusion-controlled processes in microwave-fired oxide ceramics," *Materials Research Society Symposium Proceedings*, vol. 74, p. 1675, 1991.
- [29] D. Yang and H. Conrad, "Enhanced sintering rate of zirconia (3Y-TZP) by application of a small AC electric field," *Scripta Materialia*, vol. 63, no. 3, pp. 328–331, Jan. 2010.
- [30] D. Yang, R. Raj, and H. Conrad, "Enhanced Sintering Rate of Zirconia (3Y-TZP) Through the Effect of a Weak dc Electric Field on Grain Growth," *Journal of the American Ceramic Society*, vol. 93, no. 10, pp. 2935–2937, Jan. 2010.
- [31] H. Conrad, D. Yang, and P. Becher, "Effect of an applied electric field on the flow stress of ultrafine-grained 2.5Y-TZP at high temperatures," *Materials Science and Engineering: A*, vol. 477, no. 1–2, pp. 358–365, 2008.
- [32] H. Conrad, "Space charge and the dependence of the flow stress of ceramics on an applied electric field," *Scripta Materialia(USA)*, vol. 44, no. 2, pp. 311–316, 2001.
- [33] S. D. Antolovich and H. Conrad, "The effects of electric currents and fields on deformation in metals, ceramics, and ionic materials: An interpretive survey," *Material and Manufacturing Processes*, vol. 19, no. 4, pp. 587–610, 2004.
- [34] J. Campbell, Y. Fahmy, and H. Conrad, "Influence of an electric field on the plastic deformation of fine-grained Al₂O₃," *Metallurgical and Materials Transactions A*, vol. 30, no. 11, pp. 2817–2823, 1999.
- [35] H. Conrad and D. Yang, "Effect of an electric field on the plastic deformation kinetics of electrodeposited Cu at low and intermediate temperatures," *Acta Materialia*, vol. 50, no. 11, pp. 2851–2866, 2002.
- [36] S. Ghosh, A. Chokshi, P. Lee, and R. Raj, "A Huge Effect of Weak dc Electrical Fields on Grain Growth in Zirconia," *Journal of the American Ceramic Society*, vol. 92, no. 8, pp. 1856–1859, Aug. 2009.
- [37] H. Tsubakino and N. Matsuura, "Relationship between Transformation Temperature and Time-Temperature-Transformation Curves of Tetragonal-to-Monoclinic Martensitic Transformation in Zirconia-Yttria System," *Journal of the American Ceramic Society*, vol. 85, no. 8, pp. 2102–2106, 2002.

- [38] Y. Suzuki, "Phase transition temperature of fluorite-type $ZrO_2 \square Y_2O_3$ solid solutions containing 8–44 mol% Y_2O_3 ," *Solid State Ionics*, vol. 81, no. 3–4, pp. 211–216, Nov. 1995.
- [39] G. Gritzner and C. Puchner, " V_2O_5 , Nb_2O_5 and Ta_2O_5 doped zirconia ceramics," *Journal of the European Ceramic Society*, vol. 13, no. 5, pp. 387–394, 1994.
- [40] D. M. Smyth, *The Defect Chemistry of Metal Oxides*. Oxford University Press, Inc., 2000.
- [41] K. Rajeswari, M. B. Suresh, D. Chakravarty, D. Das, and R. Johnson, "Effect of nano-grain size on the ionic conductivity of spark plasma sintered 8YSZ electrolyte," *International Journal Of Hydrogen Energy*, vol. 37, no. 1, pp. 511–517, Jan. 2012.
- [42] P. Abelard and J. F. Baumard, "The electrical conductivity of cubic stabilized zirconia: The results of an IUPAC collaborative study (Technical Report)," *Pure and applied chemistry*, vol. 67, no. 11, pp. 1891–1904, 1995.
- [43] P. Abelard and J. Baumard, "Study of the dc and ac electrical-properties of an yttria-stabilized zirconia single-crystal [$(ZrO_2)_{0.88}-(Y_2O_3)_{0.12}$]," *Physical Review B*, vol. 26, no. 2, pp. 1005–1017, Jan. 1982.
- [44] S. P. S. BADWAL, "Grain boundary resistivity in zirconia-based materials: effect of sintering temperatures and impurities," *Solid State Ionics*, vol. 76, no. 1–2, pp. 67–80, 1995.
- [45] R. Greef, R. Peat, L. M. Peter, D. Pletcher, and J. Robinson, *Instrumental Methods in Electrochemistry*. London: Ellis Horwood Ltd., 1990.
- [46] P. J. Gellings and H. J. M. Bouwmeester, *CRC Handbook of Solid State Electrochemistry*. Boca Raton: CRC Press, 1997.
- [47] S. P. S. Badwal and F. T. Ciacchi..., "A fully automated four-probe dc conductivity technique for investigating solid electrolytes," *Journal of applied electrochemistry*, Jan. 1991.
- [48] Z. Munir, U. Anselmi-Tamburini, and M. Ohyanagi, "The effect of electric field and pressure on the synthesis and consolidation of materials: A review of the spark plasma sintering method," *Journal of Materials Science*, vol. 41, no. 3, pp. 763–777, Feb. 2006.
- [49] J. S. Francis and R. Raj, "Flash-Sinterforging of Nanograin Zirconia: Field Assisted Sintering and Superplasticity," *Journal of the American Ceramic Society*, p. n/a–n/a, 2011.
- [50] B. Vaidhyanath, "Flash Sintering and Electroceramic Devices," in *Proceeding of the International Conference on Advanced Cermaics and Composites*, 2013.
- [51] M. Cologna, A. L. G. Prette, and R. Raj, "Flash-Sintering of Cubic Yttria-Stabilized Zirconia at 750 degrees C for Possible Use in SOFC Manufacturing," *Journal of the American Ceramic Society*, vol. 94, no. 2, pp. 316–319, Jan. 2011.

- [52] R. Raj, "Joule heating during flash-sintering," *JOURNAL OF THE EUROPEAN CERAMIC SOCIETY*, vol. 32, no. 10, pp. 2293–2301, 2012.
- [53] S. Kim, S. G. Kim, J. Jung, S. L. Kang, and I. Chen, "Enhanced Grain Boundary Mobility in Yttria-Stabilized Cubic Zirconia under an Electric Current," *Journal of the American Ceramic Society*, vol. 94, no. 12, pp. 4231–4238, 2011.
- [54] F. Wakai, S. Sakaguchi, and Y. Matsuno, "Superplasticity of yttria-stabilized tetragonal ZrO₂ polycrystals," *Advanced ceramic materials*, vol. 1, no. 3, pp. 259–263, 1986.
- [55] X. Hao, Y. Liu, Z. Wang, J. Qiao, and K. Sun, "A novel sintering method to obtain fully dense gadolinia doped ceria by applying a direct current," *Journal of Power Sources*, vol. 210, no. 0, pp. 86–91, Jul. 2012.
- [56] M. Cologna, J. S. C. Francis, and R. Raj, "Field assisted and flash sintering of alumina and its relationship to conductivity and MgO-doping," *Journal of the European Ceramic Society*, vol. 31, no. 15, pp. 2827–2837, Jan. 2011.
- [57] A. L. G. Prette, M. Cologna, V. Sglavo, and R. Raj, "Flash-sintering of Co₂MnO₄ spinel for solid oxide fuel cell applications," *Journal Of Power Sources*, vol. 196, no. 4, pp. 2061–2065, Jan. 2011.
- [58] A. Karakuscu, M. Cologna, D. Yarotski, J. Won, J. S. C. Francis, R. Raj, and B. P. Uberuaga, "Defect Structure of Flash-Sintered Strontium Titanate," *Journal of the American Ceramic Society*, vol. 95, no. 8, pp. 2531–2536, 2012.
- [59] J. Jamnik and J. Maier, "Defect chemistry and chemical transport involving interfaces," *Solid State Ionics*, vol. 119, no. 1–4, pp. 191–198, Jan. 1999.
- [60] J. S. Francis, M. Cologna, and R. Raj, "Particle size effects in flash sintering," *Journal of the European Ceramic Society*, vol. 32, no. 12, pp. 3129–3136, 2012.
- [61] R. Raj, M. Cologna, and J. S. C. Francis, "Influence of Externally Imposed and Internally Generated Electrical Fields on Grain Growth, Diffusional Creep, Sintering and Related Phenomena in Ceramics," *Journal of the American Ceramic Society*, vol. 94, no. 7, pp. 1941–1965, Jan. 2011.
- [62] R. Muccillo, M. Kleitz, and E. N. S. Muccillo, "Flash grain welding in yttria stabilized zirconia," *Journal of the European Ceramic Society*, vol. 31, no. 8, pp. 1517–1521, Jul. 2011.
- [63] R. Muccillo and E. N. S. Muccillo, "An experimental setup for shrinkage evaluation during electric field-assisted flash sintering: Application to yttria-stabilized zirconia," *Journal of the European Ceramic Society*, vol. 33, pp. 515–520, 2012.

- [64] R. Muccillo, "Recent developments oc electric-field assisted sintering ceramic materials," in *International Conference on Advanced Ceramics and Composites*, 2013.
- [65] X. Guo and J. Maier, "Grain Boundary Blocking Effect in Zirconia: A Schottky Barrier Analysis ," *Journal of The Electrochemical Society* , vol. 148 , no. 3 , pp. E121–E126, Jan. 2001.
- [66] "DURAMAX™ B-1000 Binder Data Sheet," p. 2, 2008.
- [67] Z. Chen, K. Ikeda, T. Murakami, and T. Takeda, "Drainage phenomenon of pastes during extrusion," *Journal of Materials Science*, vol. 35, no. 10, pp. 2517–2523, 2000.
- [68] J. Han and D. Kim, "Analysis of the proportionality constant correlating the mean intercept length to the average grain size," *Acta Metallurgica et Materialia*, vol. 43, no. 8, pp. 3185–3188, 1995.
- [69] "ASTM: C830-00. Standard Test Methods for Apparent Porosity, Liquid Absorption, Apparent Specific Gravity and Bulk Density of Refractory Shapes by Vacuum," 2009.
- [70] S. P. S. Badwal, "Electrical conductivity of single crystal and polycrystalline yttria-stabilized zirconia," *Journal of Materials Science*, vol. 19, pp. 1767–1776, 1984.
- [71] F. Paschen, "Ueber die zum Funkenübergang in Luft, Wasserstoff und Kohlensäure bei verschiedenen Drucken erforderliche Potentialdifferenz," *Annalen der Physik*, vol. 273, no. 5, pp. 69–96, 1889.
- [72] J. Lee, J. Fleig, J. Maier, D. Kim, and T. Chung, "Local Conductivity of Nitrogen-Graded Zirconia," *Journal of the American Ceramic Society*, vol. 88, no. 11, pp. 3067–3074, Nov. 2005.
- [73] J. Janek and C. Korte, "Electrochemical blackening of yttria-stabilized zirconia – morphological instability of the moving reaction front," *Solid State Ionics*, vol. 116, no. 3–4, pp. 181–195, 1999.
- [74] K. Rajeswari, M. B. Suresh, U. S. Hareesh, Y. S. Rao, D. Das, and R. Johnson, "Studies on ionic conductivity of stabilized zirconia ceramics (8YSZ) densified through conventional and non-conventional sintering methodologies," *Ceramics International*, vol. 37, no. 8, pp. 3557–3564, 2011.
- [75] R. E. W. Casselton, "Blackening in yttria stabilized zirconia due to cathodic processes at solid platinum electrodes," *Journal of Applied Electrochemistry*, vol. 4, no. 1, pp. 25–48, 1974.
- [76] J. Park and R. N. Blumenthal, "Electronic Transport in 8 Mole Percent Y 2 O 3 □ ZrO2," *Journal of The Electrochemical Society*, vol. 136, no. 10, pp. 2867–2876, 1989.
- [77] J. Janek and C. Korte, "Electrochemical blackening of yttria-stabilized zirconia – morphological instability of the moving reaction front," vol. 116, pp. 181–195, 1999.

- [78] R. Roy, D. Agrawal, J. Cheng, and S. Gedevisanishvili, "Full sintering of powdered-metal bodies in a microwave field," *Nature*, vol. 399, no. 6737, pp. 668–670, 1999.
- [79] A. West, *Solid state chemistry and its applications*. 1991.
- [80] Y. Arachi, H. Sakai, O. Yamamoto, Y. Takeda, and N. Imanishai, "Electrical conductivity of the ZrO₂-Ln₂O₃ (Ln₅ lanthanides) system," *Solid State Ionics*, vol. 121, pp. 133–139, 1999.
- [81] G. M. Fantini, "Estrusione di elettroliti in ceria drogata con gadolinia per IT-SOFC micro-tubolari (Extrusion of gadolinia doped ceria electrolytes for microtubular IT-SOFC)," Università degli Studi di Trento, 2012.
- [82] R. Buchanan, Ed., *Ceramic Materials for Electronics*, 2nd ed. New York: Marcel Dekker Inc., 1991.
- [83] K. Rajeswari, A. R. Reddy, U. S. Hareesh, B. P. Saha, and R. Johnson, "Micro structural control of stabilized zirconia ceramics (8YSZ) through modified conventional sintering methodologies," *Science of Sintering*, vol. 42, no. 1, pp. 91–97.

Appendix 1: Kröger-Vink Notation

Species	Symbol	Effective Charge
Zirconium ion and oxygen ion at normal lattice site	Zr_{Zr}^x and O_O^x	neutral
Zirconium interstitial	$Zr_i^{''''}$	+4
Oxygen interstitial	$O_i^{''}$	-2
Zirconium vacancy	$V_{Zr}^{''''}$	-4
Oxygen vacancy	$V_O^{''}$	+2
Donor cation at zirconium site	D_{Zr}^{\cdot}	+1
Acceptor cation at zirconium site	A_{Zr}^{\prime}	-1
electron	e^{\prime}	-1
Hole	h^{\cdot}	+1

Appendix 2: Grain growth

Grain growth trial and the resulting average grain size. After sintering, samples were cut in half and polished with a series of SiC paper and diamond pastes down to 1 μm . They were then thermally etched for 25 minutes at 50°C less than the sintering temperature in the same furnace. The average grain size was determined by SEM images on the etched surface using the point intercept method with a correction of 1.57.

Preparation Method	Furnace	Treatment Temperature [°C]: Time [hours]	Average Grain Size μm
Pressing	1600	1250:	0.38
	“	1300:	0.75
	“	1350:	1.40
	“	1450:	3.20
	“	1550:	7.60
	“	1575:	16.0
	1800	1400:	0.68
	“	1450:	1.29
	“	1550:	3.53
	“	1600:	4.63
	1600	2 Step*	5.84
	1600	1500: 0 min	7.60
	“	1500: 10 min	6.86
	“	1500: 0.5 hr	6.72
	“	1500: 1 hr	5.84
“	1500: 10 hr	8.31	
“	1500: 50 hr	73.9	
Extrusion	Dilatometer	1400: 2hr	2.33
	“	1450: 2hr	4.12
	“	1500: 2hr	5.59
	“	1550: 2hr	6.82

*Two-step sintering done by heating at 5°C/min to 500°C holding for 1 hour at 500°C, heating at 5°C/min to 1550°C holding 5 min cooling at 5°C/min to 1375 holding for four hours, then cooling to room temperature 5°C/min[83].

Appendix 3: Flash sintering of extruded 10GDC cylinders in dilatometric setup.

Introduction

Based on the results found from the high voltage flash sintering regarding the importance of current on the densification behavior, and that with the power supply used to apply E-fields >300 V/cm had a relatively low current limit of 120 mA resulting in low current densities in dog bone samples, the sample format was changed so that smaller samples could be used with a the PS:DLM300. In order to achieve the

So far, reported results for flash sintering are only for dog bone shaped samples. Changing to cylindrical shaped samples is still in a preliminary stages, and only low strength E-fields (60 V/cm) are being used to resolve issues before high voltages are applied to see if results for these samples can be replicated at high E-fields with the new geometry and with the high current densities believed to be required to reach full density.

Experimental

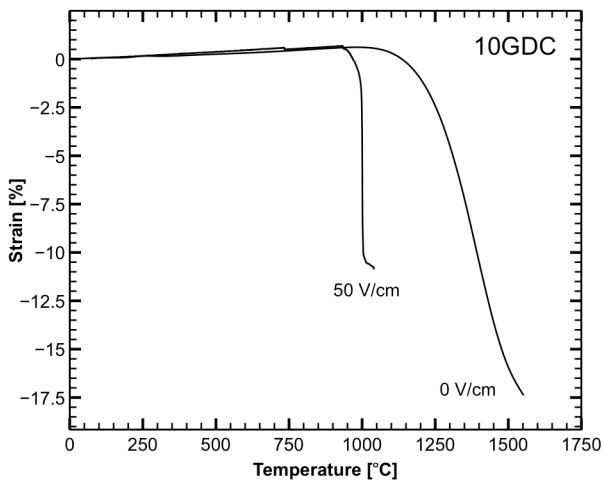
Samples of extruded 8YSZ and 10GDC were cut to a length of 70 mm. The cylindrical faces were made parallel using an jig that held samples perpendicular to SiC sand paper. The samples were placed into the dilatometric flash sintering setup. For the 8YSZ, E-fields of XXXX were applied. For 10GDC, only one E-field of XXX was applied. The samples were heated at $10^{\circ}\text{C}/\text{min}$ until flash sintering occurred.

This was the first time 10GDC had been flash sintered, so required current densities were unknown, because of its similarity to 8YSZ, an E-field of 60 V/cm was chosen

For 8YSZ, two different electrodes were used first, platinum mesh was used, but the high currents caused the mesh to melt, so the electrodes were switched to platinum foil. The foil does not have the melting issues, but the short-circuiting problem remains.

Results 8YSZ and 10GDC

The sintering behavior and flash sintering behavior for 10 mol% gadolinia-doped ceria (10GDC) is shown in Figure 5.10. With the application of 50 V/cm, 10GDC is flash sintered and successfully sintered at 1000°C. This result most importantly signifies that flash sintering is not limited to dog bone samples and done on cylindrical samples, that extruded samples can be flash sintered, and the 10GDC can be flash sintered.



Flash sintering behavior of extruded 10 mol% gadolinia doped GDC flash sintered using dilatometric setup.

Curriculum Vitae

Education:

- PhD: Materials Science and Industrial Engineering,
University of Trento, Trento, Italy(2010-2013)
Dissertation: 'Mechanism of Flash Sintering in Cubic Zirconia'
- M.S. Mechanical Engineering: Energy and Environment
Magna Cum Laude
University of Colorado, Boulder, USA (2008-2009)
- B.S Mechanical Engineering,
Magna Cum Laude
University of Colorado, Boulder (2005-2009)
Capstone Project: 'Feasibility of the implementation Anaerobic
Digesters for Methane Production at UCB'

Research Experience:

- Research Assistant:
Sintering of SiCN ceramics, Electrical properties of YSZ bicrystals
High Temperature Material Laboratory,
University of Colorado, Boulder Prof. R. Raj (2008-2009)
- Student Assistant :
Characterization and removal of biodiesel contaminants
Membrane Sciences Group, university of Colorado, Boulder,
Prof. J. Pelligrino (2007-2008)

Independent Study:

Emissions of wood fired kilns for EPA certification
Boulder Pottery Lab with Department of Mechanical Engineering,
University of Colorado, Boulder
Prof. M. Hannigan and Nancy Utterbeck

Internship:

Controls and sensors for autonomous vehicles
Perceptek Robotics, Inc. (2004-2006)

Publications and Proceedings:

Downs, J.A. and Sglavo, V.M. Electric Field Assisted Sintering of Cubic Zirconia at 390°C. *J. Am. Ceram. Soc.* DOI: 10.1111/jace.12281 (2013)

Downs, J.A., Anshu, Naik, K., Sglavo, V.M. 'Electric Field Assisted Sintering in Advanced Ceramics'. *Proceedings of the XI Convegno Nazionale AIMAT* (2012)

Sanchez, J.P., **Downs, J.A.**, Raj, R. Transient Viscous Flow During the Evolution of a Ceramic (Silicon Carbonitride) from a Polymer (Polysilazane). *J. Am. Ceram. Soc.* **93** [9] 2567-2570 (2010)

Presentations:

Downs, J.A. and Sglavo, V.M., High Voltage Flash Sintering in Cubic Zirconia. 37th International Conference and Exposition on Advanced Ceramics and Composites. Daytona Beach, FL, USA (2013)

Downs, J.A. and Sglavo, V.M., 'Flash-Like Behavior in Fully Dense Cubic Zirconia'. Materials Science & Technology Conference and Convention (2012)

Downs, J.A., Anshu, Naik, K., Sglavo, V.M. 'Electric Field Assisted Sintering in Advanced Ceramics'. XI Convegno Nazionale AIMAT (2012)

Downs, J.A., Raj, R. 'Voltage drops at grain boundary in zirconia bicrystal'. Materials Science & Technology Conference and Convention (2009)

Posters:

Naik, K. **Downs, J.A.,** Sglavo, V.M. 'Effect of Dopant on Flash-Sintering Behavior of Alumina'. Materials Science & Technology Conference and Convention (2012)

Teaching Experience:

Laboratory Assistant: Ceramics Processing & Engineering
Prof. V.M. Sglavo (2011-2013)

Teaching Assistant: Sustainable Energy
Prof. M. Hannigan (2009)

Awards and Honors:

Outstanding Senior Award, Top graduate Dec. 2008,
Department of Mechanical Engineering
University of Colorado, Boulder

Undergraduate Research Award, 2008
Department of Mechanical Engineering
University of Colorado, Boulder

Acknowledgements:

I would like to thank above all my parents, Ron and Kathy, and my sister, Michaela, for all their love and support during my adventures in Italy and throughout my carrier, and my grandparents, who are no longer here, but who have been the most influential people in my life.

To all the friends I have made in Trento that have welcomed me into their lives. Especially Aylin Karacışku and Vincenzo Catania for being there to help no matter what and being my proxy advisors, Marco Graser and his family and friends in Brendola and Vicenza especially Roma and Nino and all the adventures and stories that should go unmentioned across Europe, Andrea and Carlotta and all the amazing dinners, ski days, and days on the beach, my roommates Sinan and Fabio, Evgeny for his amazing wine descriptions, Mattia for all the coffee breaks, Teresa for the Sunday brunches. To the present and former inhabitants of Casa Nerchie the Nonesi and the Unti especially Giovanni, Laura, and Stefano for and some wild adventures in Italy and around Europe, Giulia my double agent/grape vine master and our chinese outtings, and finally Austin and Ines for giving me some grounding.

Thanks to all my friends and colleagues in the lab, Kiran, Anshu, Prandyesh, Predeep, Emanuelle, David, Giulia, Fillipo, Marzio, Francesca, Michelle, Luca, Fabio, and all the students I have helped over the last few years. You have all been a big help and a welcome distraction.

To all my friends from San Bartolameo who have spread through out the world, Milan, Jovana, Ruzzana, Kate, Beyza, Kyle, Benoit, Mohamed, Saliou, Irina, and many many others.

Finally, to all my friends, colleagues, and professors from Boulder who supported me in coming to Trento, continue to do so, and and always have a place for me when I'm visiting wherever they may be now, Robyn, Alex, John and Anna, John Francis, Heather and Michael, Laura, Julie,

Kenny and Nicole, Casey and Erin, Hallie, Brian, Joel, and Jim and Katie,
and many more from my six years there.

It's been great and the greatness shall continue...